EUROPEAN COMMISSION

Community research

Long-term Performance of Engineered Barrier Systems

PEBS

Long-term Performance of Engineered Barrier Systems PEBS

Seismic data report on EDZ and EBS evolution (HE-E)

(DELIVERABLE-N°: D2.2-10)

Contract (grant agreement) number: FP7 249681

Author(s):

Kristof Schuster (BGR)

Date of issue of this report: 14/03/2014

Start date of project: 01/03/10 Duration : 48 Months

Project co-funded by the European Commission under the Seventh Euratom Framework Programme for Nuclear Research &Training Activities (2007-2011)		
Dissemination Level		
PU	Public	**PU**
RE	Restricted to a group specified by the partners of the [acronym] project	
CO	Confidential, only for partners of the [acronym] project	

EURATOM

Table of Contents

List of figures

1 Introduction

In the frame of the EC project “Long-term performance of Engineered Barrier Systems” (PEBS) the heater experiment HE-E (Gaus et al., 2011) is performed in the Mont Terri Rock Laboratory in northwestern Switzerland. Two horizontal heaters are employed in two sections of a microtunnel with different types of buffer material (Fig. 1.1).

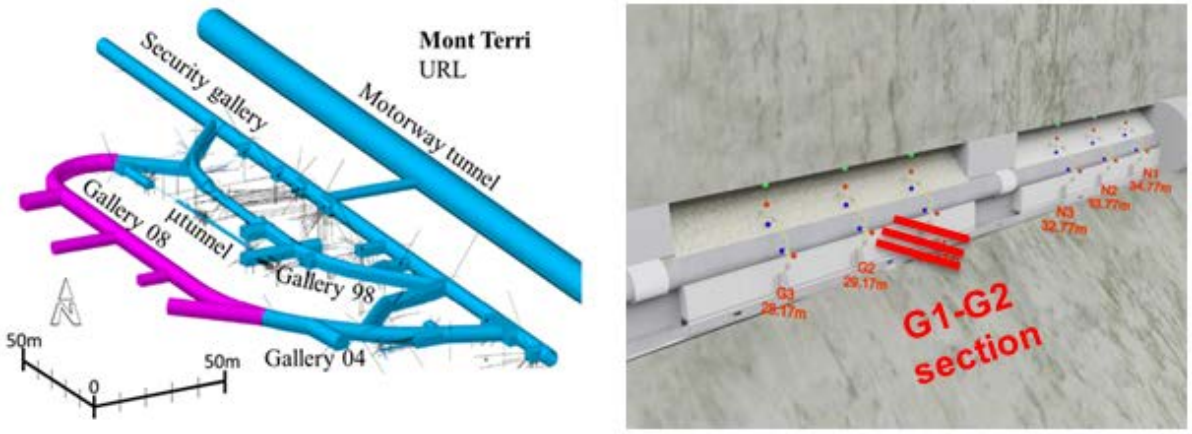

Fig. 1.1 Overview of the HE-E configuration. Left: Schematic view of the Mont Terri Rock Laboratory with the location of the microtunnel. Right: Location of 3 boreholes between the G1 and G2 section used for seismic transmission measurements (Gaus et al. 2011, modified).

BGR proposed to characterise the backfill material as well as the close vicinity of the rock within the initial phase of the experiment with seismic parameters. The section where the sand-bentonite backfill material is used was chosen for the measurements. Ultrasonic / seismic transmission measurements using three boreholes aim at the characterisation of the sand-bentonite (S/B) material and the Opalinus Clay (OPA) with the help of derived seismic parameters. Due to the de- and resaturation processes and the impact caused by the heating process and their connected reactions changes in rock properties in the vicinity of the microtunnel and especially in the S/B are expected.

The measurements with 50 different ray paths measured per day started in March 2011 and last until now. In general the data quality is very good. Trends in the data within the first 300 days can be explained fairly good with existing concepts, whereas several later trends in the data are more difficult to explain, or even not understood until now. This report focuses on the time span March 12, 2011 until September 14, 2012. It covers 553 days of daily measurements. The installation of all prefabricated components as well as the maintenance

of the measurements were performed by the subcontractor Gesellschaft für Materialprüfung und Geophysik mbH (GMuG) while data processing and interpretation are being done by BGR.

2 Objectives and Motivation

A change in rock properties in the vicinity of the microtunnel and especially in the S/B is expected due to the de- and resaturation processes, stress redistribution and the temperature impact, all caused by the installation work, the backfilling and closure of the section and finally the heating process. Seismic parameters like P-wave velocity (v_p) and the amplitudes of first arrival phases react very sensitive to appropriate changes. These parameters characterise the rock in an integral way over distances between 0.26 m and 0.86 m depending on the emitter-receiver locations. Not all correlations and dependencies between varying seismic parameters and related rock property changes are completely understood until now. In Figure 2.1 a simplified sketch for a seismic wave field traveling 50 cm between emitter and receiver in OPA illustrates the sensitivity of P-wave velocities to alterations in rock. Several options for anomalies are given on the left side: creation of an Excavation Damaged Zone (EDZ), micro cracks, increased porosity, fracture and a lithological change. For an intact OPA with a v_{p0} of 2300 m/s an integral anomaly of 10 mm, what corresponds to 2% of the total travel path length, would reduce the velocity to 2274 m/s (case 1: micro cracks, filled with “fluids” equals 98.9 % of v_{p0}) or even to 2057 m/s (case 2: pure micro cracks, “gas filled” equals 89.4 % of v_{p0}). In terms of travel times it would be: 217.4 µs (intact OPA), 219.7 µs (OPA with anomalies, case 1) and 243.1 µs (OPA with anomalies, case 2), a range of differences in time between 2.3 µs and 25.7 µs. Due to the very good data quality even the small difference of 2 µs can be resolved. In this very simplified approach no scattering effects and/or relations between seismic wave length and size and aspect ratio of anomalies (e.g. pore size) are taken into account. Both cases, all voids filled with air/gas or with fluids are extreme cases. A combination of partly gas and fluid filled pores is also conceivable and rather realistic, especially when short term developments in argillaceous rock are investigated.

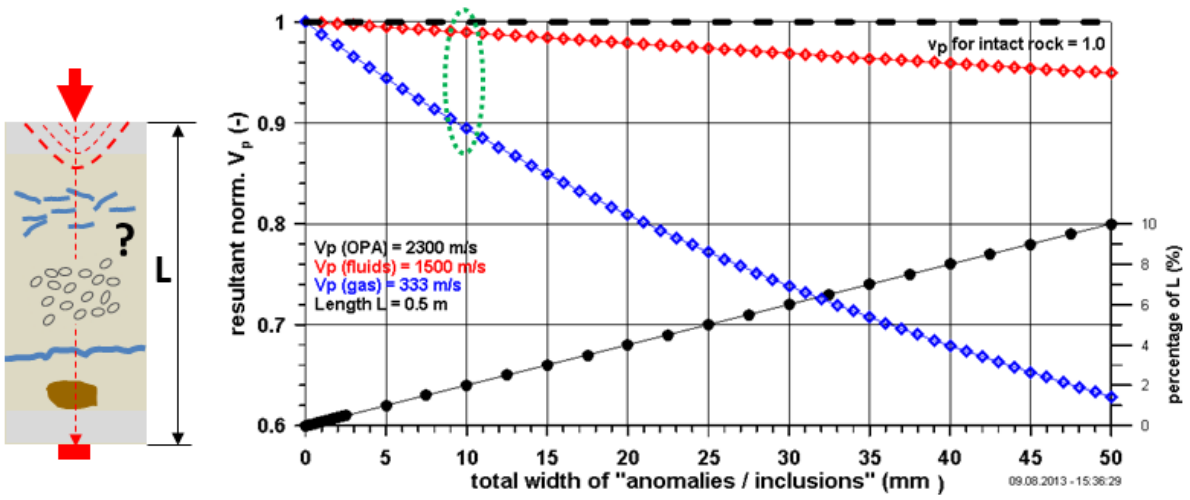

Fig. 2.1 Simplified illustration of v_p variation depending on anomalies encountered along the travel path. Left: Seismic wave field represented by a seismic ray path traveling through different anomalies in OPA. Right: Resultant normalised v_p-graphs for two extreme cases, all voids filled either with gas or with fluids.

Figure 2.2 shows a seismic section in two different resolutions covering 783 days of daily observation / recording (March 12, 2011 – May 5, 2013). The first arrival phases (P-waves) are indicated by arrows. The thin dashed line corresponds to the arrival time at day 1. The distance between emitter and receiver is 48 cm, comparable to the situation discussed in Figure 2.1. Note the very good data quality, except of some drop outs between day 300 and 350, due to a technical problem, which will be discussed in a separate section. Furthermore, there are some singular data losses, which are of minor importance.

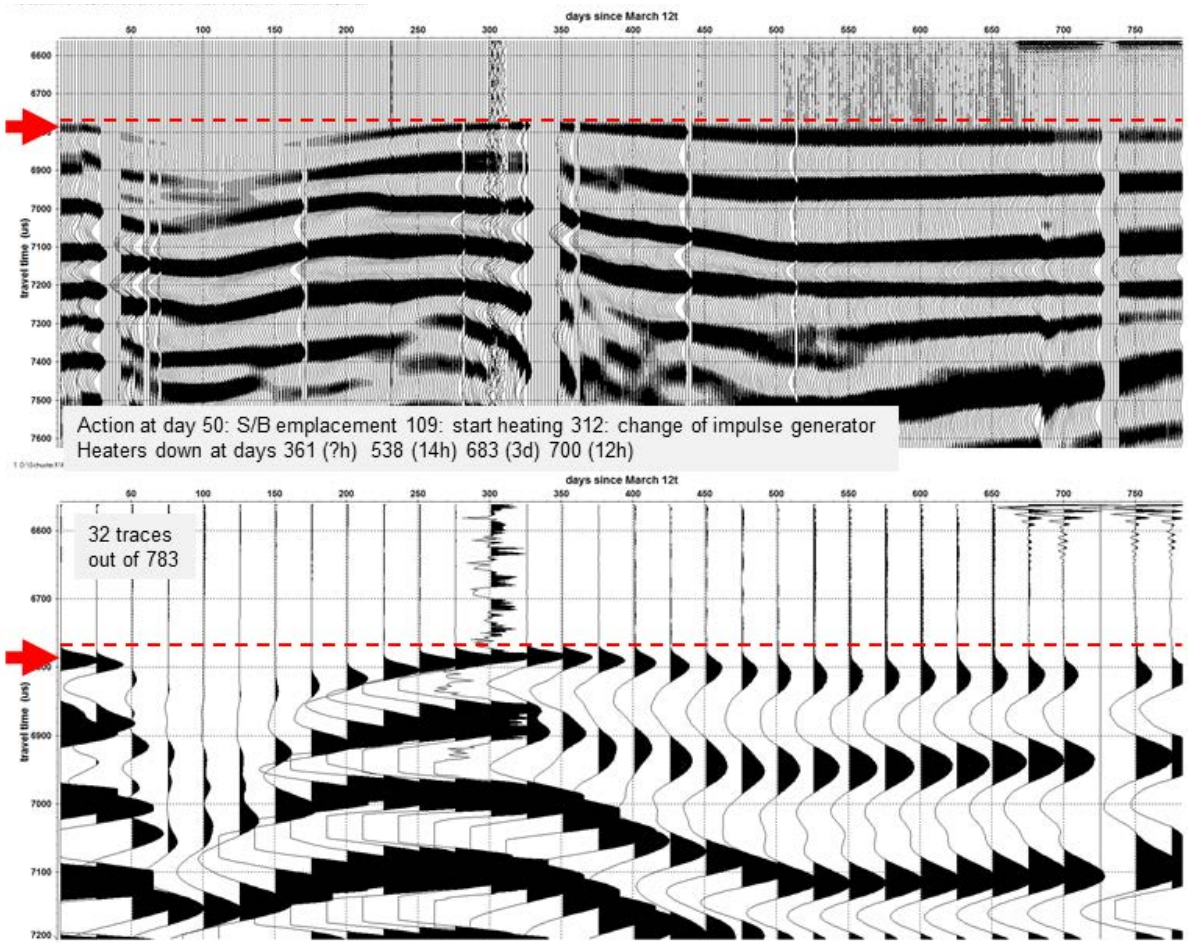

Fig. 2.2 Seismic section (E01→R10) covering 783 days of observation (March 12, 2011 – May 2, 2013). Top: all traces (trace normalized) whereas only every 2nd trace is plotted. Below: same time span, but only every 25th trace is plotted (ensemble normalized).

The seismic section represents seismic travel paths in the OPA at a distance of 10 cm from the interface S/B – OPA. This is an area where the Excavation Damaged Zone (EDZ) and/or Excavation disturbed Zone (EdZ) is well pronounced. For this emitter-receiver combination travel paths are roughly oriented 45° to bedding. P-wave phases change remarkably. In terms of first arrival times up to 55 µs which results in different p-wave velocities with a pronounced v_p decrease of up to 76 % of v_{p0} (cf. also Fig. 6.13). Furthermore, also the amplitudes varies, they change in magnitude and in frequency content. These are very clear indications that remarkable changes in rock properties occur with ongoing time.

Within the first 100 days a noticeable increase of travel times and simultaneously a decrease of amplitudes are visible, followed by a decrease of travel times and a recovery of amplitudes until day 300 where the initial situation (day 1) seems to be reached approximately. From day

360 on travel times start again to increase, stay on a constant level and start to decrease slightly, whereas amplitudes change their frequency content continuously, which can easily be seen on changing shapes of first arrival phases. What does it mean in terms of rock mechanics? All these changes among other things are close related to micro crack creation, sealing processes, swelling of OPA, stress redistribution and pore water pressure changes. Up to now only limited experiences for a sound explanation / interpretation for such seismic parameter changes in OPA exist. Some laboratory tests exist. In the following chapters a more detailed explanation will be given.

3 Layout of the seismic transmission experiment

The section where the sand – (Almeria) bentonite mixture (65/35) is used was chosen for the seismic transmission experiment because three boreholes which were used for seismic cross hole measurements in a former experiment (VE experiment) could be reused easily for this task.

3.1 Location and general layout

Three existing boreholes (diameters of 86 mm) which were used within the VE-Experiment for a seismic characterisation of the rock in October 2006 and July 2007 (Schuster, 2007) were used for the installation of a seismic array. The boreholes were inspected by swisstopo in summer 2010 and judged as stable and in good shape (pers. communication D. Jaeggi, 2010). In total 15 piezoelectric transducers were deployed. Details of the seismic array will be given in the next section. The general layout is given in Figure 3.1.

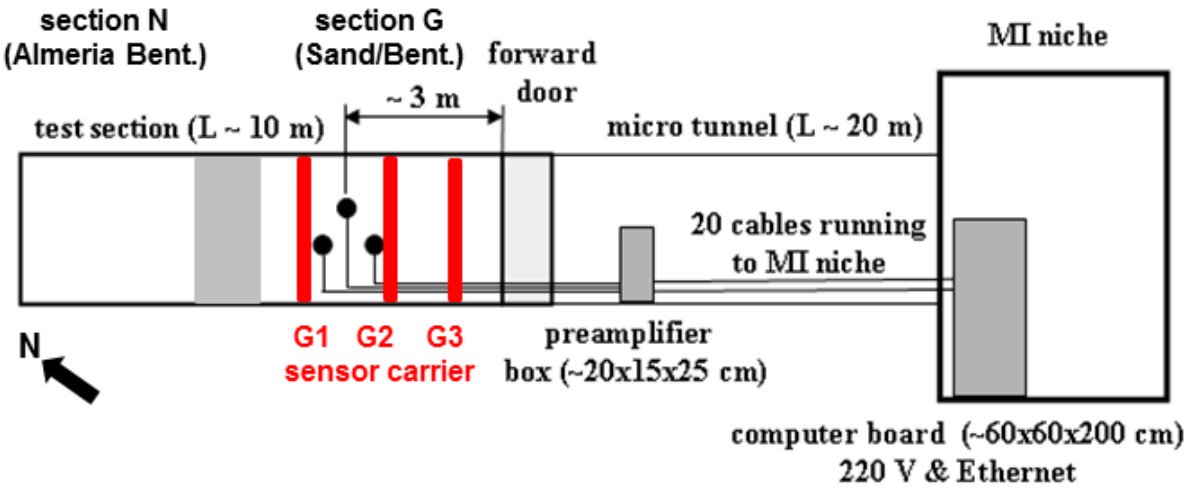

Fig. 3.1 Location and general layout of the seismic transmission experiment in the micro-tunnel.

The three borehole collars are in the space between the section carriers G1 and G2 and tend towards East (right side of the wall of the micro-tunnel, looking towards the end of the micro-tunnel).

The cable harness (~ 20 coax cables) connects the sensors inside the test section with the preamplifier box located close to the forward door. The cables (Coax RG178B/U) are temperature resistant up to 200°C. For the connection between the preamplifier box and the computer board 20 cables (normal coax cables) which were used already in the VE experiment are reused. The computer board is placed in the MI niche next to the entrance of the microtunnel. A power supply of 220 V is used for the computer board. The preamplifiers are fed from the computer board via the signal and control cables. Because of the big amount of data (full wave recording) the seismic traces are stored on portable hard disk drives (USB connection) which are changed on a monthly basis by laboratory staff and sent to the contractor which provides the raw data to BGR. At a later stage the measurement device and the data transfer could be reached / realized via internet connection.

3.2 Instrumentation / seismic array

Details of the seismic array are given in Figure 3.2. The boreholes are located on the eastern wall of the test section around 3 m away from plug 3. All three boreholes are sub-horizontal and nearly parallel. With respect to the tunnel axis they oriented ~ 30° south.

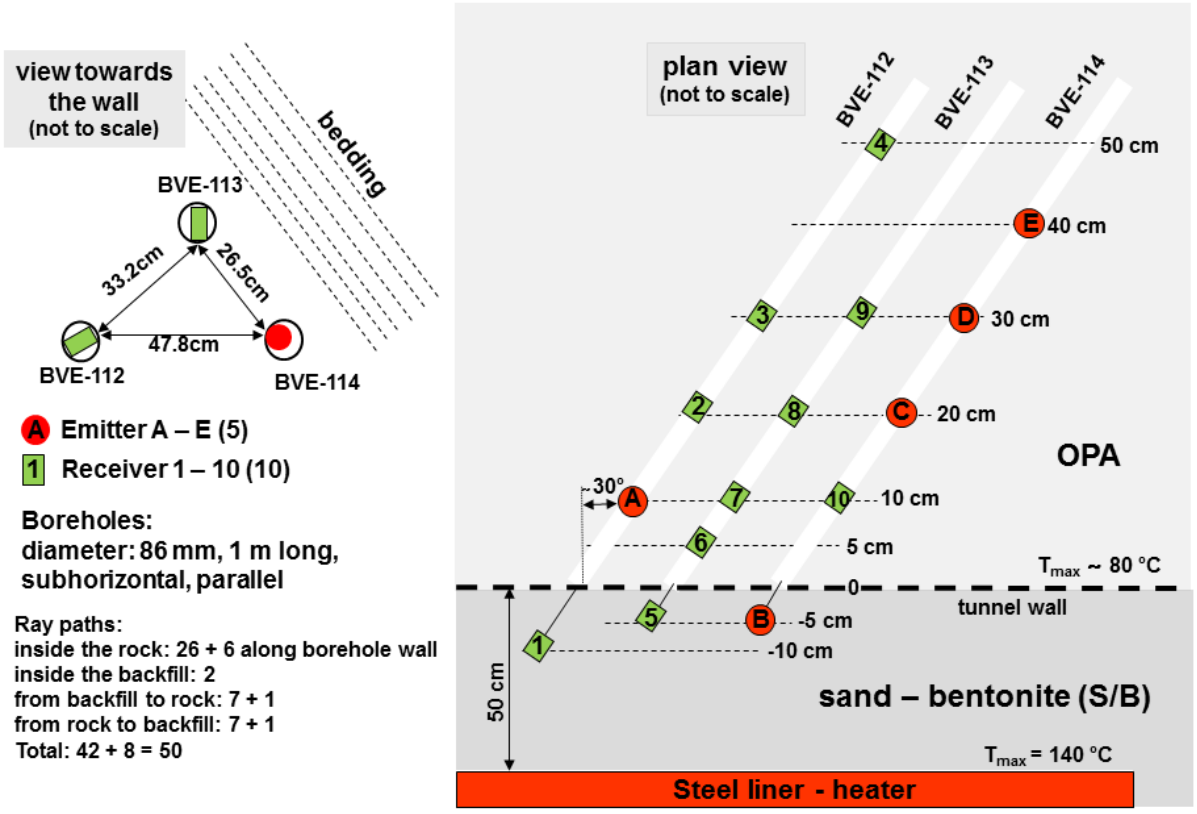

Fig. 3.2 Design of the seismic array using 3 boreholes with 15 piezoelectric transducers, 5 emitters (A-E) and 10 receivers (R01-R10).

Piezoelectric transducers were mounted on support frames and positioned in the borehole and fixed mechanically with the support of springs. In total 15 transducers are used, five emitters (sources) and ten receivers. The distribution of emitters and receivers is displayed in Fig. 3.2. Three transducers are located outside the boreholes in order to observe the development in the backfill material. Figure 3.3 shows these transducers just after the installation on February 17, 2011. This area was later, after the installation of the heaters, filled up with the sand/bentonite mixture. With this arrangement two different ray paths are realized in the S/B at distances of 5 cm and between 5 cm and 10 cm from the S/B-OPA interface.

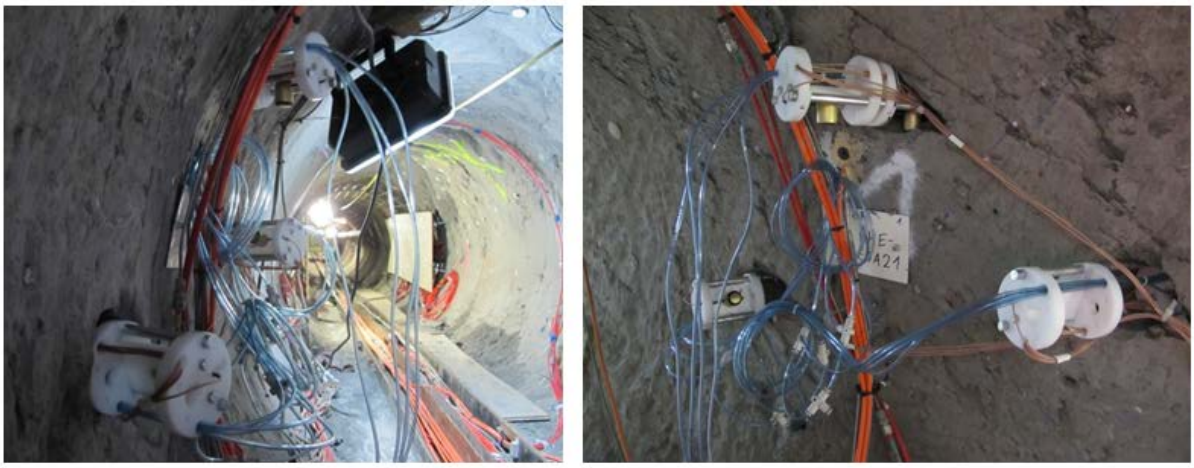

Fig. 3.3 Photographs taken during the installation work. Left: view out of the micro-tunnel towards the entrance. Right: 3 piezoelectric transducers in more detail.

The transducers installed in the boreholes allow seismic waves travelling preferably normal, parallel and with 45° towards the bedding planes of the OPA. Because the dip and the strike of the bedding planes changes slightly and the borehole orientations have some uncertainties this is a simplification for emitters and receivers at the same depth. When emitter and receiver depth differ the deviation becomes more pronounced. Concerning the coverage of different depths levels and orientations of the ray paths towards the bedding a compromise had to be made. Not all depth levels for all three orientations could be realized due to the limited number of transducers.

The automatic daily measurement between all emitter – receiver combinations results in 50 different ray paths which can be differentiated as follows:

- Ray paths inside the rock between boreholes: 26
- Ray paths inside the rock along borehole wall: 6
- Ray paths inside the backfill: 2
- Ray paths from backfill to rock between “boreholes”: 7
- Ray paths from backfill to rock along “boreholes”: 1
- Ray paths from rock to backfill between “boreholes”: 7
- Ray paths from rock to backfill along “boreholes”: 1

The most relevant orientations of ray paths are the one running directly through the OPA or through the S/B. According to the experiences made in former experiments (VE and EB) the observation focuses on the first 50 centimetres of the rock, where the main changes in rock

properties are expected. The technical details of the used equipment are compiled in a short report (German) which was provided by GMuG. It can be found in the appendix. The most important parameters are:

- Piezoelectric transducers (built by GMuG), 5 emitters and 10 receivers, prefabricated on three rods, coupling via springs, de-coupling pneumatically
- Recording system (PC based): A/D converter with 16 bit @ 500 kHz (dt = 2 µs)
- Amplification: receivers: 40 dB (30 dB pre amp + 10 dB), high-pass filter: 1 kHz
- Emitter signal (one impulse generator, located outside in the computer cabinet, switches by a relay switch between all five emitters): - 40 dB
- Recording: daily measurement at 1:10 am for about 50 minutes
- For each emitter 2048 measurements are repeated and averaged (stacked)
- Length of recordings: 32.4 ms (16384 samples)
- Pre trigger: 20 %

The installation of all components was performed between February 16 and 18, 2011 according to the planned layout. Only some minor modifications had to be made on-site in order to ensure a safer installation of the heating system. First operational tests of the seismic array at February 17, 2011 were successful. Within the test phase between February 17 and March 11, 2011 several tests were made and according to the outcomes the final recording parameters were defined.

3.3 Acoustic emission monitoring

Our subcontractor GMuG offered to record during nights and over weekends potential acoustic emission (AE) signals with the same equipment. During that time no human activities in the rock laboratory are going on what enhances the chance to record acoustic emission signals originating from processes going on in the rock, e. g. creation of cracks due to stress redistribution. Only in case of effectual and successful data acquisition an additional processing should be performed. But the outcome was rather poor. One of the reasons could be the age of the microtunnel. After more than 10 years all the major stress redistribution processes ended. Comparable AE experiments were performed around and in the EB niche which is in the prolongation of the microtunnel (see Fig. 1.1) approximately 15 m away (Spies et al., 2002, Schuster et al., 2004a). Another reason for the poor outcome could be the layout of the seismic array which was mainly designed for the active part of the seismic experiment. Therefore the AE option was not used for additional analyses.

4 Seismic Parameters and uncertainties

The discrimination between seismic methods (in-situ or mining seismic) and ultrasonic methods (laboratory seismic) is assumed by some authors for signal frequencies of 10 kHz. The dominant frequency content of the signals we are dealing with in this report is in the range between 2 kHz and 20 kHz, at which 10 kHz can be seen as the lowermost edge of the ultrasonic range. Nevertheless, we use the term seismic, also to avoid confusion in the text. The main seismic parameters derived from the recordings and used in this report are explained in this chapter. The processing, analyses and plotting of seismic records is performed with the seismic software tool Reflex Win (Sandmeier, 2013).

4.1 Derived seismic parameters

In Figure 4.1 the emitter signal for emitter E01 as generated at day 1 is displayed with the main signal characteristics used for further processing. More details concerning the source signals are discussed in the next chapter. In this context only the start time (t0) is of interest.

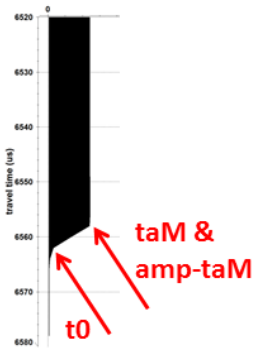

Fig. 4.1 Seismic trace witch is generated in the signal generator and used for the excitation of the piezoelectric signal transducers (emitters).

For the received signal at receiver R10 a part of a single seismic trace is shown in Figure 4.2 in order to explain the main first arrival P-wave onset characteristics used for the derivation of seismic parameters.

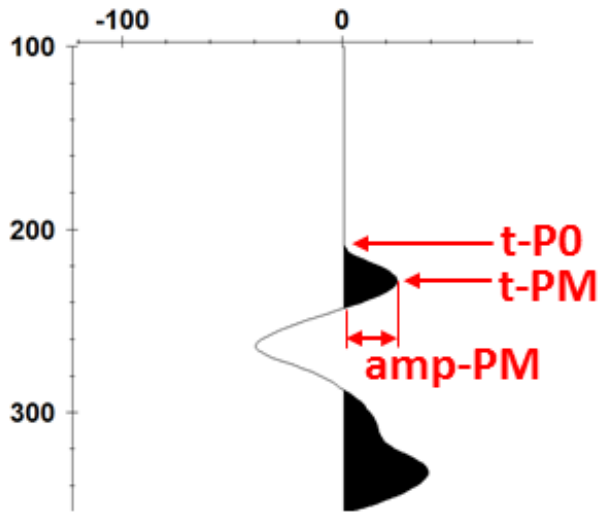

Fig. 4.2 Part of a seismic trace with derives attributes (first trace from the section displayed in Fig. 2.2, only pre-trigger time subtracted).

The following characteristic signal attributes are determined from the traces. The analyses, especially phase correlations and time picking of relevant phases, have to be made manually, because an automatic processing would not be precise enough. This is a time consuming part of the analyses.

- t-P0: travel time of first arrival P-wave onset (us)
- t-PM: time of amplitude maximum of P-wave first arrival phase (µs)
- amp-PM: amplitude of maximum of P-wave first arrival phase (V)
- t0: source signal (start time, start of emitted source signal (µs), see Fig. 4.1)
- taM: source signal (time when max. amplitude of emitter signal is reached (µs), see Fig. 4.1)
- amp-taM: max. amplitude of source signal (V)

For further analyses the data are processed slightly in three steps:

- Subtraction of possible DC shifts
- Subtraction of pre trigger time
- Moderate filter, meanfilter

During the conversion process where the data are transformed from binary apparatus format to a PC-readable format all receiver data are corrected to a normalized peak amplitude value

of 100 V by taking different amplitudes of the source signal into account. This guarantees that all amplitudes of the received signals are directly comparable. The emitter start time is not affected by this processing step.

With the derived travel times (t) and the calculated distances (L) between piezoelectric emitters and receivers seismic P-wave velocities (v_p) are calculated (v_p = L / t) assuming straight ray propagation. To optimise the comparison all velocities are normalised to the values derived for day 1 of the measurements for each emitter – receiver combination. This characterises the start situation (initial stage). Furthermore, due to minor uncertainties in the distance estimation with a v_p normalisation an "over interpretation" of the absolute v_p-values is avoided. All absolute v_p values are lower than the values obtained in former own in-situ investigations outside the EDZ at comparable locations. But the relative differences between the derived absolute velocities for the three orientations are in line with the anisotropic structure of the OPA (v_p-normal < v_p-45° < v_p-parallel). The frequencies of the P-wave phases are in the range between 12 kHz and 20 kHz. Again, a part of the seismic section E01-R10 (see also Fig. 2.2) is shown in Figure 4.3 to emphasise in a simple and clear way, together with the derived parameters listed in Table 4.1, the variation of derived seismic parameters from the first arrival P-wave phase (around 200 µs).

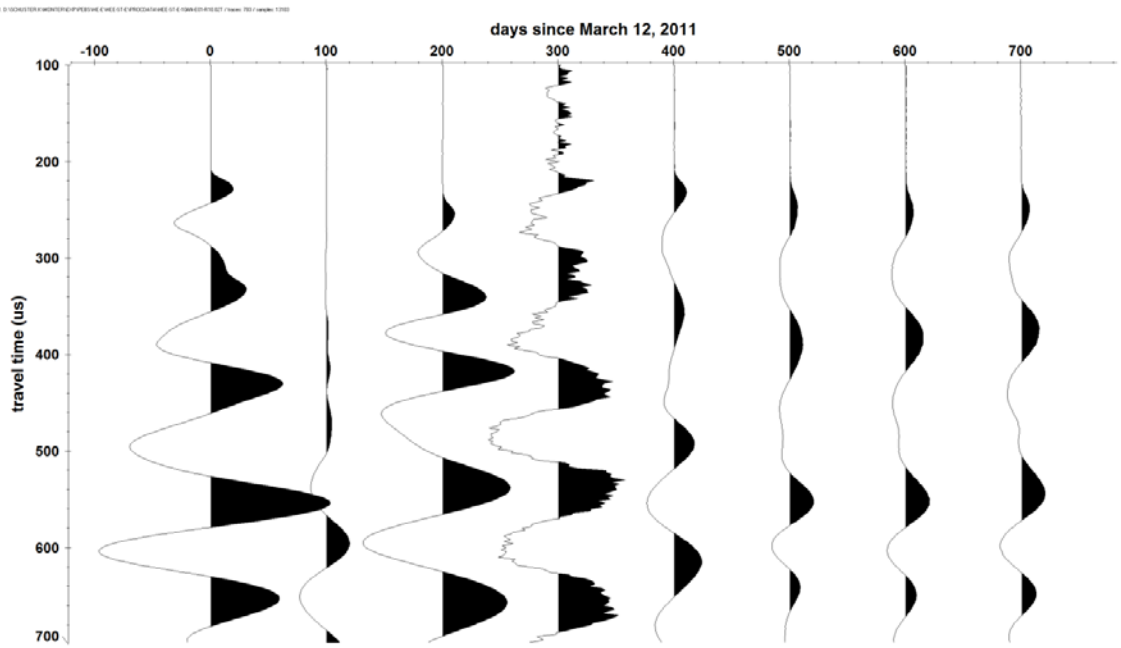

Fig. 4.3 Ensemble normalised part of seismic section E01-R10, only every 100th trace is plotted (see also Fig. 2.2). A clear variation of seismic P-wave phases is visible.

Exemplarily, the derived parameters from first arrival phases (P-wave phases) are compiled in Table 4.1. Later phases are difficult to distinguish due to the relatively short emitter – receiver distances what leads to interference of reverberating P-wave phases with possible S-wave phase onsets. Therefore we concentrate on P-wave phases.

Tab. 4.1 Seismic P-wave parameters at different days derived from emitter – receiver combination E01-R10 (see Fig. 4.3).

	travel time	Distance L	v_p	norm v_p	Norm Amp	App. Freq.
day	µs	m	m/s	-	-	(kHz)
1	206.000	0.485	2355.39	1.000	1.000	11.36
100	272.147	0.485	1782.97	0.757	-0.03	not clear
200	224.558	0.485	2160.81	0.917	0.775	10.66
300	205.500	0.485	2361.22	1.002	1.126	14.18
400	205.776	0.485	2358.05	1.001	0.56	9.53
500	218.143	0.485	2224.36	0.944	0.327	8.37
600	217.726	0.485	2228.63	0.946	0.341	6.77
700	221.739	0.485	2188.29	0.929	0.343	9.25

4.2 Uncertainties – error estimation

Concerning the uncertainties we have to distinguish between technical failures, identification and correlation of seismic phases, picking of travel times as well as other signal attributes and geometrical parameters. The start time is important. It is controlled manually and found to be sufficiently good (see section 4.1 and 5.1). Travel time picking is more challenging, but due to the very good quality of P-wave arrivals the first arrival picks (t-P0) can be determined with an uncertainty better than ± 0.5 µs for most of the traces. Only in cases where the attenuation is very strong the uncertainty goes up to values around ± 2 µs. In Figure 4.4 an example of first arrival phase picks is given, where the pick accuracy is rather ± 0.5 µs. When we consider an error in time of ± 2 µs it would result in a dv_p of 21 m/s for L = 0.5 m and a v_p of 2300 m/s. For the normalized v_p it would be ± 0.9 %. Amplitudes were corrected during the conversion process as described in section 5.1.

Furthermore, we have to mention that all the processing is done by one person, the author, and therefore the ineluctable errors should be similar (“constant shift”).

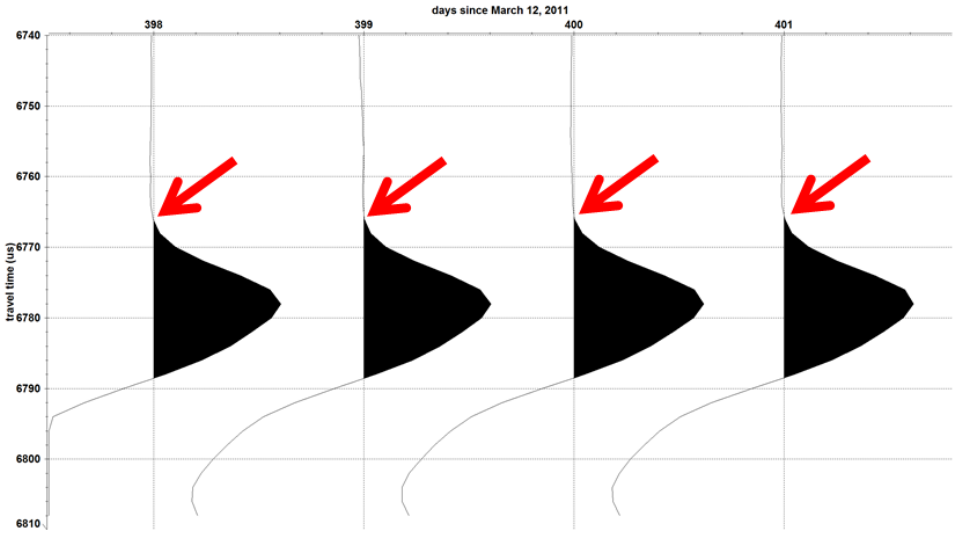

Fig. 4.4 Examples of first arrival picks for the emitter–receiver pair E03-R02, 20 cm from the S/B-OPA interface. Picks are marked with red arrows. The time between two gridlines is 10 µs.

The distance is less important because for most of the interpretations and related plots a v_p - normalisation was chosen, what allows a clear time depending assessment of the variations. Exact orientation of propagation paths towards bedding could only be assessed very roughly and for convenience reasons grouped into three groups (normal, parallel and 45°).

5 Data

The automatic daily measurement between all emitter – receiver combinations results in 50 different ray paths. The regular measuring phase started on March 12th, 2011 with one measurement phase every night at about 1 o'clock am. During this measuring phase of approximately 50 minutes the ten seismic receivers record successively seismic signals emitted by the five emitters. Each recording is repeated 2048 times in order to improve the signal to noise ratio. In total 50 different seismic traces are recorded every night. From these data, seismic parameters are derived for further interpretation. In this stage the focus is on the P-wave arrival phases. More data can be analysed in a later stage.

5.1 Source signal data

The start time t0 describes the moment of emission of the seismic signal into the rock. It is derived from the signal sent from the signal generator to the emitter transducers. In Figure 5.1 (left) the emitter signal for emitter E01 as generated at day 1 is displayed in full. The source signal is characterized by a continuous and slow build-up of voltage over approximately 5000 µs and a sudden release at a defined time which generates the mechanical impulse in the piezoelectric transducer. As a consequence the seismic wave field is emitted and can be received at all 10 piezoelectric receivers. On the right side in Figure 5.1 the maximum amplitude (amp-taM) and the time which is used as start time (t0) are marked in the zoom-in display (60 µs) for day 1 and for several other days. Please note that the difference between taM and t0 is only 4 µs what corresponds to two sample steps.

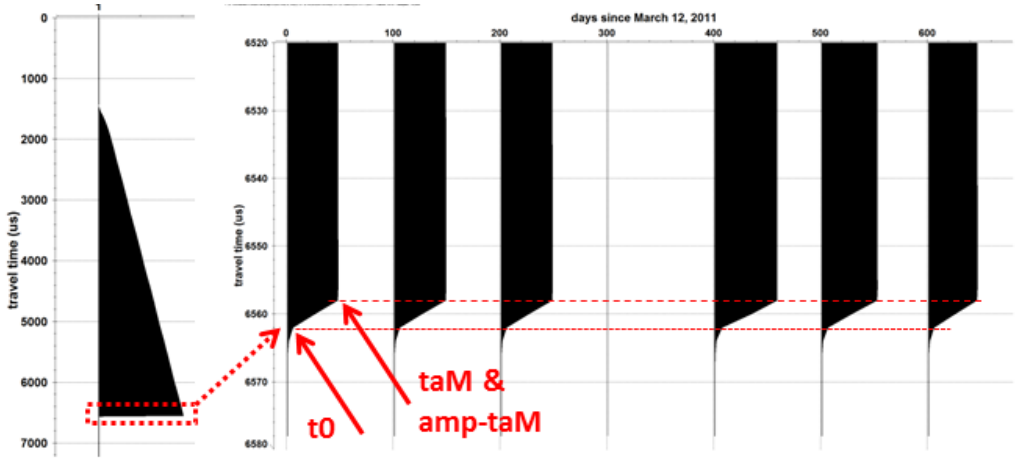

Fig. 5.1 Seismic traces with are generated in the signal generator and used for the excitation of the piezoelectric signal transducers (emitters).

In order to emphasize that the start time for the emission of seismic pulses are well controlled and nearly constant over the time in Figure 5.2 a selection of the five emitter signals are displayed. A clear bisection can be seen, until day 300 and beyond day 350. Until day 300 the build-up of the signal amplitude starts around 1480 µs and continuous gradually until 6558 µs (see also Fig. 5.1), where the maximum amplitude is reached (circa 94 V). Then, within 4 µs the amplitude drop to circa 10 V (6562 µs). This is the time we are taking as the start time (t0) for emitting the seismic pulse. After another 2 µs the amplitude is nearly zero. The signal generator broke at day 300 (January 6, 2012) and was replaced (see next section). The continuous monitoring mode was reestablished at day 348 (February 22, 2012). From day 350 on the start point of the build-up of the emitter signal lies outside the recording window. This is not of interest. Important for the velocity calculations is the fact,

that the decline of the ramp like signal behaves in the same way as discussed before. This is the case at all days. For the five emitters only the amplitudes of the exciting signals vary with different intensities and gradients. An amplitude correction is applied during the conversion process as discussed in section 5.4.

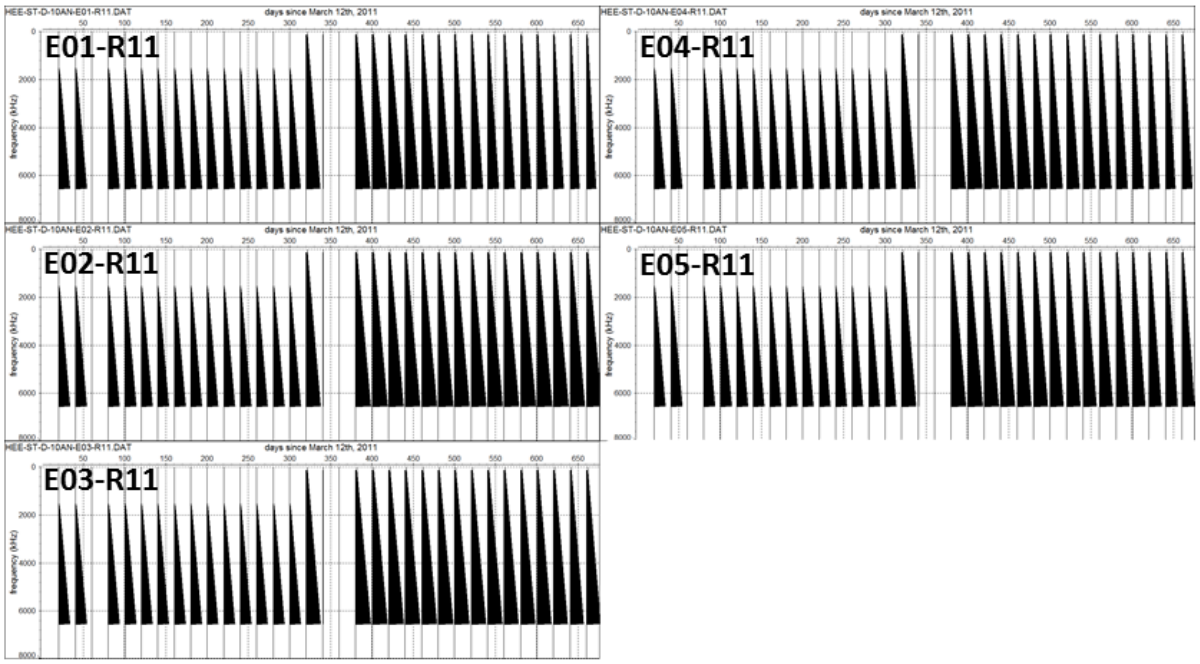

Fig. 5.2 Compilation of signals recorded for the five emitters (E01 – E05) which are generated in the signal generator and used for the excitation of the piezoelectric signal transducers (emitters). Every 20th record is plotted (days 1 – 670).

5.2 Data from S/B

As an example a seismic section where the emitter-receiver pair is located in the S/B material is shown in Figure 5.3 covering the time March 12, 2011 (day 1) until September 14, 2012 (day 553). Only every second trace is plotted in order to get a clearer visualisation. Some recordings are defective, for example around day 310. The section is ensemble normalized what enables a direct comparison of amplitudes along the section. Seismic traces for emitter E02 (B) and receiver 1 (R01), both located in the S/B at 5 cm and 10 cm distance from the interface S/B-OPA, are shown (cf. Figure 10). A correlative wave phases are highlighted. Between day 1 and day 51 no seismic signals can be correlated because no

buffer material was emplaced and consequently no seismic energy could propagate properly. Instead, as a side effect, we observe the arrival of an air wave which is propagated with a velocity of circa 330 m/s.

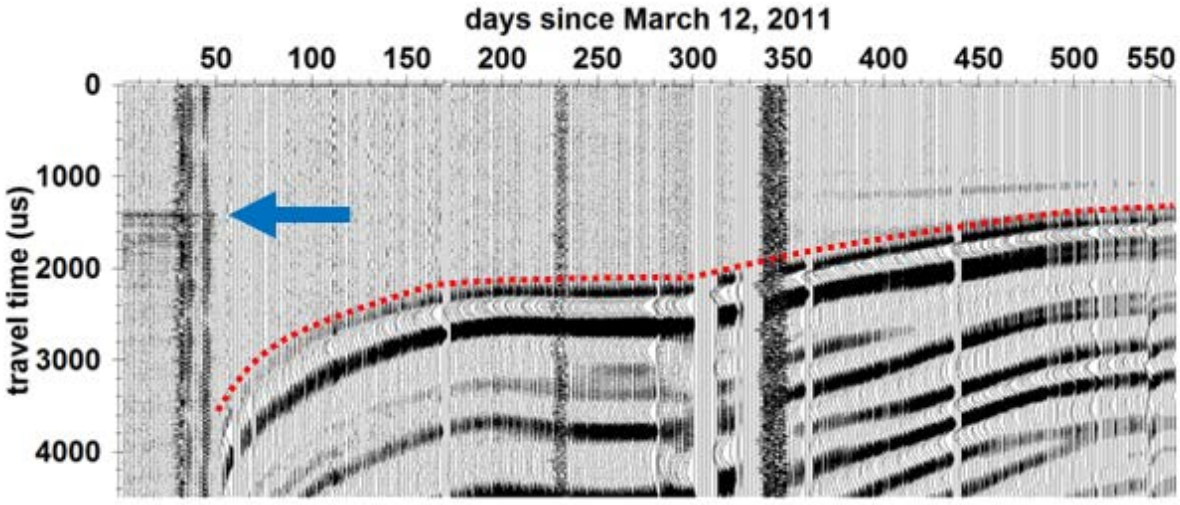

Fig. 5.3 Seismic section from the S/B material. Recording between emitter E02 and receiver R01, both located in the S/B at distances of 5 cm and 10 cm from the interface S/B-OPA. Only every 2nd trace is plotted.

The emplacement of the sand-bentonite mixture started on day 52. Starting from this day the seismic signals become stronger and seismic P-wave phases can be correlated clearly. A decrease of travel times corresponds to an increase in P-wave velocity (v_p). This process continues until day 180 followed by nearly constant values until day 300. Then travel times decrease in two different steps, between day 300 and day 500 with a higher gradient as between day 500 and 553. The corresponding v graph is shown in Figure 6.11.

The second emitter – receiver combination where both transducers are located in the S/B is displayed in Figure 5.4. In this case emitter E02 and receiver R05 are both located at 5 cm distance from the interface S/B-OPA. Data are plotted in a point mode with colour coded amplitudes which allows to rate the variation of the amplitude evolution in an easier way. The amplitude variations are given in voltage (V). The red arrows indicate the dates for the emplacement of the sand-bentonite mixture (day 52) and the day where a power failure occured (day 538). The heaters were without power for about 14 hours. The later incident shows that interrupting the heating results immediately in a change of the seismic signals what on the other hand indicates that the seismic wave field was influenced by temporal changes in the S/B material. It punctuates furthermore the sensitivity of the seismic

transmission method to small changes in rock parameters. Both discussed incidents can also be seen in Fig. 5.3.

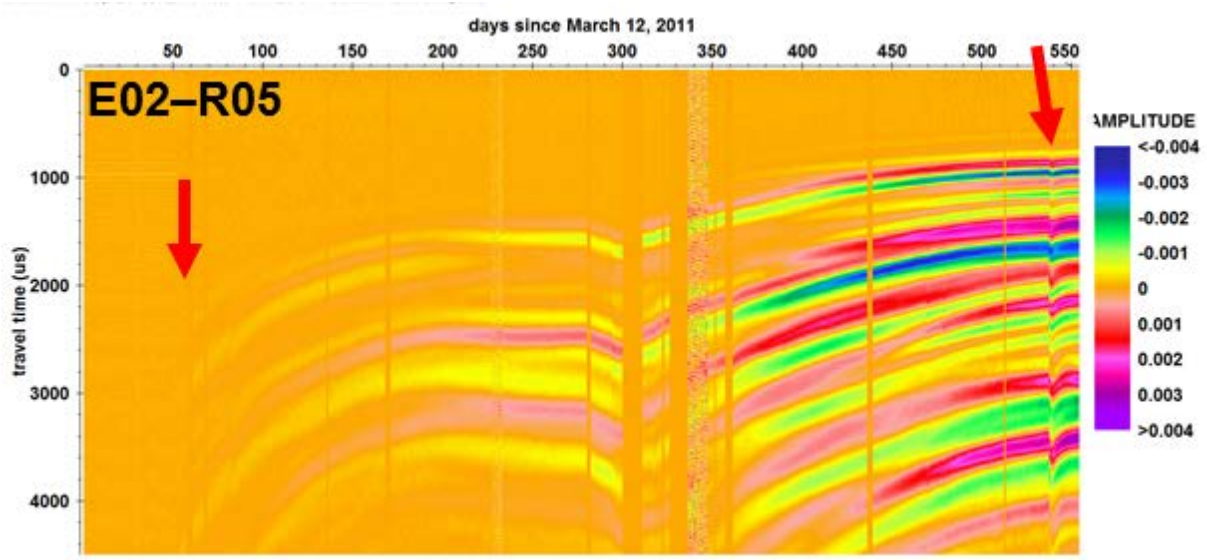

Fig. 5.4 Seismic section from the S/B material. Recording between emitter E02 and receiver R05, both located in the S/B at a distance of 5 cm from the interface S/B-OPA. Ensemble normalized display with colour coded amplitudes.

A closer analysis of seismic traces recorded in the S/B material around day 550 allowed a rough estimation of the absolute P- and S-wave velocity. The estimation is a bit uncertain, but the values are comprehensible.

The following values were derived:

	v_p (m/s)	v_s (m/s)	v_p / vs
E02 (5cm) – R01 (5cm)	585	340	1.72
E02 (5cm) – R05 (10cm)	490	375	1.31

5.3 Data from OPA

In this section exemplarily for one emitter–receiver combination (E01-R10) different plots are presented which allows to assess the evolution of seismic parameters derived in the OPA in a qualitative way. Figure 5.5 shows the seismic section for ray path running in the OPA approximately at 45° towards the bedding at a distance of 10 cm from the interface S/B-OPA

(cf. Fig. 3.2). The P-wave arrivals can be identified very clearly at around 210 µs (day 1). The pronounced variation of these first arrival phases (travel time and amplitude) with time is a clear indication for changes of petrophysical properties of the OPA along the travel path. Around day 25 the travel times start to increase (v_p drops) and the strength of amplitudes drops. During that time the installation work and the emplacement of EBS in the rear section of the tunnel started what was combined with an intensive ventilation of the section. The test section was closed at day 53. The heater elements were switched on at day 109. From day 130 on the amplitudes start to become stronger and v_p increases. Around day 300 travel times and amplitudes are very close to the starting situation. At day 350 travel times start to increase again (v_p drops). This process continues till the end of the actual observation phase. The P-wave phases change in the same time towards a lower frequency-content ("broader signal") and lower amplitudes (not visible in this data representation). This could be an indication for an increase in saturation of the OPA. The appropriate derived and normalised seismic P-wave velocities are plotted in Figure 6.13.

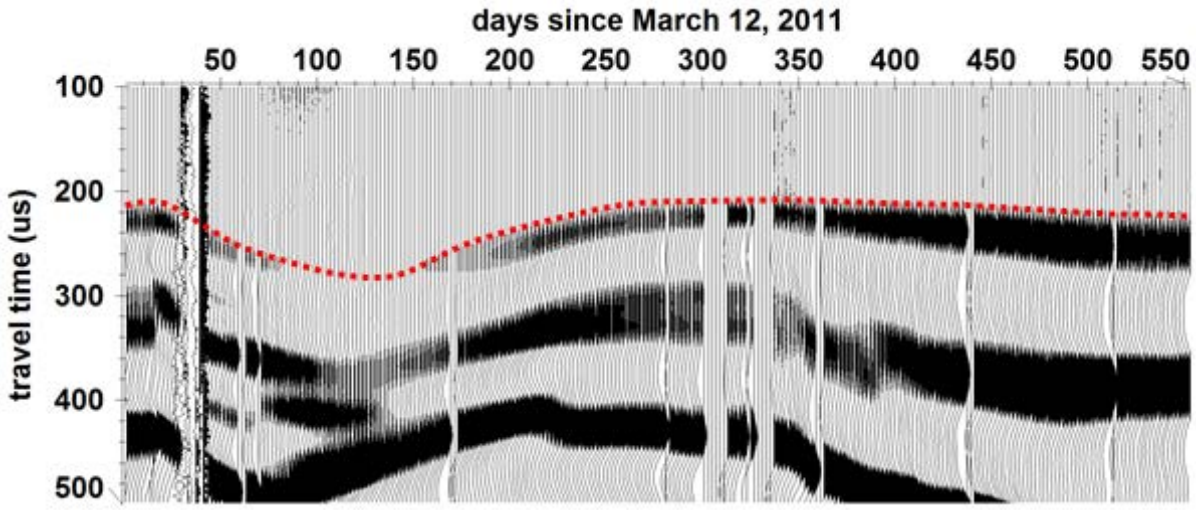

Fig. 5.5 Seismic section recorded in the OPA between emitter E01 and receiver R10, both located in the OPA at a distance of 10 cm from the interface S/B-OPA. Trace normalized, only every 2nd trace is plotted.

Figure 5.6 shows the same data set in a point mode plot with colour coded amplitudes and as an ensemble normalised section what allows a better assessment of the dynamic evolution of the scanned rock mass. For example we see around day 100 that nearly the entire seismic signal energy dropped to very low values compared with the start phase and the time around day 260. From day 280 on a slight decay in signal strength starts.

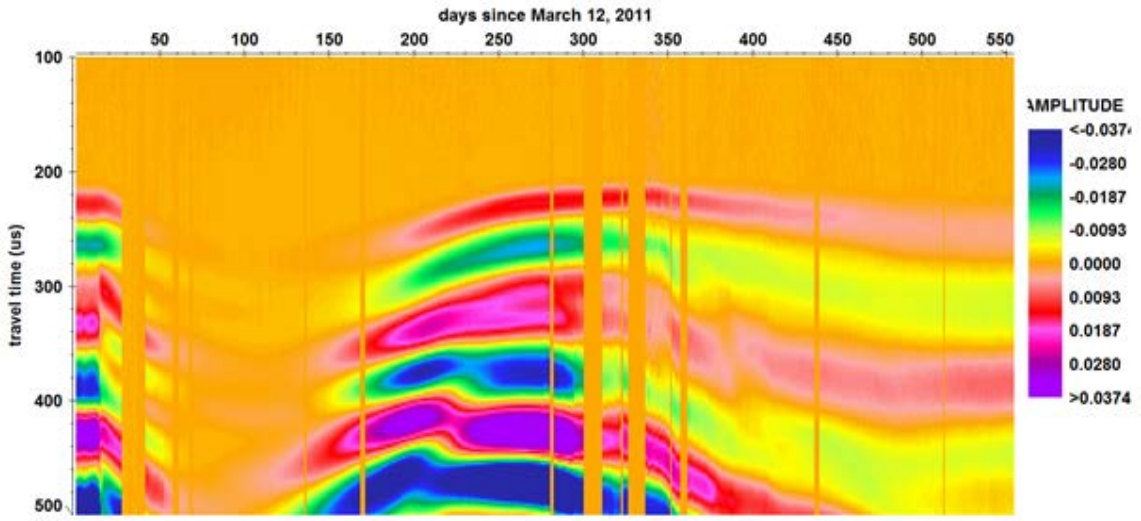

Fig. 5.6 Same data as in Fig. 5.5 (E01-R10) but with colour coded amplitudes. Ensemble normalized display.

In the following Figure 5.7 the frequency content of each seismic trace was calculated and all frequency trace spectra are displayed in a colour coded plot. Such plots show the variability of the shape of the seismic signals in a quantitative manner whereas a rather qualitative impression can be obtained already in the wiggle mode display in Figure 5.5. Until day 280 a broad range between 6 kHz and 12 kHz dominates the plot and between days 170 and 280 even frequencies up to 17 kHz are significant. From day 280 on the main frequency content moves towards lower values. Although the band between 1 kHz and 2 kHz is already present from the beginning it develops and appears to be stronger towards day 553.

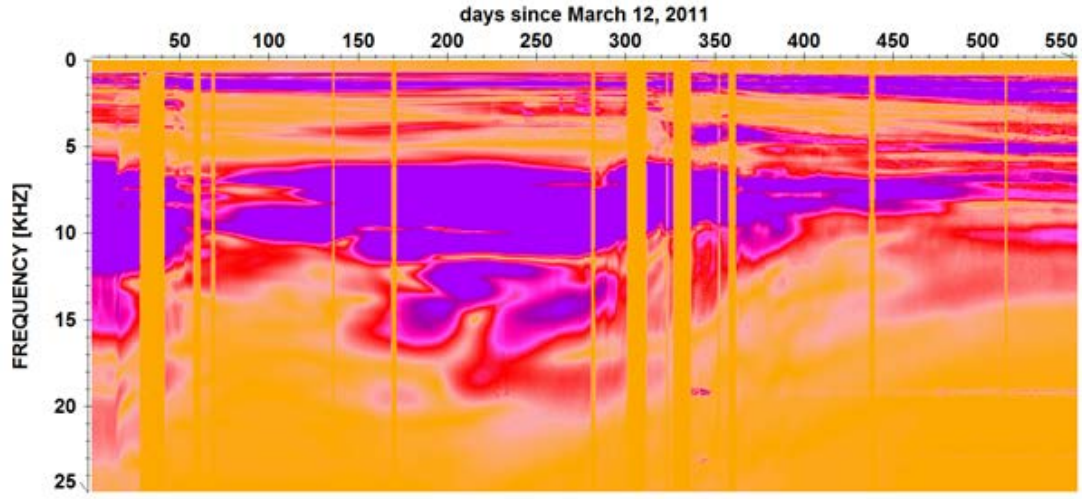

Fig. 5.7 Frequency content of the data set displayed in Fig. 5.5 (E01-R10). Ensemble normalized display with colour coded amplitudes.

The total variability of seismic signals is shown exemplarily for one emitter (E01) and nine related receivers in Figure 5.8 as trace normalised wiggle plots. The same compilation of data but displayed in an ensemble normalised version and with colour coded amplitudes is displayed in Figure 5.9. The appropriate receiver numbers can be found in each sub plot in the top line, for example: HEE-ST-D-10AN-E01-R01.03T, for the emitter-receiver pair. E01-R01. All fifty seismic sections are compiled in Appendix I.

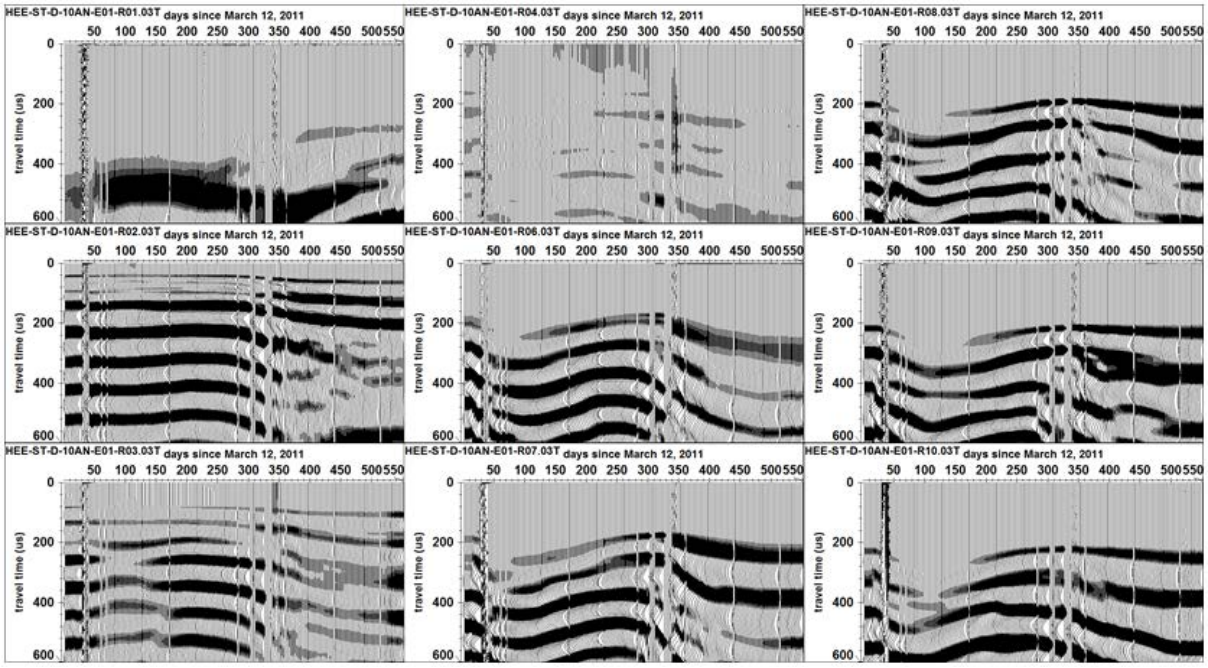

Fig. 5.8 Compilation of seismic sections belonging to emitter (E01) and nine receivers (R01- R10, without R05). All sections are trace normalized.

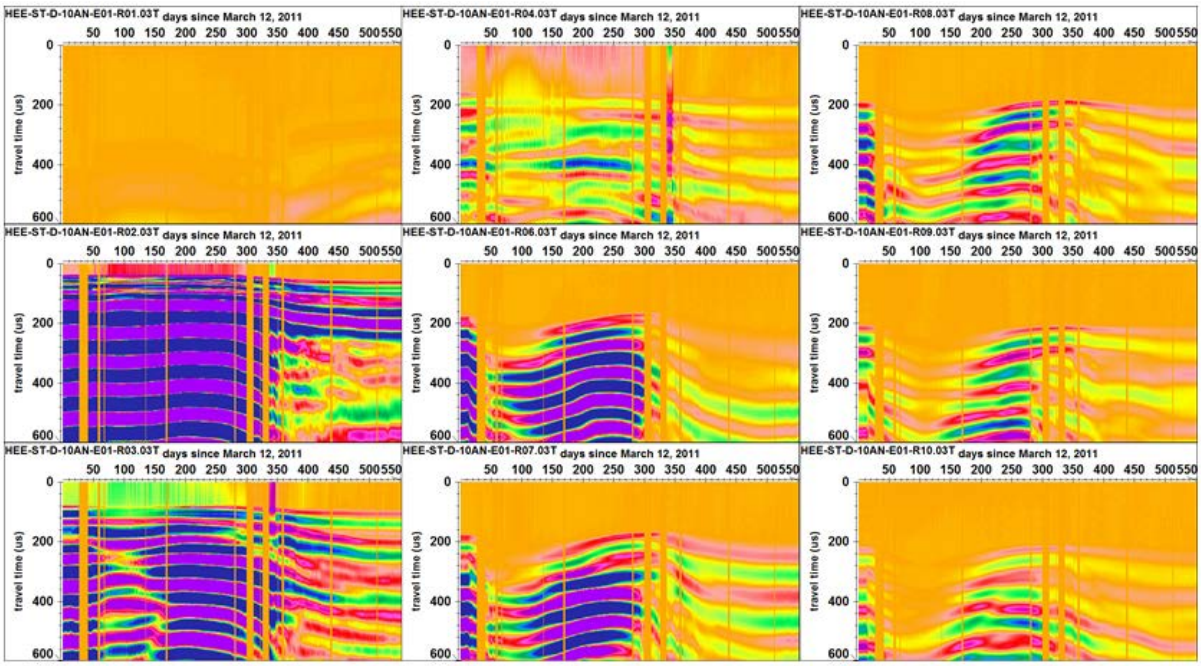

Fig. 5.9 Same data set (E01-RNN) as in Fig. 5.8 but the total display is ensemble normalized and amplitudes are colour coded.

Seismic trace plots from different distances, from 5 cm to 45 cm, for example see Figure 5.10 in the next section, show a clear qualitative trend: the further the travel paths from the S/B-OPA interface the less the P-wave phase variation is distinctive. This holds for travel times, frequencies and amplitudes of first arrival phases.

The propagation paths for some emitter – receiver combinations cross the interface S/B-OPA, for example E01 → R01 (OPA → S/B). In such cases the interpretation becomes more complicate (see section 5.5).

5.4 Dependency of seismic parameters from distance to the interface S/B - OPA

Figure 5.10 shows qualitatively how diverse the seismic wave field is affected by the EDZ / EdZ. A strong dependency from the distance of the interface S/B-OPA is obvious. The area near the interface S/B-OPA seems to be more affected what can be clearly seen by travel times increase, amplitude are becoming weaker and the shape of the first arrival phases change. This is in good accordance with features which are characterizing the degree and the extent of an EDZ. See also section 6.1 (EDZ relevant parameters).

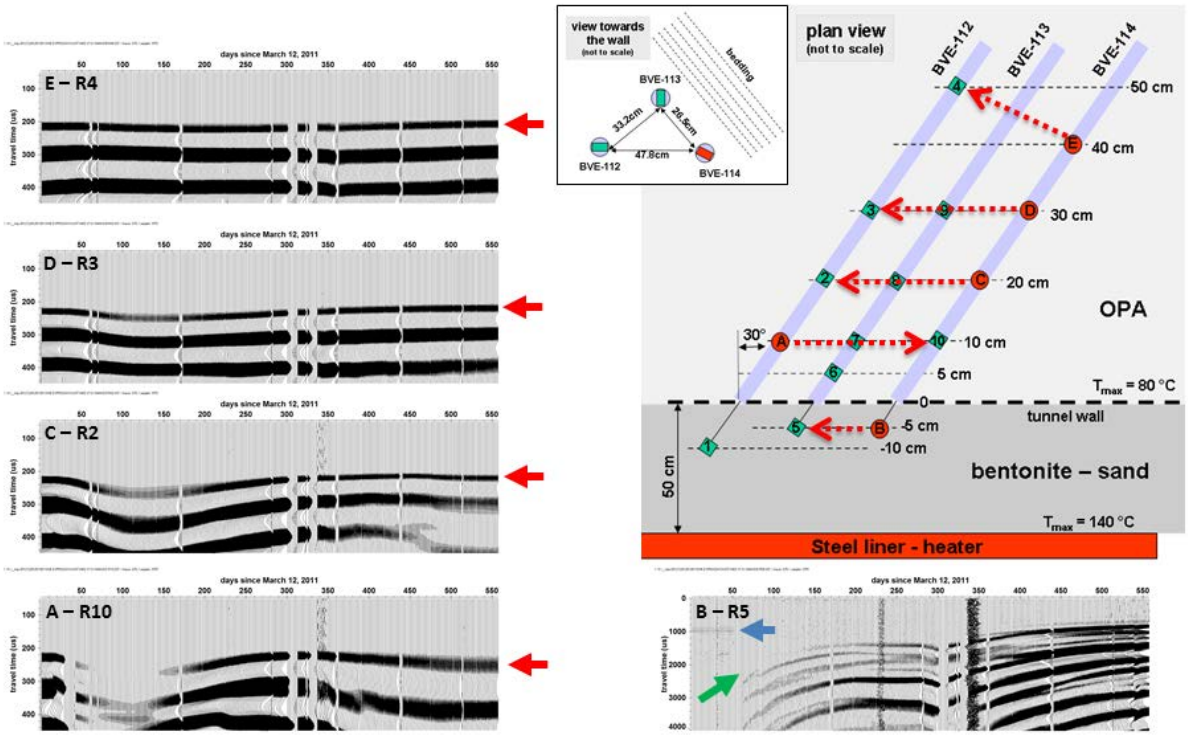

Fig. 5.10 Seismic sections representing different distances of the propagation paths of the seismic wave field from the interface S/B-OPA. Trace normalized display, only every 2nd trace plotted.

5.5 Temporal technical problem

A technical problem occurred on January 5, 2012 (day 300) when the signal generator which is responsible for generating the voltage for the five emitter transducers failed. It was replaced on January 17, 2012 (day 312) followed by several tests and adjustments until February 24, 2012 (day 350) before the system was set back to the continuous daily recording mode. The signal generator is located outside, circa 35 m away from the experimental side, placed in the computer cabinet in the MI-niche. As a result of this change the peak voltage of the signal generator was set from 96 V (until day 300) to 124 V (during the test phase) to 130 V (from day 350 on). In section 4.1 and 5.1 the emitter voltage characteristic (ramp like signal) was discussed detailed. Figure 5.10 show the peak voltage (amplitude) for each day as used at the five emitter transducers. Until day 300 the amplitudes are relatively constant, only a slight decrease is visible. Between days 312 and 320 (test phase) and more pronounced from day 350 on the amplitudes start to scatter and to decrease continuously. The peak amplitudes drop from 130 V at day 350 to 58 V at day 850 for emitter E03 (C), and to 98 V for emitter E05 (D). Ostentatiously for emitter E02 (B) which

is located directly in the S/B material amplitudes stay constant around 130 V, they even increase slightly.

The reason for this is unclear until now, although a lot of checks and tests were done. One explanation could be that the coax cables came under mechanical pressure inside the boreholes what could change the electrical impedance (Fischer/Philipp, 2012, pers. commun.) and finally the voltage amplitude. Another reason could be that free water or moisture affects the contacts at the piezoelectric transducers what similarly could change the electrical impedance with comparable consequences.

As explained in section 5.1 the moment for emitting the signal (t0) is not influenced by this decrease of peak voltage. This time stays stable over the total monitoring time. This means, that also the derived velocities are not affected by the emitter amplitude decrease. The situation is different for the received amplitudes. In order to allow a comparison of the amplitudes over the total time of observation they have to be corrected. During the conversion process where the data are transformed from binary apparatus format to a PC-readable format all amplitudes are normalized by taking different amplitudes of the source signal into account. All amplitudes are corrected to a normalised emitter output peak voltage of 100 V. This guarantees that all amplitudes of the received signals are directly comparable. As mentioned before, the emitter start time is not affected by this processing step. In spite of the steep gradients of the output voltage until day 550 all peak amplitudes stay above the initially applied 96 V.

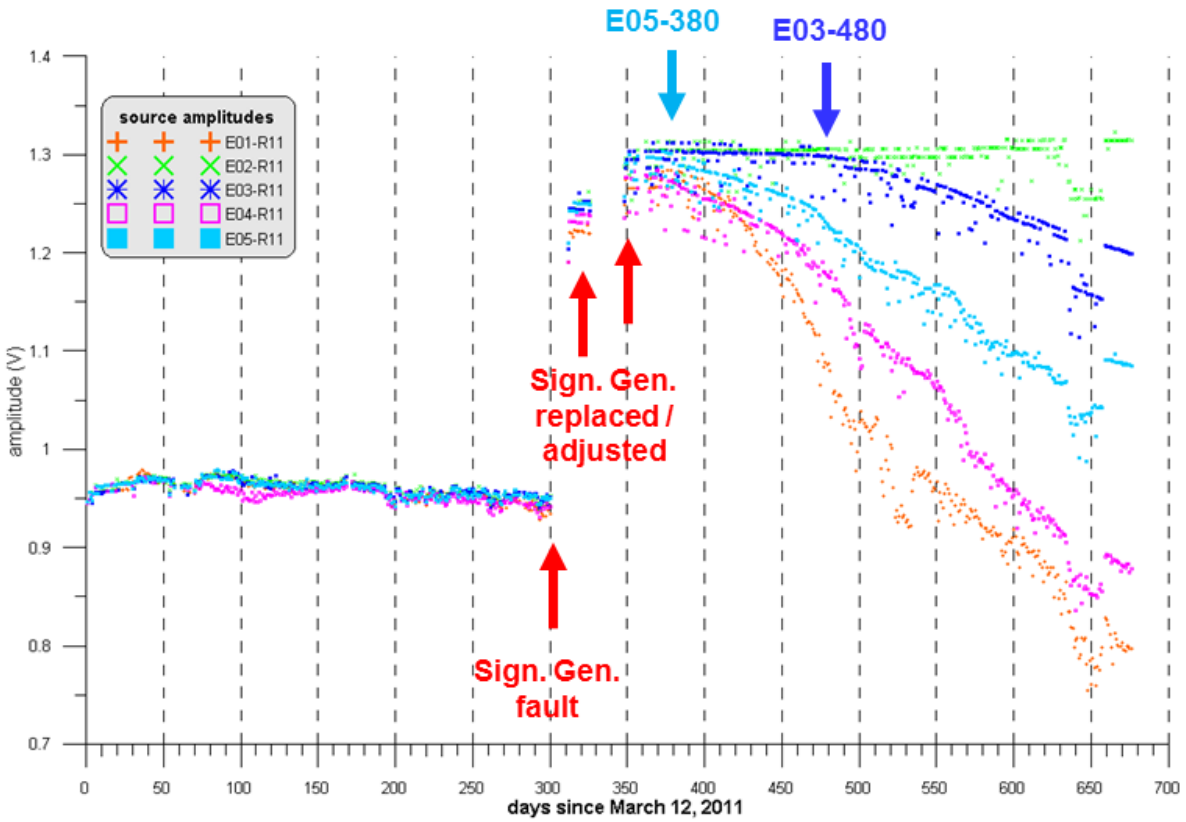

Fig. 5.11 Maximum voltage of emitter signals. Please note that displayed voltage has to be multiplied by 100.

After day 350 the peak amplitudes start to decrease at different times and also the gradient of decrease is different. Some peak voltage amplitudes drop faster than others, for example E01 peak voltage starts earlier to decrease and drops faster than E03 voltage.

Due to this distinct differentiation in start time of peak voltage decrease and also of the different gradients of decrease we proposed several criteria in order to extract a possible trend which could correlate with the distance of emitter-receiver pairs from the S/B-OPA interface. Such an indication could give hints of a propagating vapor front or a “stress redistribution front”. The following criteria are proposed:

- (1) Moment of beginning of peak voltage decrease (day)
- (2) Moment when peak voltage drop by 10 V from the former plateau (day)
- (3) Slope of decrease (arctan)

As can be seen in Figure 5.11 a clear trend can only be accepted for criteria (2) and (3) if the values for emitter C (E03) at a distance of 30 cm from the S/B-OPA interface are neglected or treated separately.

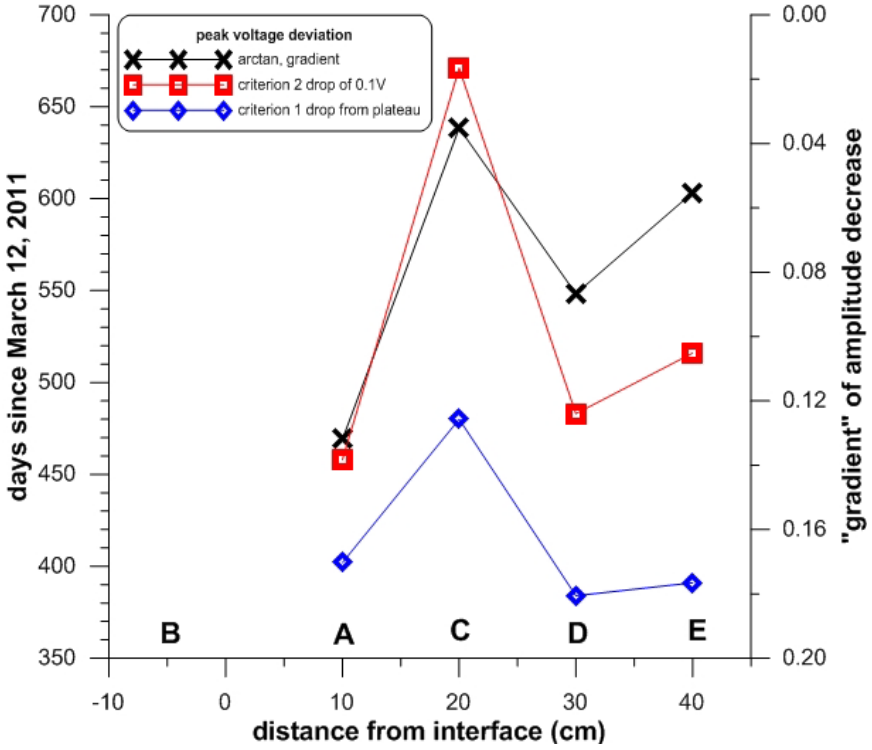

Fig. 5.12 Criteria applied to the emitter peak voltage data as displayed in Fig. 5.11. The explanation is given in the text.

Exemplarily for emitter E03 (C) in Figure 5.13 the decay of the peak voltage (black dots) is plotted together with all corrected receiver amplitudes (coloured dots). In spite of the decay of the emitter amplitude most of the receiver amplitudes increase, stay constant or decay only slightly. It seems that the driving force for this behavior is related to developments in the OPA itself.

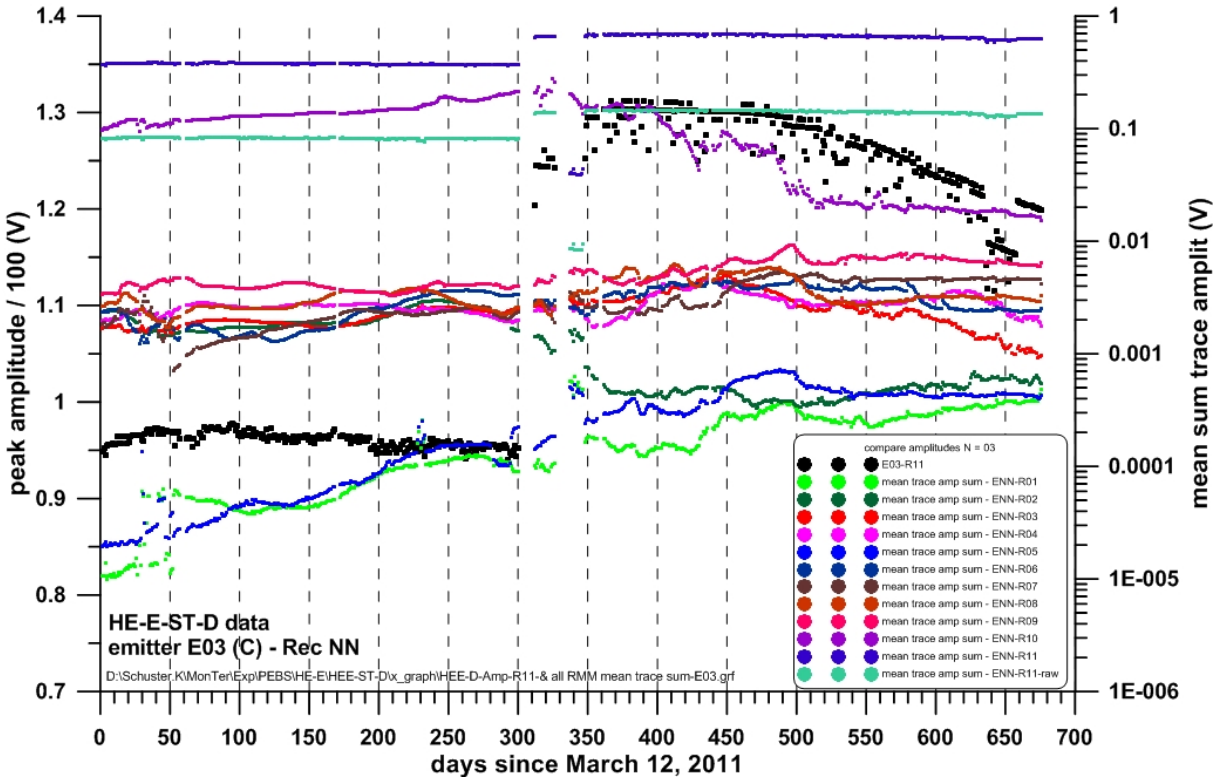

Fig. 5.13 Decrease of emitter peak amplitude (left Y-axis and black dots) and evolution of all receiver amplitudes (right Y-axis). For this calculation the arithmetic mean of the sum of amplitudes for each trace was taken into account.

In Figure 5.14 for the emitter-receiver pairs E01(A)-R06&R07 and E02(B)-R06&R07 seismic traces and peak amplitudes of emitters are plotted for days 220 to 480. This time window was chosen in order to discuss a possible influence of the exchange of the signal generator and the higher peak voltage used from day 350 on for the emitters.

In the upper part data from the OPA are displayed (E01(A)-R06&R07). In the seismic sections already from day 280 on a very slight increase of travel times seems to start, twenty days before the signal generator failed. Although the emitter voltage was increased the P-wave receiver amplitudes decrease continuously in combination with an increase of travel times. In the lower part of Fig. 5.14 data are displayed where the seismic signals crossing from the S/B material (emitter E02) to the OPA, to receiver R06 at 5 cm from the interface and to receiver R07 at 10 cm from the interface. Here we also observe from day 280 on continuously increasing travel times until day 350 followed by a continuous decrease combined with a pronounced strengthening of amplitudes. The reason for that is most probably that the consolidation process in the S/B starts from day 300 on with a very high

rate. In Figure 6.11 the derived normalised velocity stays constant between day 200 and 300 and increases very rapidly from day 300 on.

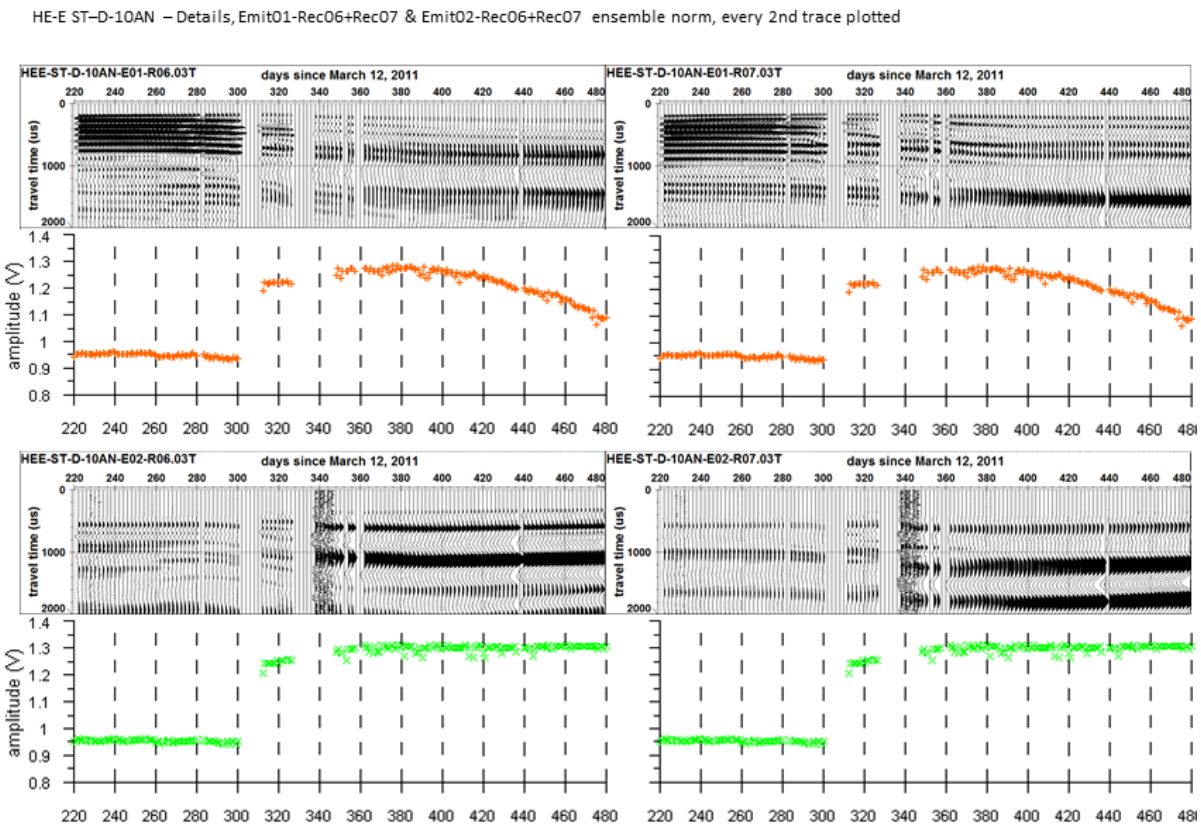

Fig. 5.14 For the emitter-receiver pairs E01(A)-R06&R07 (top) and E02(B)-R06&R07 (below) seismic traces and peak amplitudes of emitters are plotted for days 220 to 480. Only every 2nd trace is plotted.

In order to assess the evolution of the frequency content of the same data sets each trace was transformed to a trace spectrum and all spectra were combined in appropriate ensemble normalized sections (see Fig. 5.15). For the sections related to the OPA (upper part) a continuous evolution towards lower frequencies can be seen. For the data which cross from S/B to OPA (lower part) a contrary development is visible. The frequency content tends towards higher frequencies, more pronounced for the shorter distance (R06 at 5 cm from the interface). As discussed before, the second stage of a rapid consolidation of the S/B starting at day 300 (see Fig. 6.11) could be the reason.

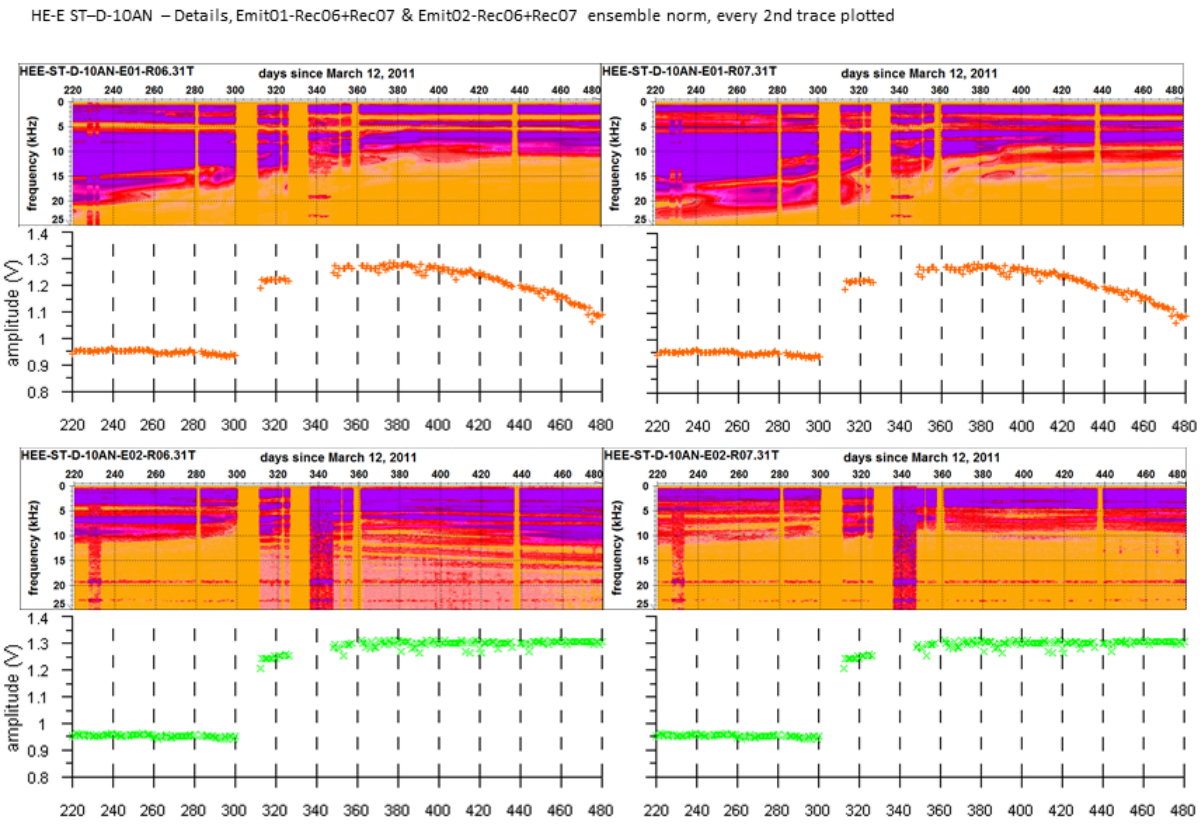

Fig. 5.15 Same data sets as plotted in Fig 5.14 but transformed to seismic trace spectra in order to show the evolution of the frequency content of the entire sections (E01(A)-R06&R07 (top) and E02(B)-R06&R07 (below), again with peak amplitudes of emitters for days 220 to 480. Data are ensemble normalized.

We can conclude, that the changes between day 300 and day 350 are most probably not related to technical reasons (exchange of signal generator and increased emitter peak voltage), because the trend in change of signal characteristics (travel times, amplitudes and frequency contents) starts already around day 280, twenty days before the technical failure.

6 Results

The recorded data were processed and analysed as described in chapter 4. Additionally, due to the temporal technical problem (see section 5.5) all receiver amplitudes were corrected. All emitter peak amplitudes were normalized during the conversion process to a value of

100 V. Seismic parameters like P-wave velocities, attenuation of P-waves (amplitudes) and apparent frequencies of first arrival phases were derived. Furthermore, the recordings were classified according to their travel paths. In total 50 different propagation paths can be extracted. We differentiate between recordings in the S/B material and in the OPA, whereat for the latter we separate the travel paths along the borehole wall from the more important data which describe the scans within the OPA. Taking the pronounced anisotropy of the OPA into account we differentiate three propagation paths for the seismic wave field towards the bedding, parallel, normal and circa 45°. The three orientations towards the bedding are only rough estimates. Finally, some of the propagation paths are mixed, for instance signals excited in the OPA and recorded in the S/B or vice versa. A different evolution of seismic parameters was expected in these groups. In order to guarantee a better comparability of all results the derived parameters are presented in most of the cases normalized. Values at day 1 of the recording was chosen as the reference value (= 1.0).

We classified the data into the following main groups:

- Propagation paths in the S/B material
- Travel paths in the OPA, 45° to bedding
- Travel paths in the OPA, normal to bedding
- Travel paths in the OPA, parallel to bedding
- Travel paths in the OPA, along the borehole wall

Due to the huge amount of records not all data could be analysed until now in detail. For a part of the data only a plausibility test was made. These tests showed that the evolution of seismic parameters like travel time (resulting in v_p) and amplitudes are comparable to the results obtained for the data which were analysed more detailed and presented here. In general the trends in these groups are similar.

In order to rate the derived v_p we compare them in several cases with results obtained from former own investigations in the Mont Terri rock laboratory. For example, concerning the seismic anisotropy, we obtained in the EZ-B niche v_p -values in the range between 2200 m/s (normal to bedding) and 3500 m/s (parallel to bedding).

A rather qualitative explanation for the v_p variation can be given according to experiences gained at several own ultrasonic in-situ experiments at the Mont Terri Rock Laboratory. In general, a drop in v_p can be explained with a loosening of the rock and an increase of v_p with

a consolidation of the material. Loosening can be caused by the creation of micro cracks, even when they are macroscopically not visible, or an increase of porosity. The consolidation of the rock can be explained by swelling of the OPA (water uptake and sealing of micro cracks). Furthermore, a v_p increase can also be caused by an increase of saturation. A pore pressure variation can also influence the v_p. Interpretations concerning the influences of pore pressure and saturation in relation to signal and v_p variations mainly known from ultrasonic laboratory investigations on sandstones.

6.1 Related geotechnical data

Partly our results are compared with geotechnical data which were measured in parallel at nearby locations. In Figure 6.1 these locations are compiled and highlighted if they are relevant for the actual discussion. Many sensors were already used in the former VE experiment and were included in the actual HE-E project.

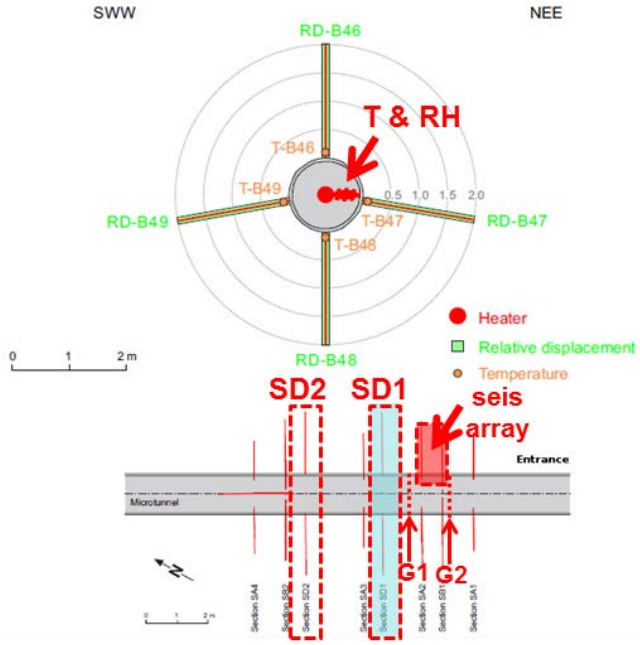

Fig. 6.1 Location of the relative displacement measurements, the seismic array and the T- and RH sensors along G1- and G2-section in the microtunnel (Garcià-Sineriz et al., 2005, modified).

The temperature (T) and the relative humidity (RH) are measured continuously within the experiment at different distances around the heater elements. Figure 6.2 shows the T- and RH- evolution exemplarily from section G1 (see Fig. 6.1) which is close to the seismic array.

at three distances in the S/B, close to the heater (blue symbols), in the middle (red symbols) and at the OPA, close to the S/B-OPA interface during the first 750 days. All three T-graphs start at circa 17 °C, stay constant and develop very similar after the heater was switched on (day 109). Of course, with steeper gradients and higher absolute values near the heater. The notches in the T-graphs (days 361, 538 and 683) originate from a malfunction (power blackout) of the heaters. An immediate response in several seismic sections can be observed, for example in Fig. 5.2.

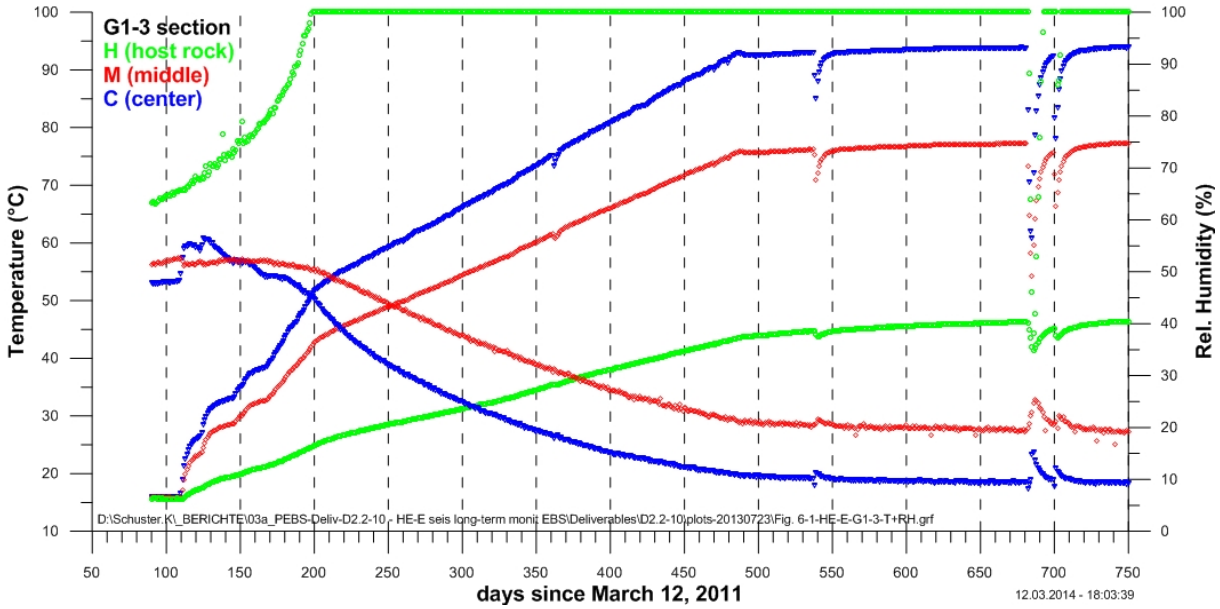

Fig. 6.2 Temperature and relative humidity evolution within the first 750 days in section G1 at 3 o'clock, orientation towards the seismic array. All three T-graphs start at circa 17 °C.

Thee RH-graphs seem to correlate very close with the T-evolution. The RH-graphs near the heater (blue symbols) drop from 50 % (day 80) to 10 % (day 750). The RH-graph related to sensor in the middle (red symbols) drops only to 20 % (day 750), whereas the RH-sensors at the OPA reach already at day 200, 90 days after the heater was switched on, a value of 100 %. We observe a gradual 'desaturation' of the inner part of the S/B and a quick and full saturation of the RH sensor at the interface. This supports the assumption that a vapor front is propagating towards the S/B-OPA interface. We assume furthermore, that this vapor front propagates further into the OPA.

That the temperature evolution is a driving force can be derived from the contrary development of the power failure related notches in the T- and RH graphs, for example at

day 683. A decrease in T leads to an immediate increase in RH, even at the interface, with astonishing amplitudes. T drops from 45 °C to 40 °C and the RH sensor responds with a drop from 100 % to 40 %.

The relative displacement evolutions displayed in Figure 6.3 and Figure 6.4 show that movements in the rock, close to the micro tunnel wall, in the order of 20 mm are observed. Both sections (SD1 and SD2) are close to the seismic array (see Fig. 6.1).

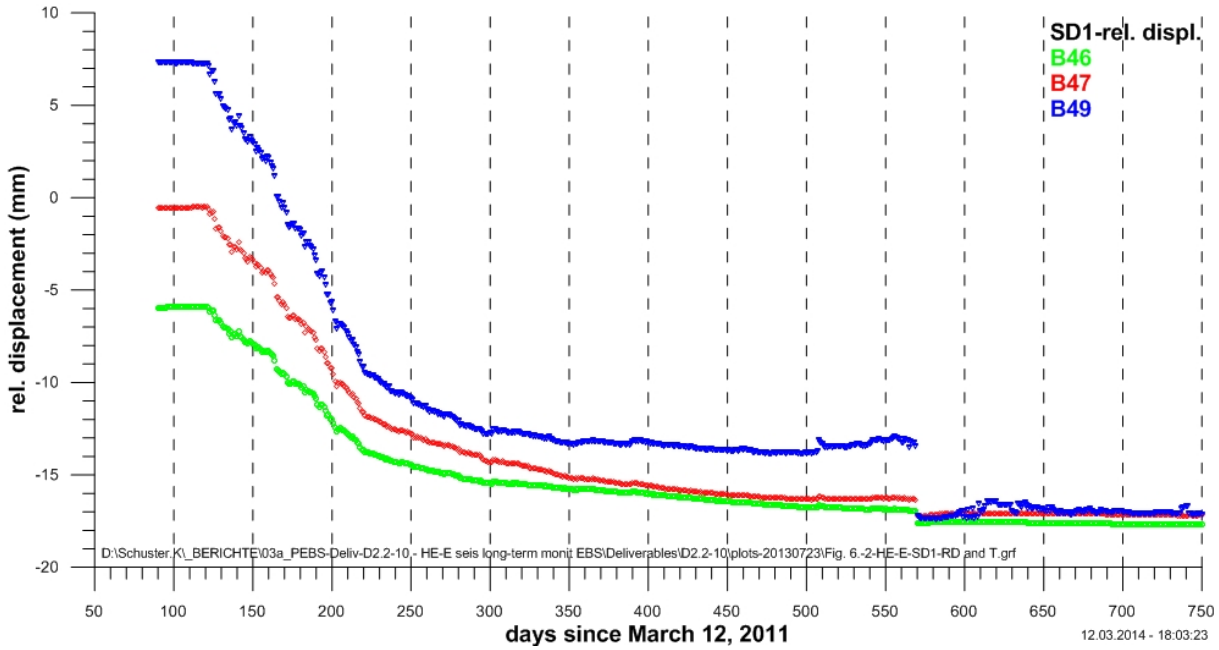

Fig. 6.3 Relative displacement evolution within the first 750 days in section SD1 (see Fig. 6.1).

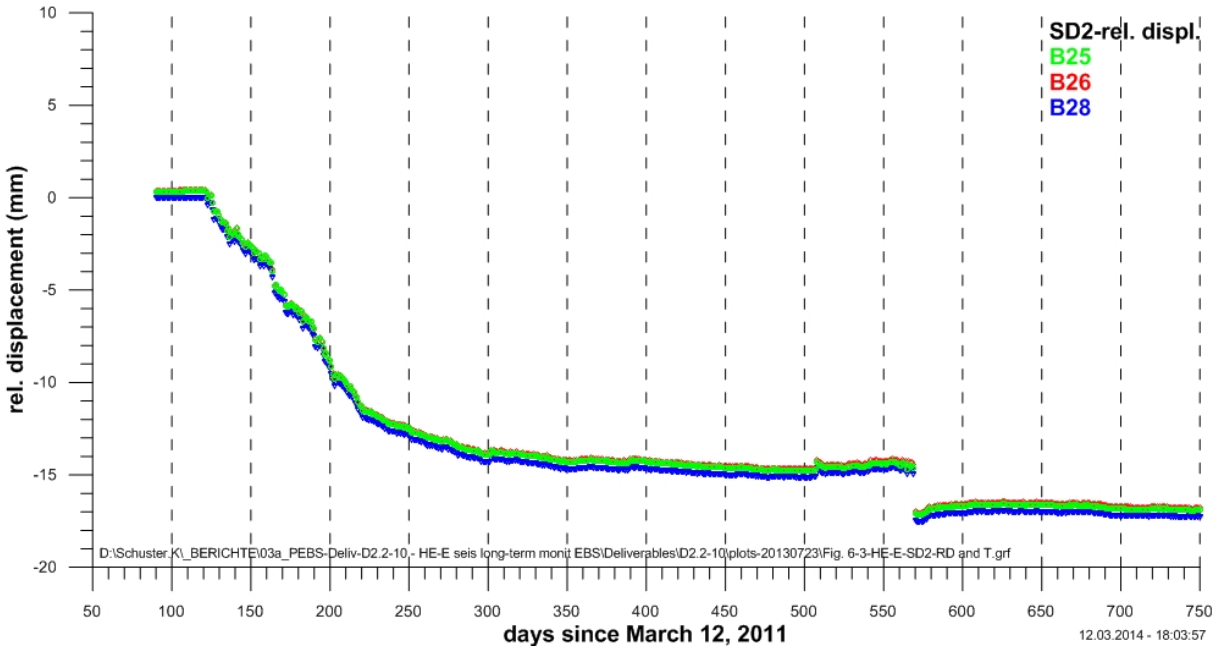

Fig. 6.4 Relative displacement evolution within the first 750 days in section SD2 (see Fig. 6.1).

6.2 EDZ related parameters

The P-wave velocity can be regarded as a good indicator for the existence, degree and extend of the EDZ/EdZ as could be shown in several own experiments at the Mont Terri Rock Laboratory.

6.2.1 Absolute velocities

In Figure 6.5 the derived P-wave velocities derived from P-wave onsets are plotted. Only the selection of emitters and receivers from boreholes BEV112 and BVE114 allow covering different, nearly equidistantly spaced distances from the interface S/B-OPA. In this case the propagation paths are circa 45° towards the bedding and distances of 10 cm, 20 cm, 30 cm and 45 cm are realised. All derived absolute velocities at the beginning of the monitoring phase are in a range which is comparable with own measurements performed in the same area within the VE experiment (Schuster, 2007). Conspicuous is, that the v_p for the 10 cm, 20 cm and 30 cm distance very similar. This could be related to an uncertainty in the borehole coordinates.

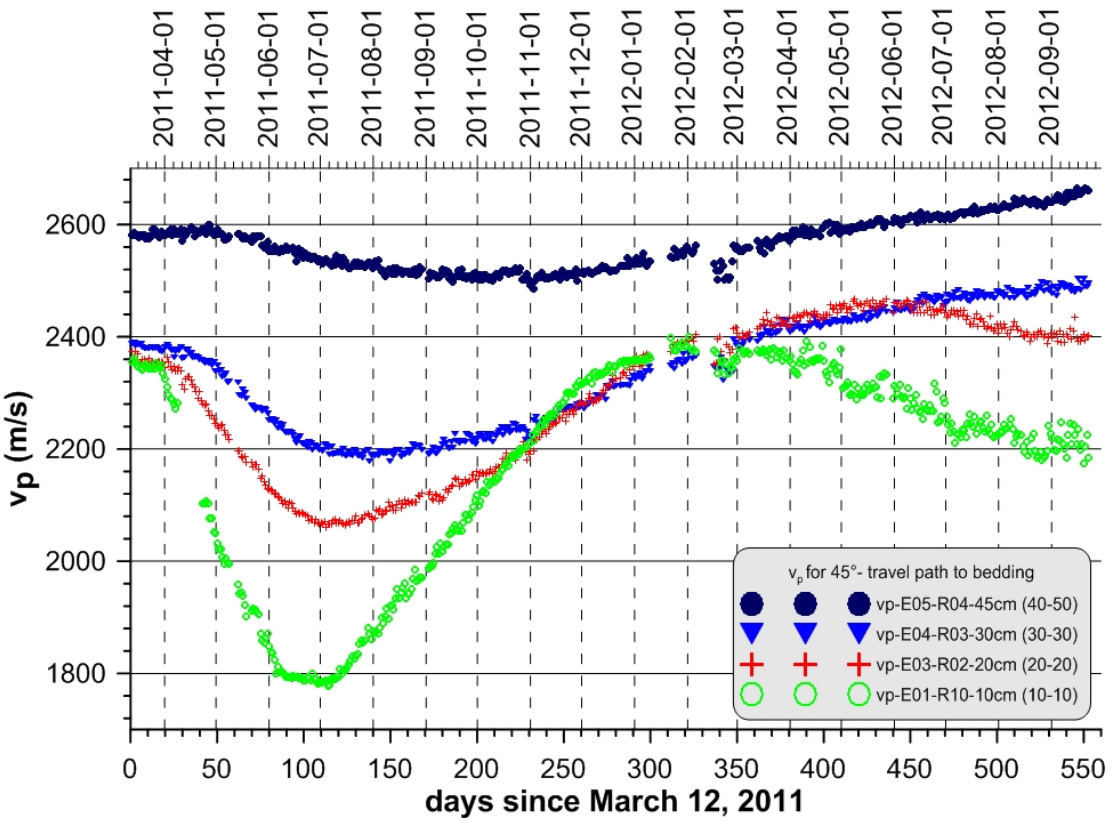

Fig. 6.5 Seismic P-wave velocities for different distances from the interface S/B-OPA with propagation paths circa 45° towards bedding.

In Figure 6.6 the absolute P-wave velocities which were derived in the beginning and at the end of the actual discussed monitoring phase are compared. The arithmetic mean value for the days 1 to 11 (blue symbols) and days 544 to 553 (red symbols) was calculated and plotted dependent on the distance to the interface. A clear distance dependent and except for the 10 cm distance a clear time dependent evolution is visible. It can be attributed to the consolidation of the rock mass. For the 'undisturbed' OPA a v_p of 2700 m/s for the 45° orientation towards the bedding was found in several own measurements at the Mont Terri RL (Schuster, 2009).

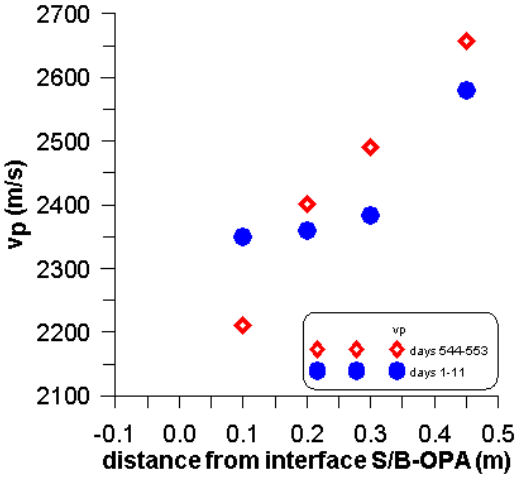

Fig. 6.6 Seismic P-wave velocities for different distances from the interface S/B-OPA at the beginning and at the end of the monitoring phase with propagation paths circa 45° towards bedding.

6.2.2 Absolute amplitudes

For the data set discussed in section 6.2.1 in Figure 6.7 the absolute values for the derived amplitudes are plotted. A clear dependency of the attenuation of seismic wave energy from the distance to the interface is visible. As farther the distance of the travel paths from the interface as lesser the amplitude damping.

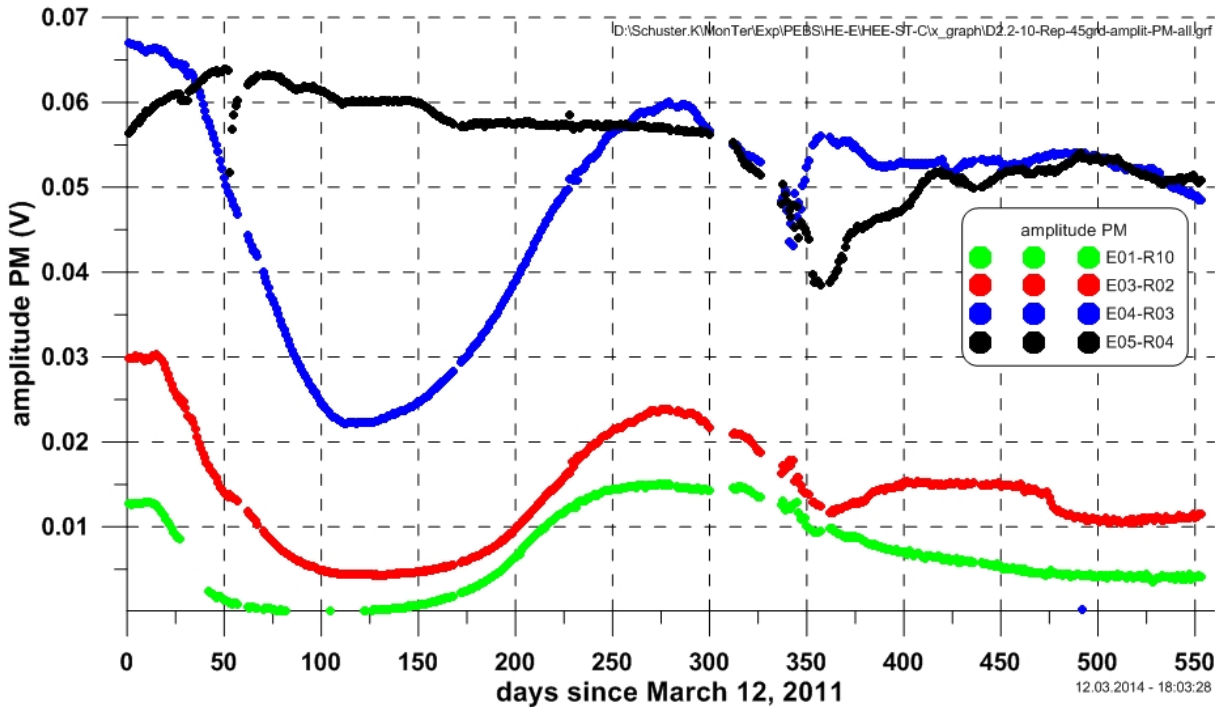

Fig. 6.7 Seismic amplitudes PM for different distances from the interface S/B-OPA with propagation paths circa 45° towards bedding.

In Figure 6.8 the absolute P-wave amplitudes (PM) which were derived in the beginning and at the end of the actual discussed monitoring phase are compared. The arithmetic mean value for the days 1 to 11 (blue symbols) and days 544 to 553 (red symbols) was calculated and plotted dependent on the distance to the interface. A clear distance and time dependent evolution is visible. Noticeable is the time dependent evolution of amplitudes. For each distance from the interface the amplitudes around days 553 are lower than at the beginning. This means that the wave attenuation seems to increase with time and is more pronounced near the interface.

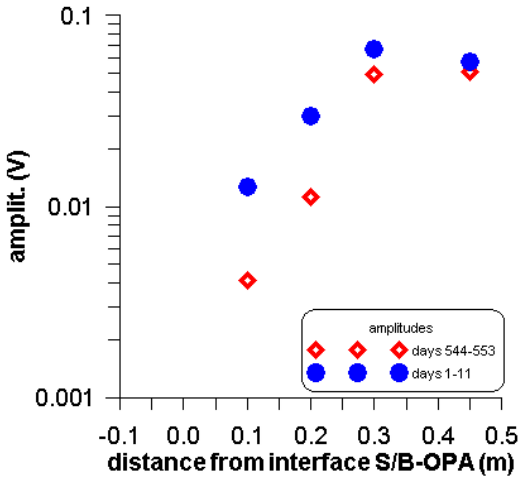

Fig. 6.8 Seismic amplitudes PM for different distances from the interface S/B-OPA at the beginning and at the end of the monitoring phase with propagation paths circa 45° towards bedding.

6.2.3 Absolute frequency content

For the up to now discussed data set the apparent frequencies of the first arrival P-wave signal was calculated and plotted in Figure 6.9. Except for the 10 cm distance values the graphs plot in the range between 6 kHz and 20 kHz. Values for the 10 cm distance between days 50 and 150 are not reliable due to the extreme attenuation in this phase.

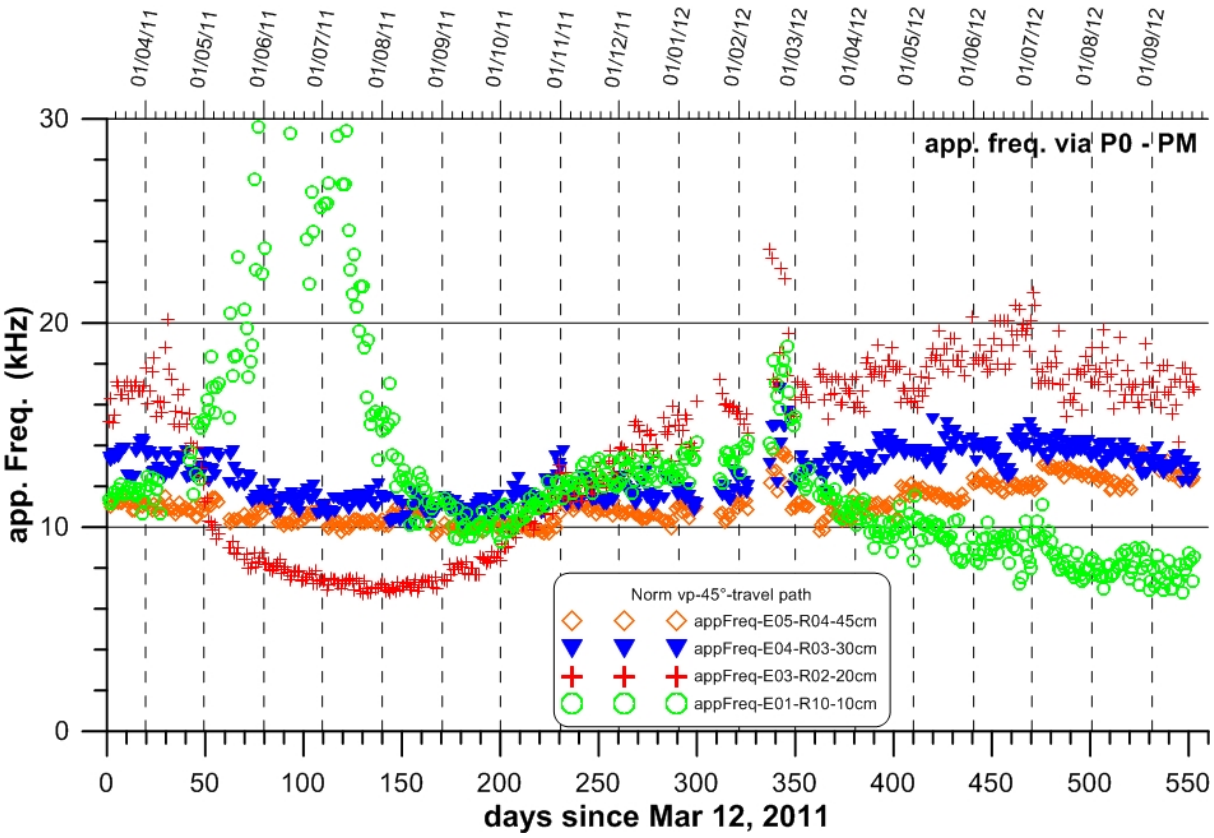

Fig. 6.9 Apparent frequency content of first arrival P-wave phases for different distances from the interface S/B-OPA with propagation paths circa 45° towards bedding.

In Figure 6.10 the apparent frequencies of the first arrival P-wave signals which were derived in the beginning and at the end of the actual discussed monitoring phase are compared. The arithmetic mean value for the days 1 to 11 (blue symbols) and days 544 to 553 (red symbols) was calculated and plotted dependent on the distance to the interface. No constant distance and time dependent evolution is visible. Noticeable is the distance dependent evolution of apparent frequencies from 10 cm to 20 cm distance and the reverse evolution from 20 cm to 45 cm.

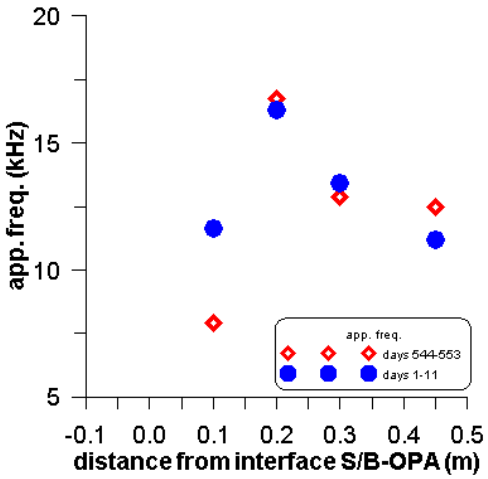

Fig. 6.10 Apparent frequencies of first arrival phases for different distances from the interface S/B-OPA at the beginning and at the end of the monitoring phase with propagation paths circa 45° towards bedding.

6.3 Results derived from the sand-bentonite material

In the S/B material two travel paths are realised, one piezoelectric emitter at 5 cm and two receivers, one at 5 cm and the other one at 10 cm distance from the interface S/B – OPA. All three transducers are fully covered by the backfill material.

6.3.1 Normalised velocities

In Figure 6.11 the derived normalized velocity of correlative phases are displayed. At this stage it is not clear if the phase is a P-wave phase or an S-wave phase, according to the derived absolute velocities.

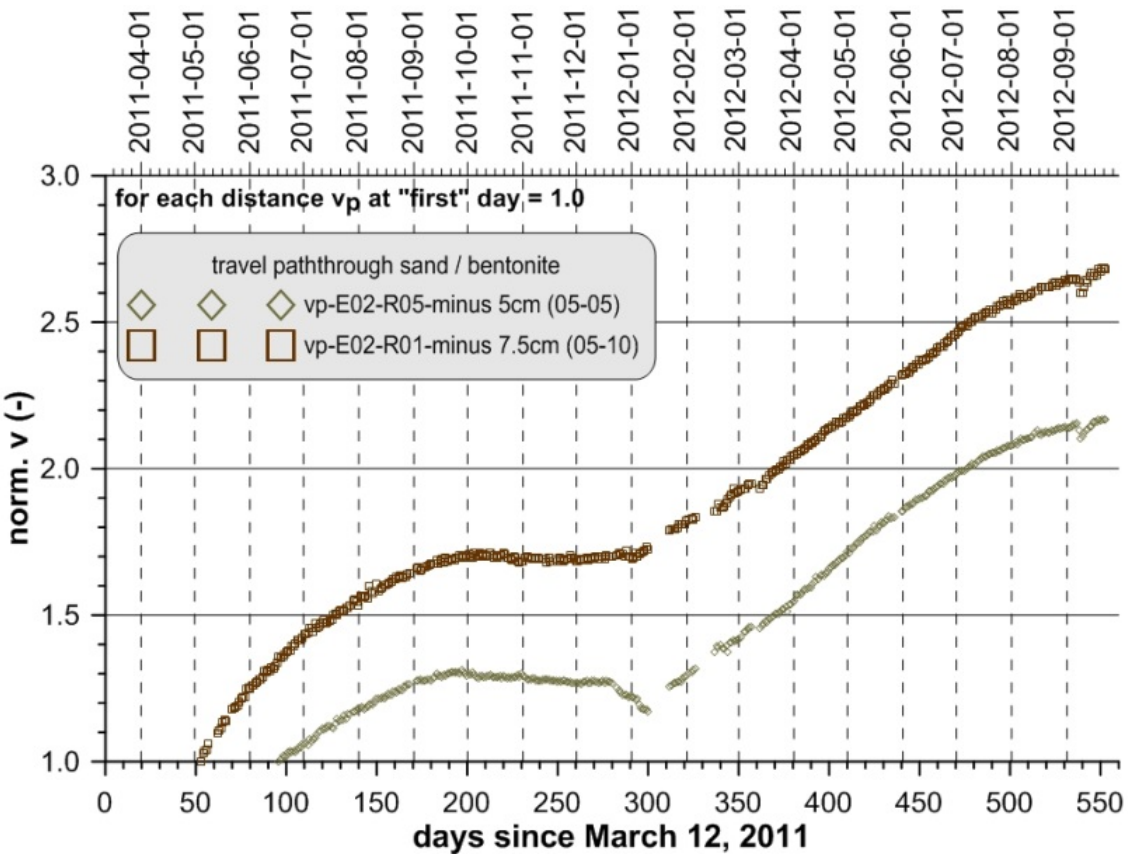

Fig. 6.11 Normalised seismic velocities for two distances from the interface S/B-OPA with propagation paths in the S/B.

Very clear different stages of the normalized velocity evolution in the sand bentonite mixture can be distinguished. For example, earlier correlative phase detection farther away from the interface (day 52, 7.5 cm) than for the propagation path closer to the interface (day 95, 5 cm). In both graphs a constant phase during the evolution is visible between days 200 and 290 followed by a steep increase until day 500 and a lower steep gradient from day 500 on. Two notches in the graphs at days 361 and 538 correlate with a power breakdown of the heaters (see. section 6.1). More details are discussed in chapter 7.

6.3.2 Normalised amplitudes

Normalised amplitudes derived in the S/B are plotted in Figure 6.12. Until day 410 the evolution of both graphs are comparable, but from this day on the gradient of the shorter distance amplitude data start to increase very fast. This could be related to an stronger consolidation of the S/B close to the interface.

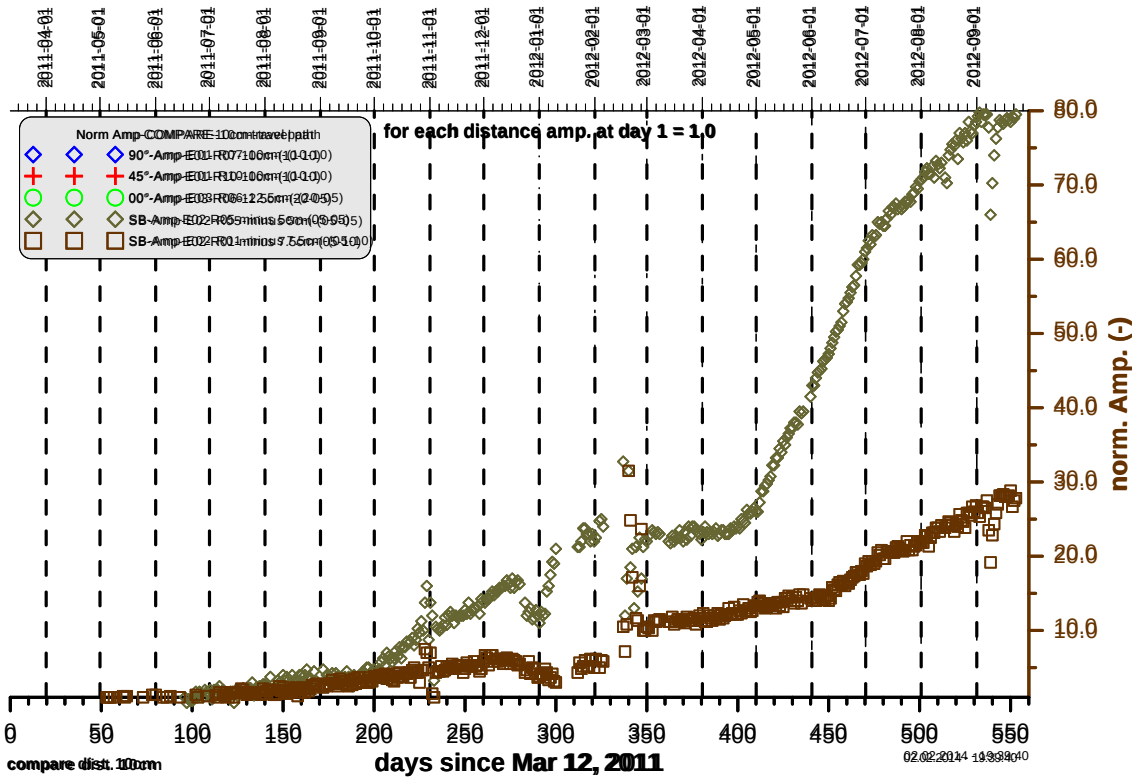

Fig. 6.12 Normalised seismic amplitudes (PM) for two distances from the interface S/B-OPA with propagation paths in the S/B.

6.3.3 Normalised frequency content

No frequency content of the S/B data was determined up to now.

6.4 Results derived from data within the OPA – 45° raypaths

For the travel paths orientation nearly 45° to bedding four emitter – receiver combinations were analysed, covering distances to the interface S/B-OPA between 10 cm and 45 cm. Emitters and receivers are located in boreholes BVE112 and BVE114.

6.4.1 Normalised velocities

The normalized v_p data derived for four distances to the interface and an orientation of 45° to the bedding is plotted in Figure 6.13.

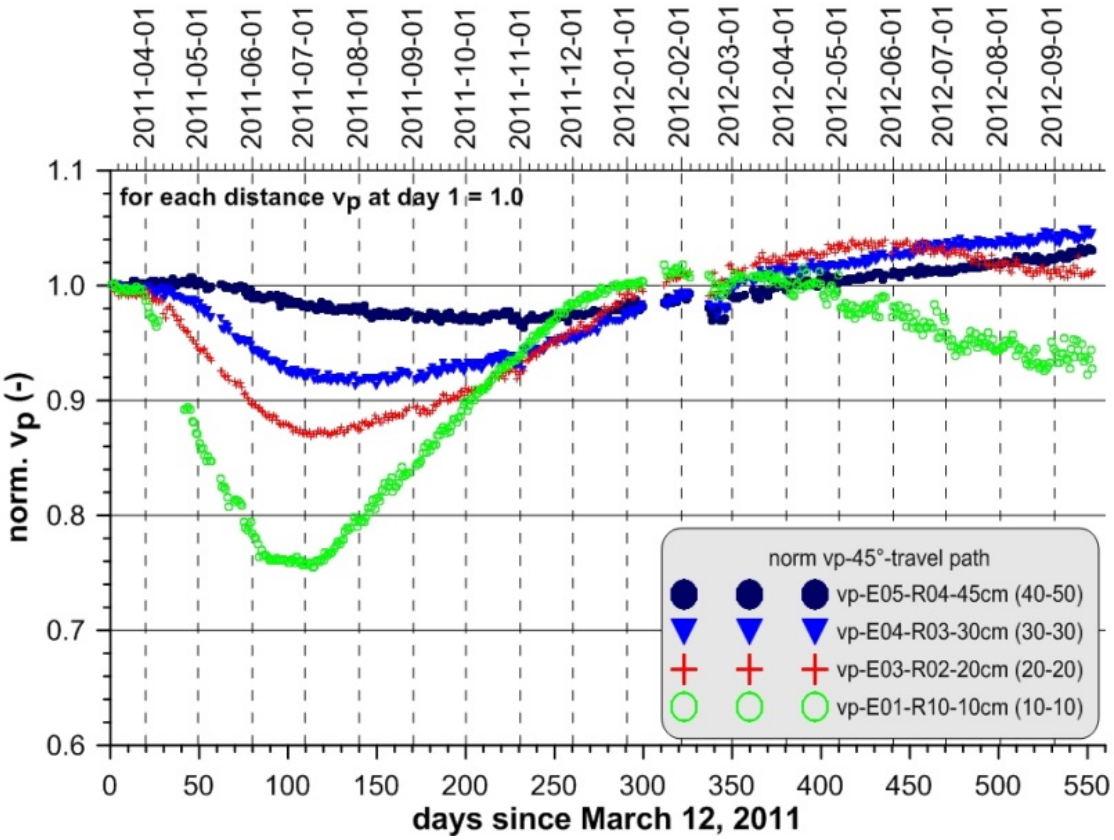

Fig. 6.13 Normalised seismic P-wave velocities for different distances from the interface S/B-OPA with propagation paths circa 45° towards bedding.

6.4.2 Normalised amplitudes

The trends of the normalised amplitudes are very similar for distances up to 30 cm (see Fig. 6.14). Normalised amplitudes for the 10 cm data (green symbols) drop to zero around day 100 and recover around day 225 (norm. amp. PM = 1) and increase further to 1.2 at day 275 before it decrease continuously to 0.3.The 20 cm data (red symbols) and 30 cm data (bkue symbols) do not recover fully, they stay with 0.8 and 0.9 below 1.0.

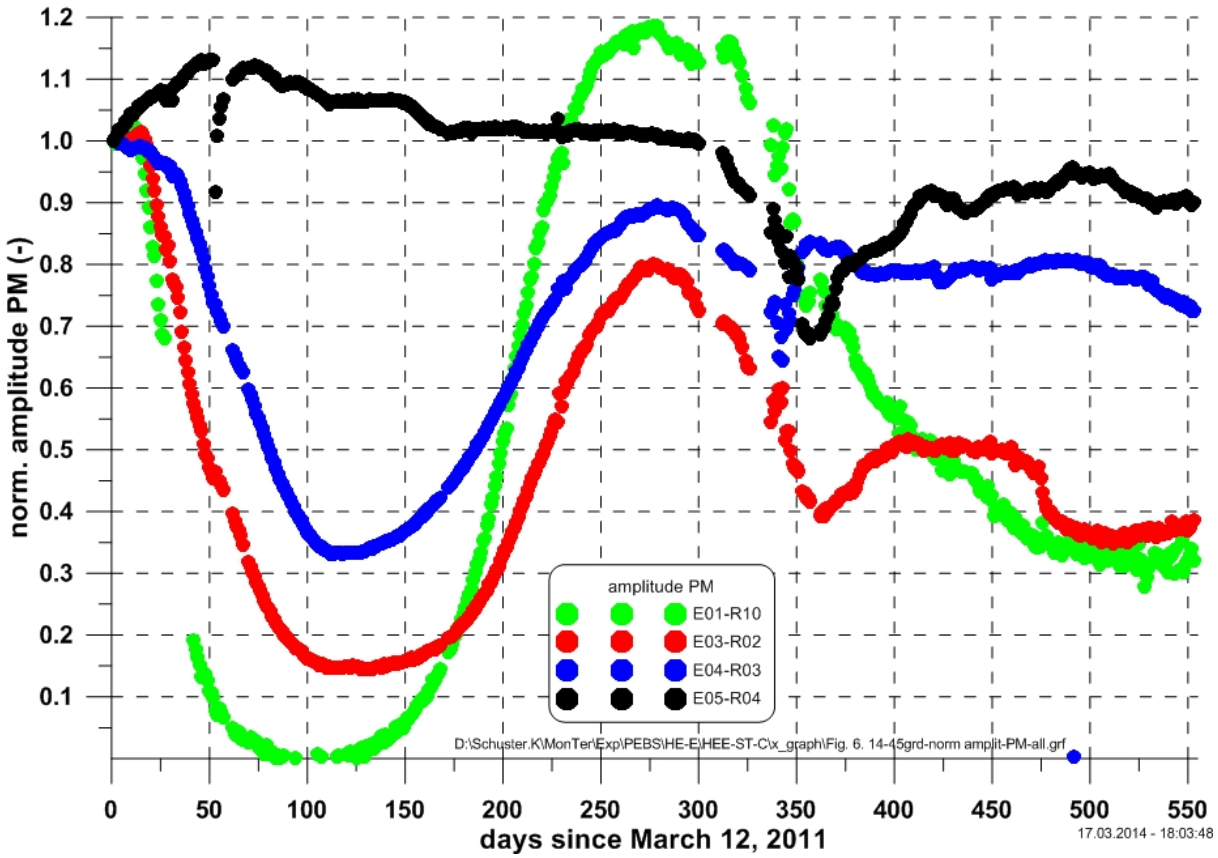

Fig. 6.14 Normalised P-wave amplitudes (PM) for different distances from the interface S/B-OPA with propagation paths circa 45° towards bedding.

6.4.3 Normalised frequency content

No normalized frequency content of the 45° data was determined up to now.

6.5 Results derived from data within the OPA – normal raypaths towards bedding

For the travel paths orientation nearly normal to bedding four emitter – receiver combinations were analysed, covering distances to the interface S/B-OPA between 7.5 cm and 20 cm. Emitter E01 (A) in borehole BVE112 and 4 receivers in borehole BVE113. Only the transducer pair E01 (A) – R07 is really normal oriented to bedding.

6.5.1 Normalised velocities

The v_p evolution (see Fig. 6.15) shows until day 300 a similar behavior like for the 45° orientation, except that the recovery values around day 300 are higher and that there is not such a clear differentiation around day 100 for the 10 cm and 20 cm distance data, even an inverse situation occurs around day 100, v_p at 10cm declines less than v_p at 20 cm distance. Furthermore, the decline beyond day 300 starts earlier.

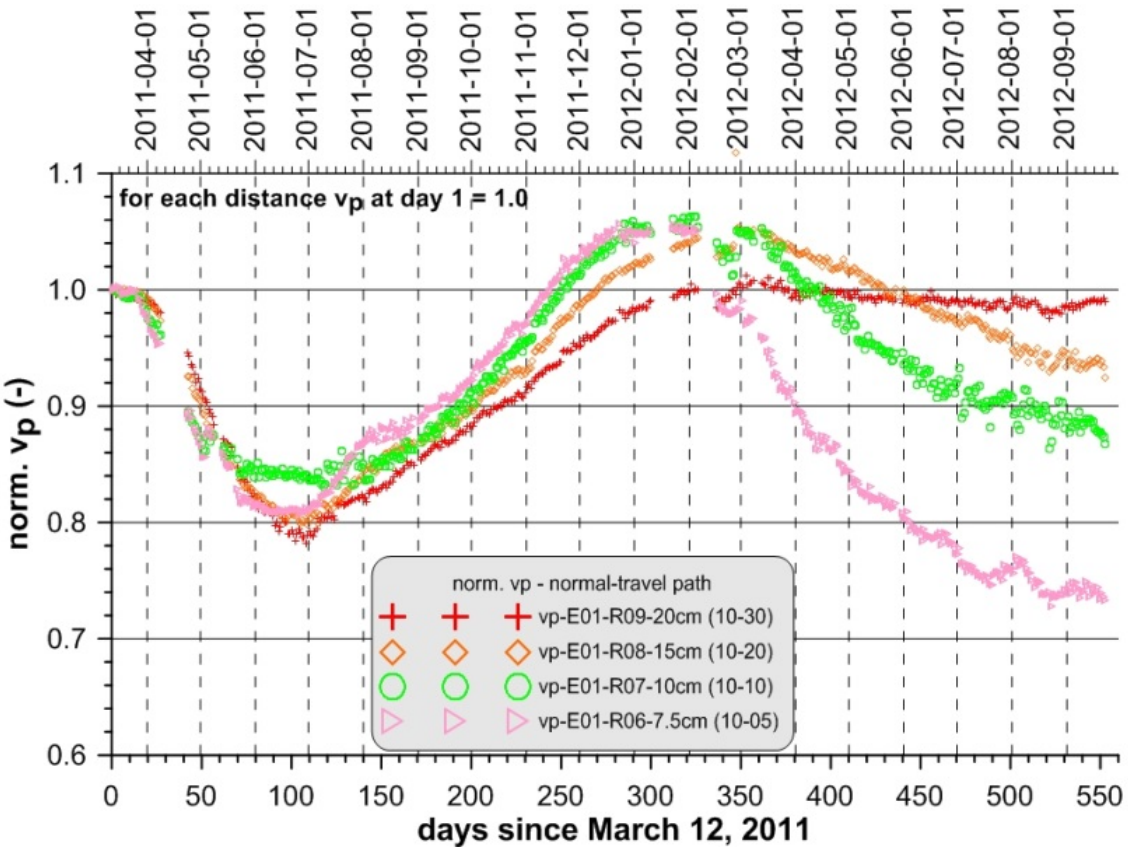

Fig. 6.15 Normalised seismic P-wave velocities for different distances from the interface S/B-OPA with propagation paths circa normal towards bedding.

6.5.2 Normalised amplitudes

The normalized amplitude evolution for the normal to bedding orientation as shown in Figure 6.16 is comparable with the data derived for the 45° orientation (see Fig. 6.14) except that for the 30 cm distance (blue symbols) amplitudes drop to zero between days 90 and 125.

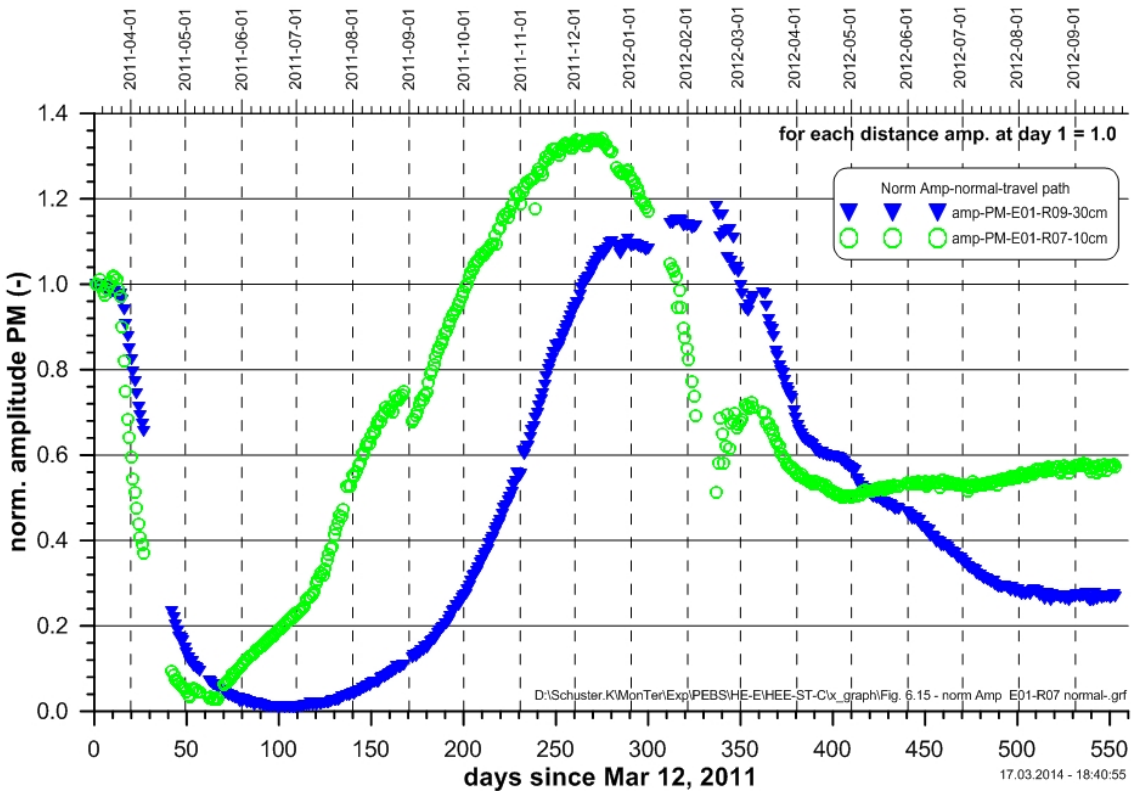

Fig. 6.16 Normalised P-wave amplitudes (PM) for different distances from the interface S/B-OPA with propagation paths circa normal towards bedding.

6.5.3 Normalised frequency content

No normalized frequency content of the normal orientation data was determined up to now.

6.6 Results derived from data within the OPA – parallel raypaths towards bedding

For the travel paths orientation nearly parallel to bedding three emitter–receiver combinations were analysed, covering distances to the interface S/B-OPA between 12.5 cm and 20 cm. Emitters and receivers are located in boreholes BVE114 and BVE113. Only the transducer pair E03 (C) – R08 is really parallel oriented to bedding.

6.6.1 Normalised velocities

The parallel to the bedding oriented travel paths v_p data (see Fig.6.17) are partly comparable to the other two orientations. The v_p at 20 cm declines only very little, whereas the v_p at 12.5 cm declines very strong, to values of 0.6. In this case we have to consider, that the source is located at 20 cm distance from the interface and the receiver at 5 cm only, what complicates a direct comparison.

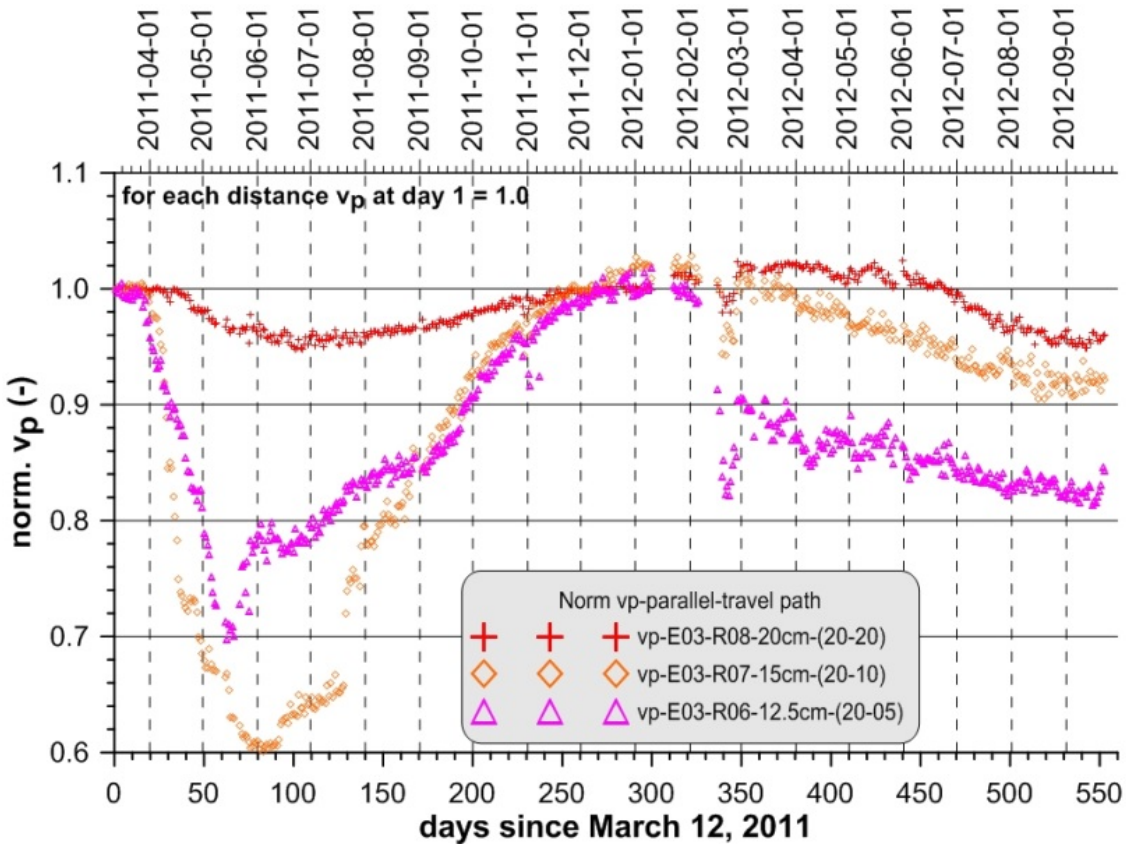

Fig. 6.17 Normalised seismic P-wave velocities for different distances from the interface S/B-OPA with propagation paths circa parallel towards bedding.

6.6.2 Normalised amplitudes

The related normalized amplitude graphs (see Fig. 6.18) are conspicuous because the amplitudes stay for a long time (between days 75 and 175) around zero for the short distances to the interface (12.5 cm and 15 cm). Furthermore, the recovery values between days 300 and 400 are very high compared to the data derived for the other orientations to the

bedding, where the highest values reach only 1.2 (45° orientation) and 1.4 (normal orientation).

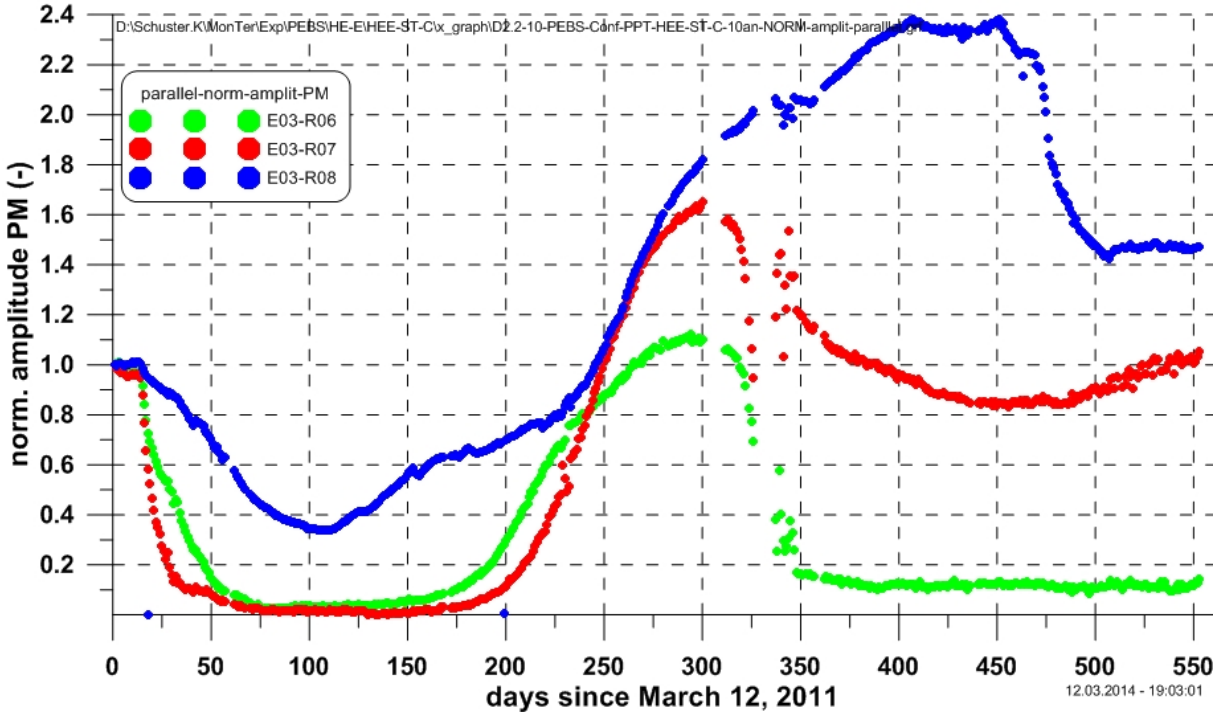

Fig. 6.18 Normalised P-wave amplitudes (PM) for different distances from the interface S/B-OPA with propagation paths circa parallel towards bedding. Distances to the interface: 12.5 cm (green symbols), 15 cm (red), 20 cm (blue).

6.6.3 Frequency content

In Figure 6.19 the absolute apparent frequencies for three distances to the bedding for the parallel to the bedding oriented travel paths are shown. In general a trend towards the end of the actual observation phase (day 553) from higher to lower frequencies for all three distances can be seen and several distinct variations in the graphs.

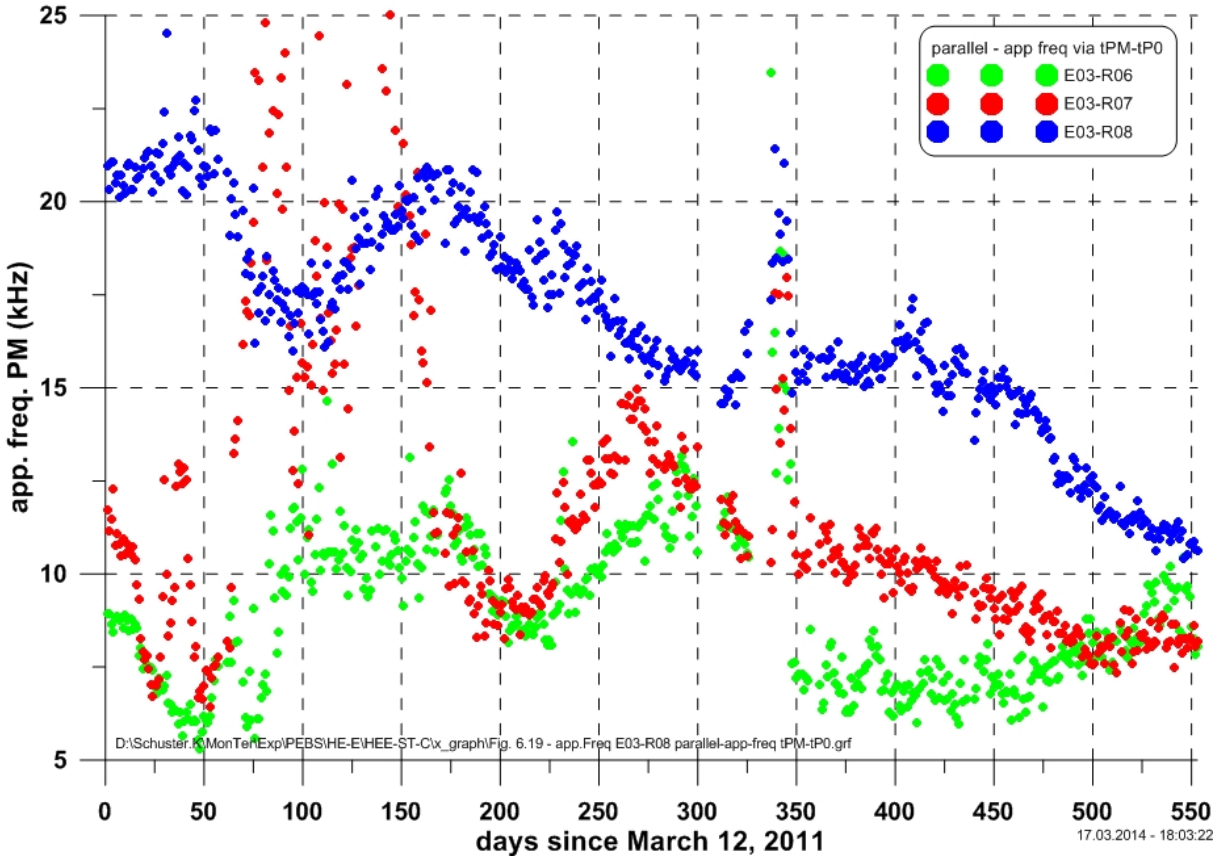

Fig. 6.19 Apparent frequency content of first arrival P-wave phases for different distances from the interface S/B-OPA with propagation paths circa parallel towards bedding. Distances to the interface: 12.5 cm (green symbols), 15 cm (red), 20 cm (blue).

6.7 Results derived from data within the OPA – raypaths along the borehole wall

For the travel paths orientation along the borehole wall borehole BVE112 with emitter E01 (A) and receivers R02, R03 and R04 could be used, covering distances between emitter and receivers of 10 cm, 20 cm and 40 cm. In the second borehole BVE114 receiver R10 and emitters E03 (C), E04 (D) and E05 (E) data were analysed. All piezoelectric transducers are pressed at circa 60° (BVE112) and circa 285° (BVE114) to the borehole wall (if looking into the horizontal boreholes). From this geometrical point of view both situations are very similar.

This type of travel time analyses has a clear analogy to interval velocity measurements we performed with our BGR borehole probe in numerous borehole investigations (Schuster et al., 2001). With the help of repetition measurements also the development of the borehole disturbed wall zone (BdZ) could be detected and seismically characterized (Schuster, 2009).

6.7.1 Velocities

The first constellation (interval velocity measurements in borehole BVE 112) corresponds to a common shot point section (CSP) with an emitter at 10 cm and receivers at 10 cm, 20 cm and 40 cm. The derived P-wave velocities are plotted in Figure 6.20.

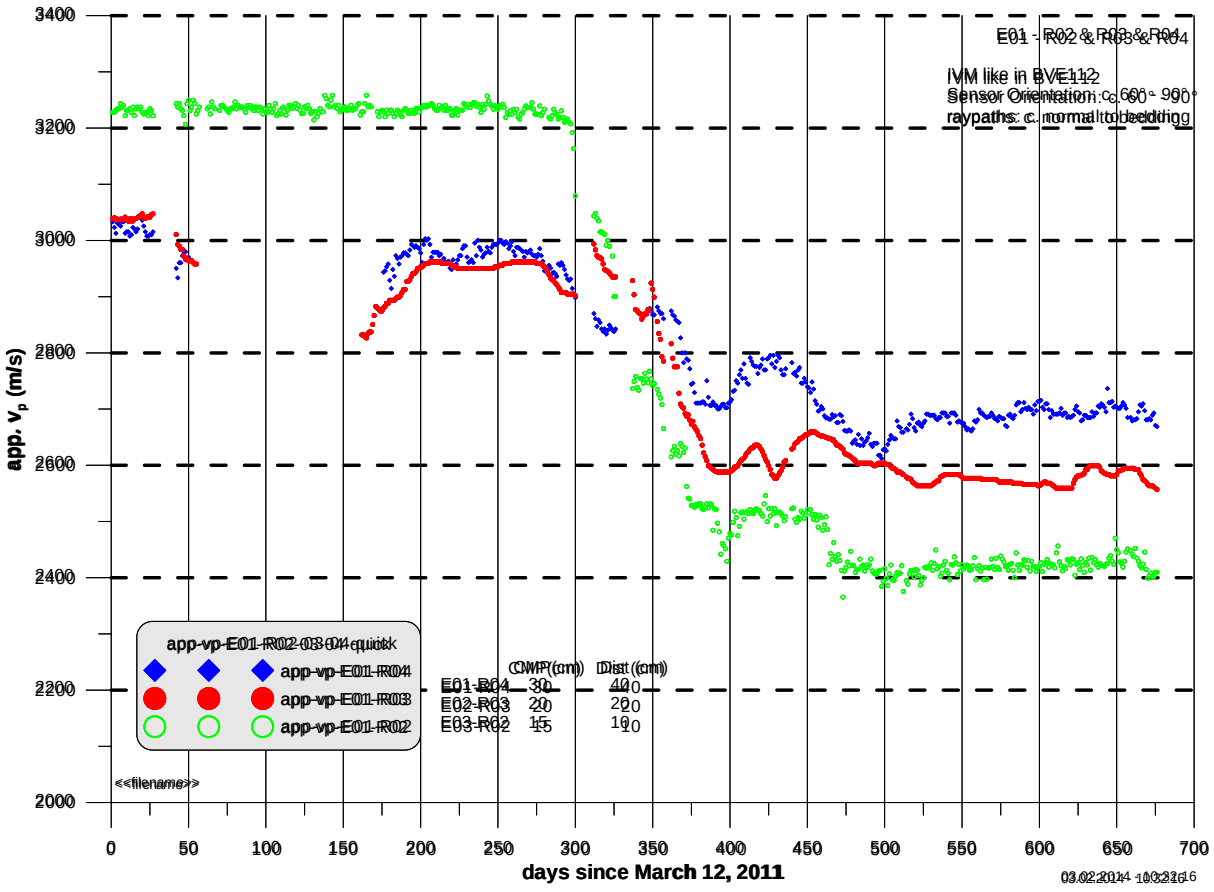

Fig. 6.20 Seismic P-wave velocities along the borehole wall in borehole BVE112 (comparable to interval velocities) for different distances between one emitter and three receivers.

Remarkable is the emitter-receiver related order of derived velocities. For most of the up to now investigated boreholes in clay rocks at different European underground research laboratories we found the following order: lowest v_p for the short distances and highest v_p for the greatest distance between emitter and receiver. This is an indication for a “normal” borehole wall with a positive radial velocity gradient. The differences between the individual v_p are related to the extent of the BdZ (Schuster, 2009). As greater the differences of individual v_p as greater the extent of the BdZ. In Figure 6.20 we see a astonishing evolution. For the shortest distance (10 cm, green graph) we derived the highest v_p (3200 m/s) until day

300 followed by a gradual decrease between days 300 and 400 to a v_p of 2400 m/s which increases only slightly towards day 670. From day 400 on we see the “normal” order of derived v_p, which is close to common v_p in the sense of absolute values as well as in the sense of differences. Until day day 300 we would describe the borehole wall as an eggshell like wall with a stiff (high v_p) thin layer. We observed changes of a borehole wall (BdZ) as a consequence of the drilling process at Mont Terri RL (Schuster, 2009). The derived v_p distribution is very similar to the distribution plotted in Figure 6.20.

The second constellation (interval velocity measurements in borehole BVE 114) corresponds to a common receiver point section (CRP) with one receiver at 10 cm and three emitters at distances of 10 cm, 20 cm and 30 cm. Due to the general law of reciprocity of travel time between emitter and receiver both sections are comparable from the principle physical point of view. The derived P-wave velocities are plotted in Figure 6.21.

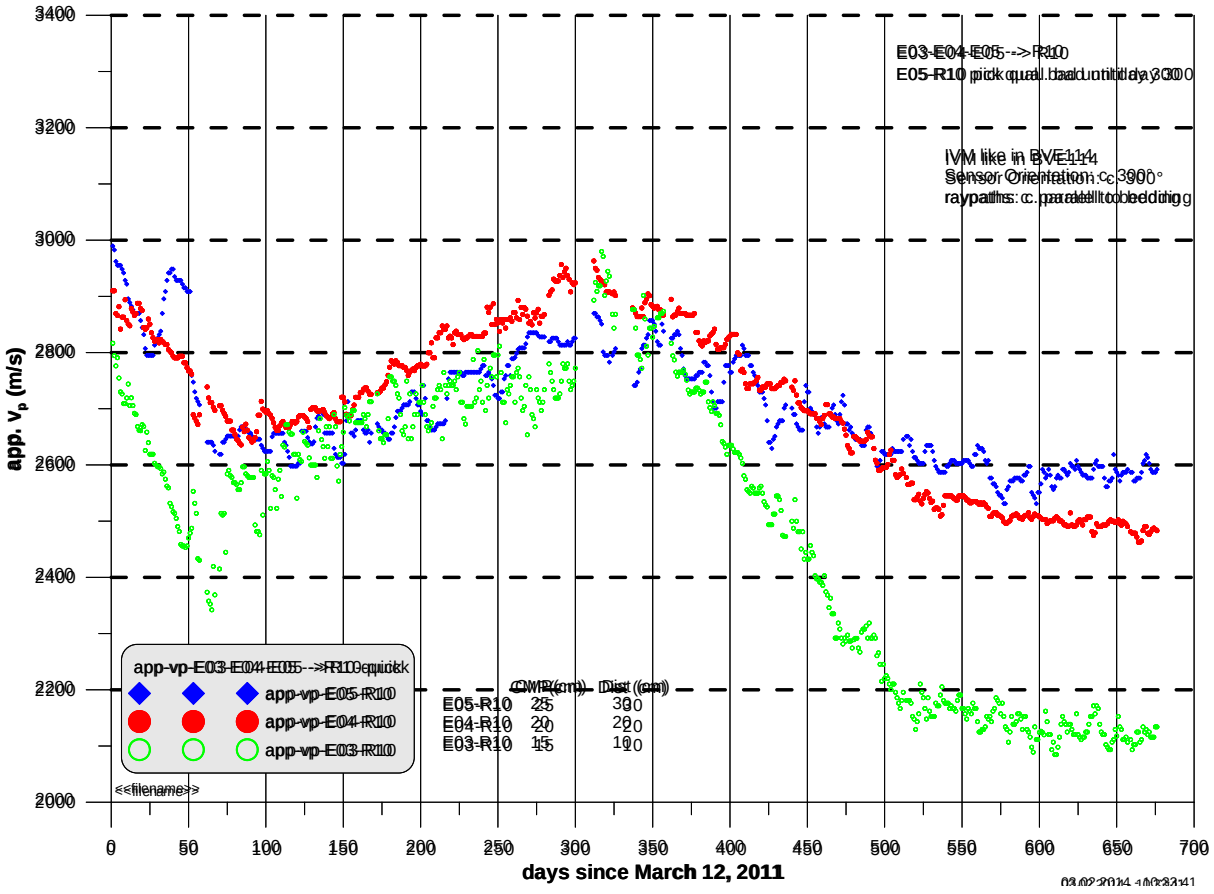

Fig. 6.21 Seismic P-wave velocities along the borehole wall in borehole BVE114 (comparable to interval velocities) for different distances between one receiver and three emitters.

The derived individual velocities in borehole BVE114 are lower until day 300, than they also decrease. From day 550 on they stay at a slightly lower level as the velocities derived in borehole BVE112.

From a geometrical point of view both boreholes are comparable. They are at the same level (see Fig. 3.2) and both are sub horizontal. Nevertheless the individual v_p are different as well as the evolution with time. One difference are the propagation paths of the seismic wave field. Wave filed propagation in BVE112 is a combination of normal and parallel oriented towards the bedding, whereas in BVE114 the wave field propagates rather parallel to the bedding.

7 Preliminary interpretation and conclusion

Not all correlations and dependencies between varying seismic parameters and related rock property changes are completely understood until now. In Figure 7.1 the most important normalized velocity graphs which were discussed until now from different distances of the ray paths from the S/B-OPA interface and three orientations towards the bedding are comprised. All velocities are normalised (v_p = 1 for day 1). Additionally, the velocity evolution between 5 cm and approximately 7.5 cm distance from the S/B-OPA interface in the **sand/bentonite mixture** is given. The backfill material (S/B) was emplaced at day 51 and 52. Therefore no correlative signals in the S/B section were expected before. Until day 52 only an air wave was recorded (see Fig. 5.10, blue arrow, v = 335 m/s). For the 5 cm distance from the interface a phase starting from day 95 on was taken as certain for a correlation. For the 7.5 cm distance the phases could be correlated immediately after the backfilling and closure of the section (day 52). This means that the backfill in the gap at the interface was not tightly filled. In the S/B material a rather stepwise velocity increase can be observed in both graphs which indicate a clear stepwise consolidation of the S/B mixture. Remarkable are the plateaus between days 200 and 300 and the bend in the graphs around day 500 several days after the heaters were hold at constant temperature. The notch in the v graphs at day 540 results most probably from a power failure that produced similar notches in the temperature and RH graphs several days before (see Fig. 6.1, 6.2 and 6.3). This underlines exemplarily that seismic parameters react very sensitive and instant to changes in material parameters.

Comparing the four v_p -graphs for the **45° orientation of travel paths** a similarity in the general trend can be seen but it is obvious that the rock material closer to the interface S/B-OPA (10 cm) is more affected, most probably by creation and a later sealing of micro cracks than at greater distances (20, 30 and 45 cm). The decline of v_p starts between days 20 (v_p at 10 cm) and day 50 (v_p at 45 cm). Likewise the absolute minima are reached at different times and different intensities, varying between 25 % (v_p at 10 cm, day 112) and 3 % (v_p at 45 cm, day 240). The ventilation (desaturation near the microtunnel) during the installation is most probably responsible for that. Between day 280 and 380 the four v_p graphs reach their start values (1), with a greater but comparable delay as they declined between day 20 and 50. The start values are exceeded by several percent. A hydration of the OPA (gradual closing of micro cracks) due to vapor coming from the drying S/B would support this. v_p values derived near the interface (10 cm and 20 cm) start to decline at day 410 and day 480 although the relative humidity RH measured at the interface stays constant at 100 % from day 250 on. An expansion of the OPA into the still unconsolidated S/B could explain this v_p reduction partly. From nearby locations (instrumentation sections SD1 and SD2, see Fig. 6.2 and 6.3) displacements in the range of up to minus 20 mm were measured between days 110 and 350. Also a pore water pressure increase, as predicted in the models, however for greater distances from the interface, could also lead to a v_p decrease in certain situations.

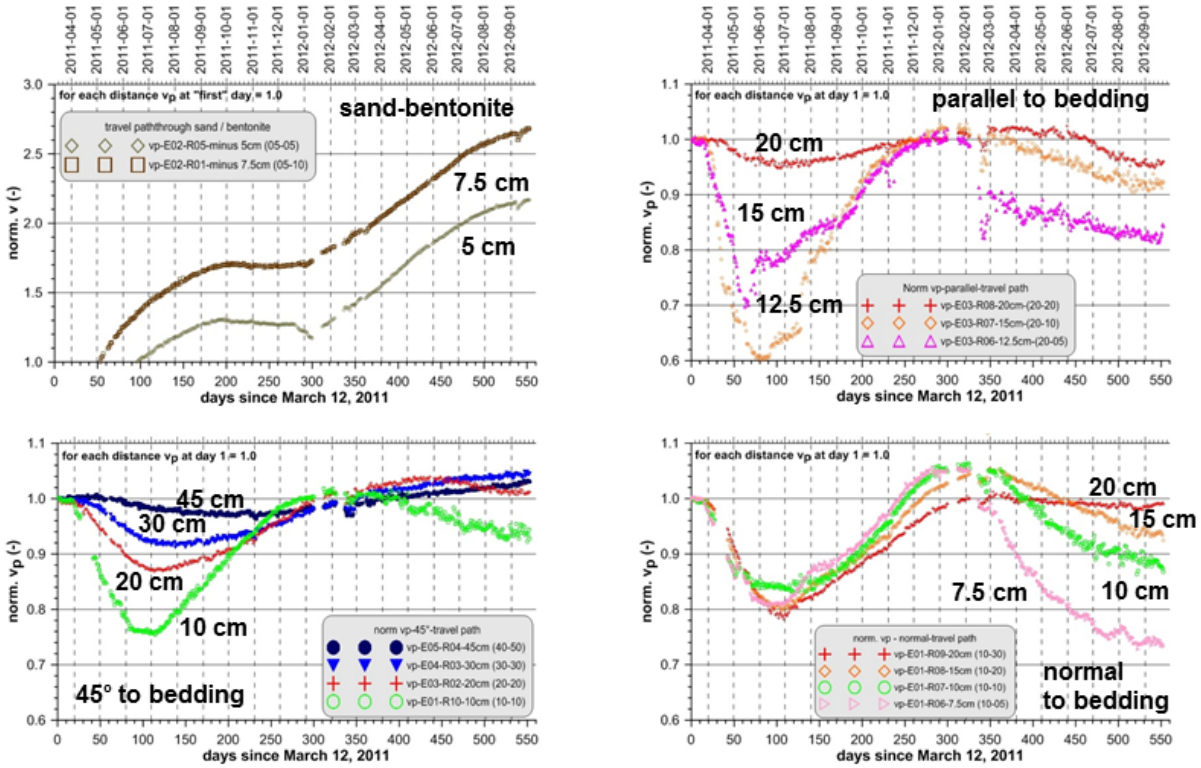

Fig. 7.1 Derived normalised velocities for three orientations of travel paths in the OPA towards the bedding and travel paths through the sand-bentonite mixture.

For the other orientations of travel paths towards the bedding only distances between 7.5 cm and 20 cm from the interface are taken into account due to the chosen layout. Additionally, most of them do not run parallel to the interface, what complicates a direct comparison of different orientations for the same distance from the interface.

The v_p evolution in OPA for **travel paths normal towards bedding** shows until day 300 a similar behavior like for the 45° orientation, except that the recovery values around day 300 are higher and that there is not such a clear differentiation around day 100 for the 10 cm and 20 cm distance data, even an inverse situation occurs around day 100, v_p at 10 cm declines less than v_p at 20 cm distance. Furthermore, the decline beyond day 300 starts earlier.

The **parallel to the bedding oriented travel paths** data are partly comparable to the other two orientations. The v_p at 20 cm declines only very little, whereas the v_p at 12.5 cm declines very strong, to values of 0.6. In this case we have to consider, that the source is located at 20 cm distance from the interface and the receiver at 5 cm only, what complicates a direct comparison.

All shown normalised v_p variations range between 1.06 and 0.6 what underlines that remarkable time dependent changes in material parameters are going on. In Figure 7.2 these results are compiled in a simplified graph which gives the range of possible widths of “anomalies”.

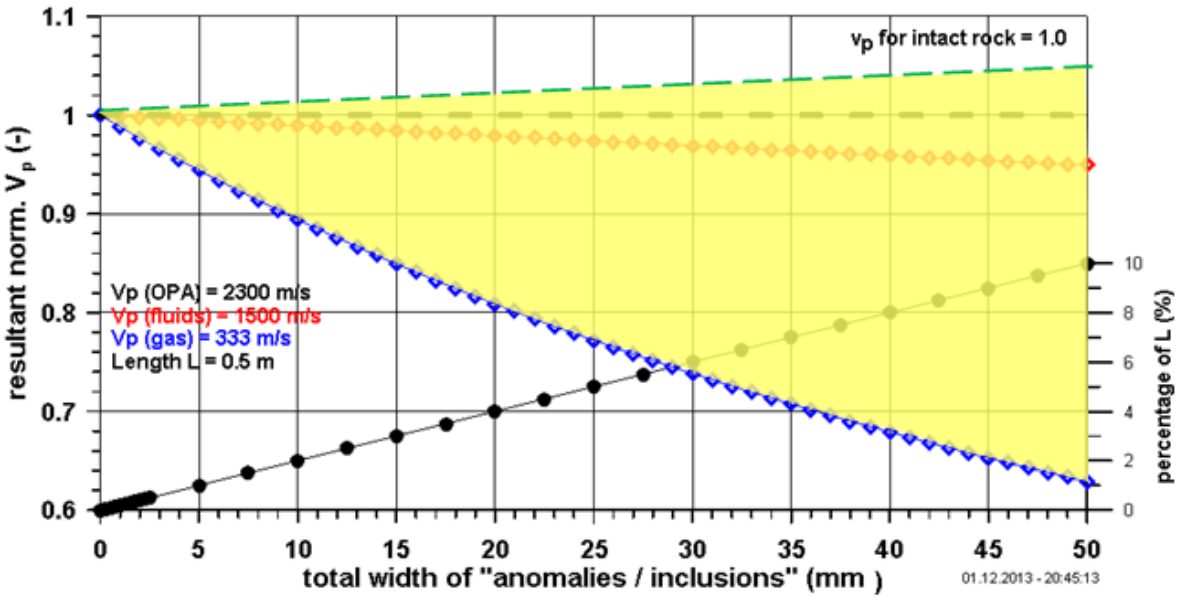

Fig. 7.2 Simplified illustration of the variability of normalized seismic P-wave velocities as derived in the course of the first 553 days of seismic transmission measurement monitoring (yellow area).

Generally, a clear dependency between the intensity of seismic parameter changes and the distance from the interface S/B-OPA can be seen in all results. For shorter distances the variations are more pronounced than for greater distances. Furthermore, it is worth mentioning that several tens of days after the velocity in the S/B starts to rise (day 300, increasing consolidation), the v_p for the short distances in the OPA start to decline. It seems that a “pulse” is entering the rock, and at later stages coming from the rock, but with a distinctive dependency from the orientation to the bedding (anisotropy of OPA). Which driving forces (thermal impact, vapor pressure, degree of saturation) generate this “pulse” and what process interactions define its origin needs further attention. It is shown however that seismic monitoring is a useful tool for the characterisation of continuously ongoing changes of rock properties.

Does a relation between relative displacement and normalised v_p evolution exist? In Figures 6.3 and 6.4 we see that the relative displacement is most developed between days 120 and 220 (steepest slope). During this time the first stage of the consolidation process of the S/B (see Fig. 7.1) took place and the recovery of the normalised v_p in the OPA is strongest for all orientations (see also Fig. 7.1).

For all v_p calculations the distances between emitters and receivers are assumed to be constant. Therefore the influence of thermal expansion was checked by taking a difference in temperature of 35 K (see Fig. 6.2) and a thermal expansion coefficient for the OPA of 1.9E-05 K^{-1} ($S_\perp$ -sample, 1st heating, Bock, 2009) into account. The resultant change in length is less than 1 mm for a distance of 0.5 m and is therefore not sufficient to explain the normalised v_p variations.

The v_p variations along the borehole walls in boreholes BVE112 and BVE114, as discussed in Figures 6.20 and 6.21, could be caused by processes related to vapor which propagates through the borehole into the OPA or coming out of the OPA.

Up to now we mainly compile results and tried to give some first explanations and / or interpretations. An integrative approach for an overall explanation has to be found later.

In Figures 7.3 and 7.4 for the three propagation paths of the seismic wave field towards the bedding normalised amplitudes (PM) for the distance of 10 cm and 20 cm to the interface are compiled.

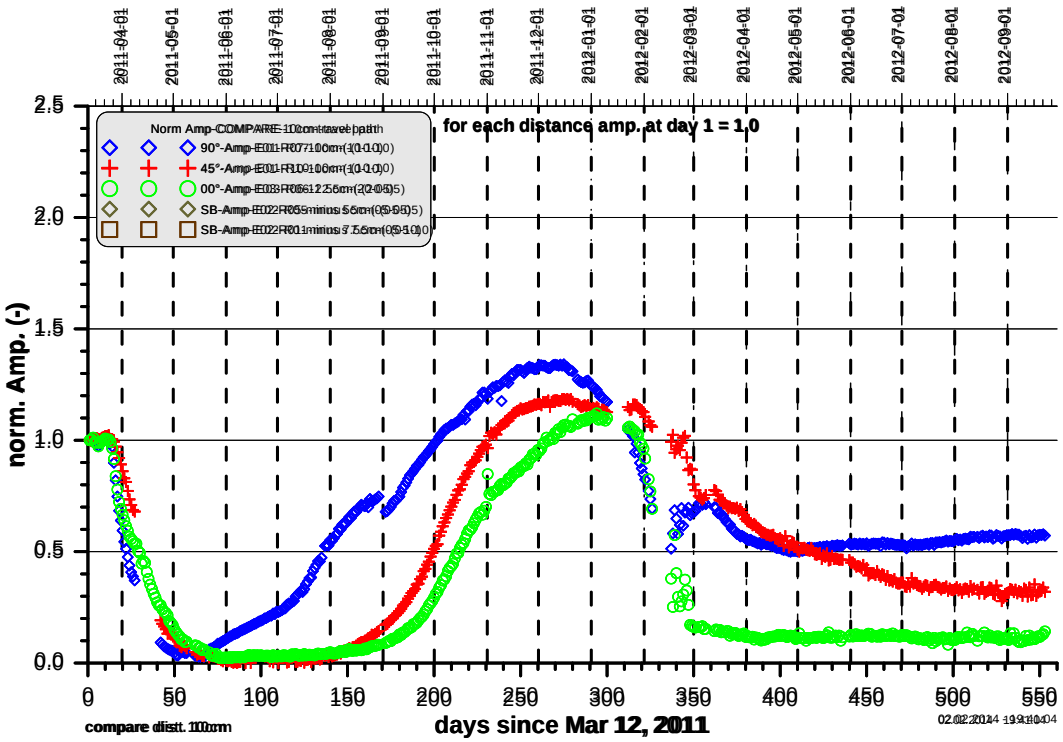

Fig. 7.3 Comparison of derived normalised amplitudes (PM) for three orientations of travel paths in the OPA towards the bedding at a distance of 10 cm to the S/B-OPA interface.

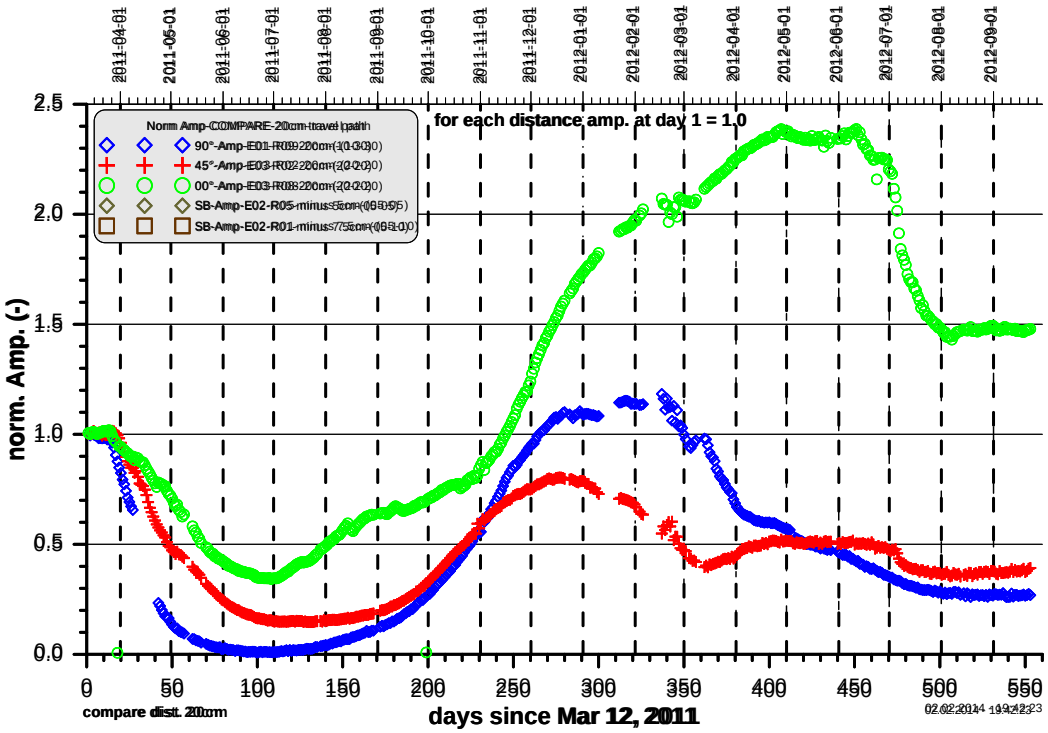

Fig. 7.4 Comparison of derived normalised amplitudes (PM) for three orientations of travel paths in the OPA towards the bedding at a distance of 20 cm to the S/B-OPA interface.

From the normalised v_p graphs presented for example in Figure 7.1 as a compilation we try to extract dependencies concerning the evolution in time, distance to the interface and the orientation of the propagation paths of the wave field towards the bedding. The graphs in Figures 7.5 shows after how many days the minimum value of normalised v_p is reached. For all distances to the interface S/B-OPA the sequence related to the propagation paths orientations is as follows: 1) parallel, 2) normal and 3) 45°. In Figure 7.6, except of some "outliers", a similar tendency for the recovery of the normalised v_p can be seen.

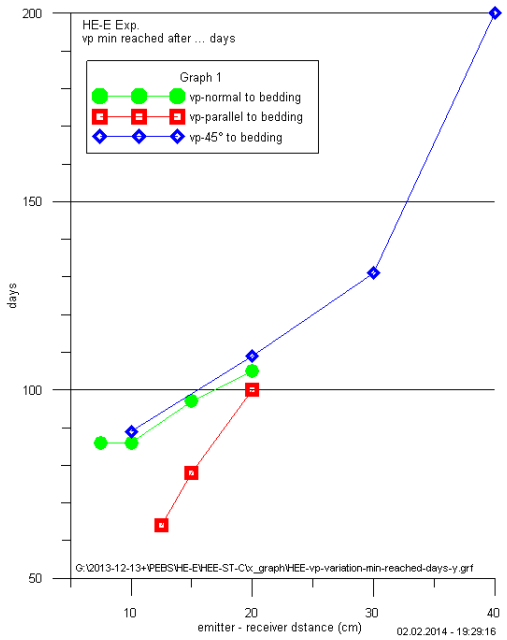

Fig. 7.5 Dependencies related to propagation path orientation. After how many days the minimum value of normalised $\mathbf{v_p}$ is reached?

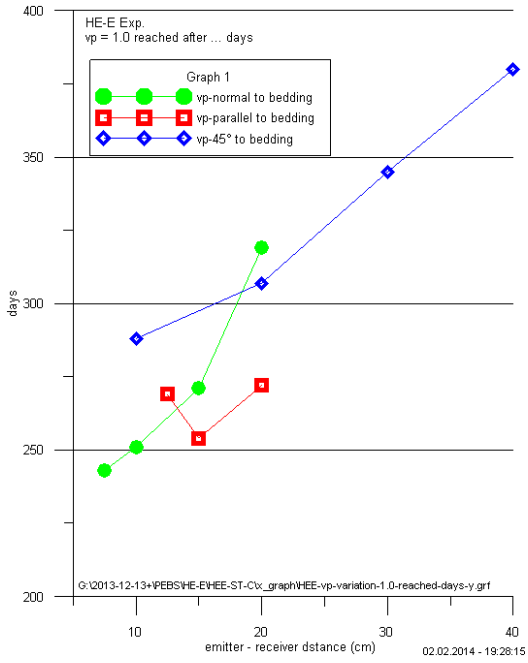

Fig. 7.6 Dependencies related to propagation path orientation. After how many days the start value of normalised $\mathbf{v_p}$ is reached ($\mathbf{v_p}$ = 1)?

8 Acknowledgement

The research leading to these results has received funding from the European Atomic Energy Community's Seventh Framework Programme (FP7/2007-2011) under grant agreement n° 249681.

The BGR contribution is co-funded by the German Ministry of Economy and Technology (BMWi), FKZ 02 E 10689.

9 References

Bock, H. (2009): RA Experiment: Updated review of the rock mechanics properties of the Opalinus Clay of the, Mont Terri URL based on laboratory and field testing, Mont Terri Technical Report TR 2008-04, swisstopo, Wabern, Switzerland.

Gaus I., Wieczorek K., Mayor J.C., Trick, T., Garcià-Sineriz, J.-L., Schuster K., Garitte B., Kuhlmann, U., (2011), EBS behaviour immediately after repository closure in a clay host rock: HE-E experiment (Mont Terri URL), Proceedings of the 14th Int. Conference on Environmental Remediation and Radioactive Waste Management, ICEM'11, September 25-29, 2011, Reims, France

Garcià-Sineriz, J. L. et al. (2005): NF PRO RTD C$ WP 4.3, EDZ short term evolution Task 1 & Task 3, Deliverable 4.3.2 (D 1) Test Plan

Mayor, J. C., et al, (2007a): Engineered barrier emplacement experiment in Opalinus Clay for the disposal of radioactive waste in underground repositories. In: Bossart, P. and Nussbaum, C. (Eds.): Mont Terri Project – Heater Experiment, Engineered Barriers Emplacement and Ventilation Tests (p. 115-179). – Rep. Swiss Geol. Surv. I.

Mayor, J. C., et al, (2007b): Ventilation experiment in Opalinus Clay for the disposal of radioactive waste in underground repositories. In: Bossart, P. and Nussbaum, C. (Eds.): Mont Terri Project – Heater Experiment, Engineered Barriers Emplacement and Ventilation Tests (p. 181-240). – Rep. Swiss Geol. Surv. I.

Sandmeier, K.-J. (2013): Reflex-Win, Version 7, Sandmeier scientific software, http://www.sandmeier-geo.de/

Schuster, K., Alheid, H.-J. & Böddener, D. (2001): Seismic investigation of the Excavation damaged zone in Opalinus Clay, Engng. Geol. 61: 189-197.

Schuster, K., Alheid, H.-J., Kruschwitz, S., Siebrands, S., Yaramanci, U., Trick, T., Manthei, G. (2004a), Observation of an Engineered Barrier Experiment in the Opalinus Clay of the Mont Terri Rock Laboratory (CH) with Geophysical and Hydraulic Methods, 2 posters and abstract, Euradwaste'04, Radioactive waste management - Community policy and research initiatives, Sixth European Commission Conference on the Management and Disposal of Radiactive Waste, 29. March - 1. April 2004, Luxembourg.

Schuster, K. (2007): High resolution seismic investigations within the VE-Experiment, Mont Terri Technical Report TR 07-06, swisstopo, Wabern, Switzerland.

Schuster, K. (2009): Detection of borehole wall disturbed zones and small scale rock heterogeneities with geophysical methods, Proceedings of the EC-TIMODAZ-THERESA THMC-Conference, Luxemburg, 29 Sep. - 1 Oct. 2009

Spies, T., Heidrich, D., Kruschwitz, S. (2002): Geophysical Characterisation of the Excavation Disturbed Zone (ED-C): Acoustic emission measurements during the excavation of the EN niche – a mine-by experiment, Mont Terri Technical Note TN 2002-08 (internal report), swisstopo, Wabern, Switzerland.

10 Appendix I – seismic sections of all 50 emitter - receiver combinations

In this appendix all 50 seismic data sets which were recorded within the first 553 days of monitoring are presented as a whole. This data set contains the combination of all emitters (E01 (A) – E05 (E)) with all related receivers (R01 – R10). It results in a total number of 27'650 single seismic traces. Not all of them were shown or discussed in the report. This compilation allows additionally a rough overview over the data quality, even main features can be compared individually, like travel time and amplitude evolutions. In Figure 10.1 the locations of all piezoelectric transducers (emitters and receivers) are shown once more.

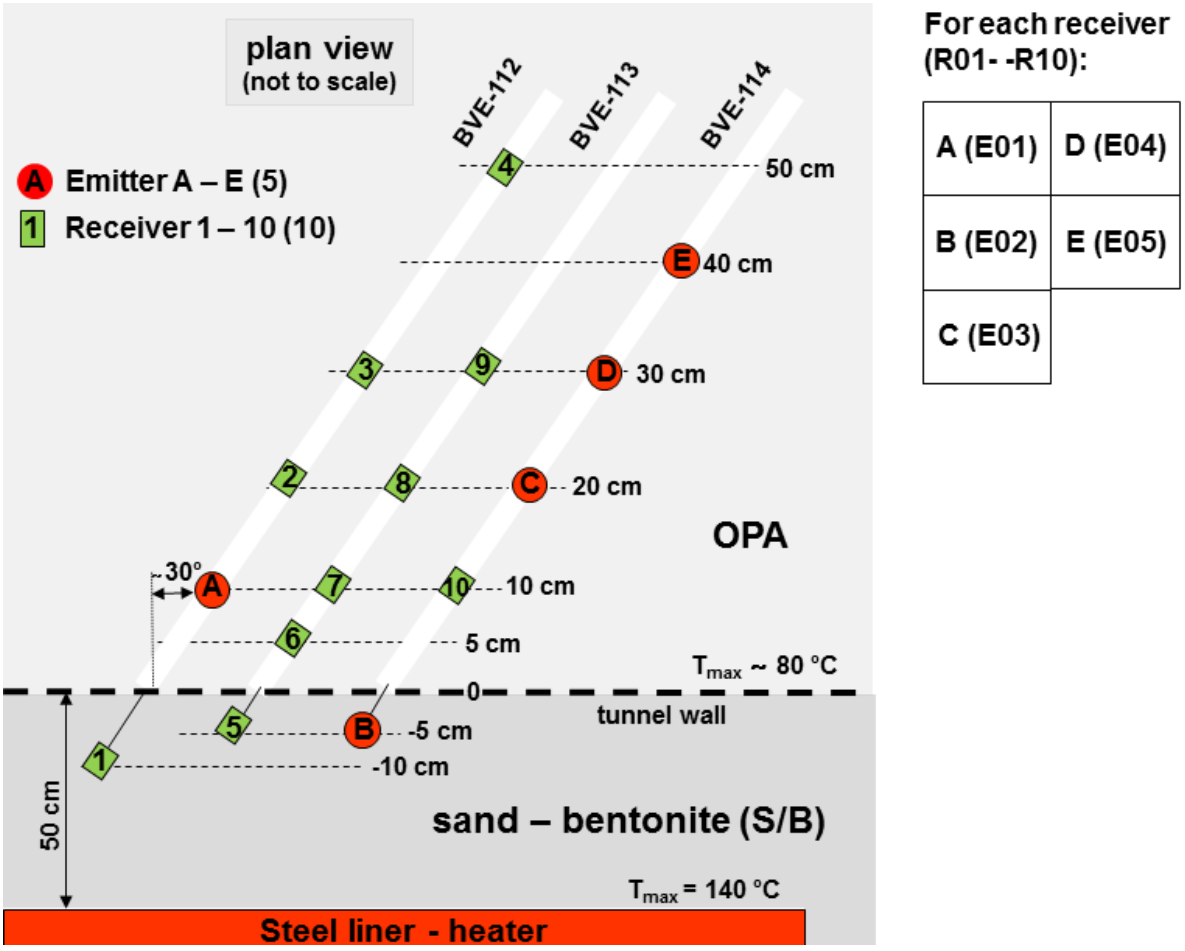

Fig. 10.1 Overview of the locations of five emitters A (E01) – E (E05) and ten receivers (R01 – R10) in three boreholes.

All seismic sections are presented in the following order. They are sorted according to receiver numbers. On each page in the upper part for one receiver all five belonging emitter combinations are displayed in a trace normalized mode. This plot mode allows to assess the

data quality of each seismic trace individually. Below the same data set is plotted in an ensemble normalised mode, which gives access to comparison of selected traces and even of sections among themselves. Additionally, all seismic sections were transformed to their trace spectra and presented on the following pages in an ensemble normalized mode. For all ensemble normalised plots a compromise had to be made concerning the magnification. Nevertheless it can't be excluded that in certain situations one section is overexcited whereas another one is hardly visible. This represents the whole dynamic range.

For a better overview a sketch of the plot order four each sub section is given in Figure 7.1 (upper right side).

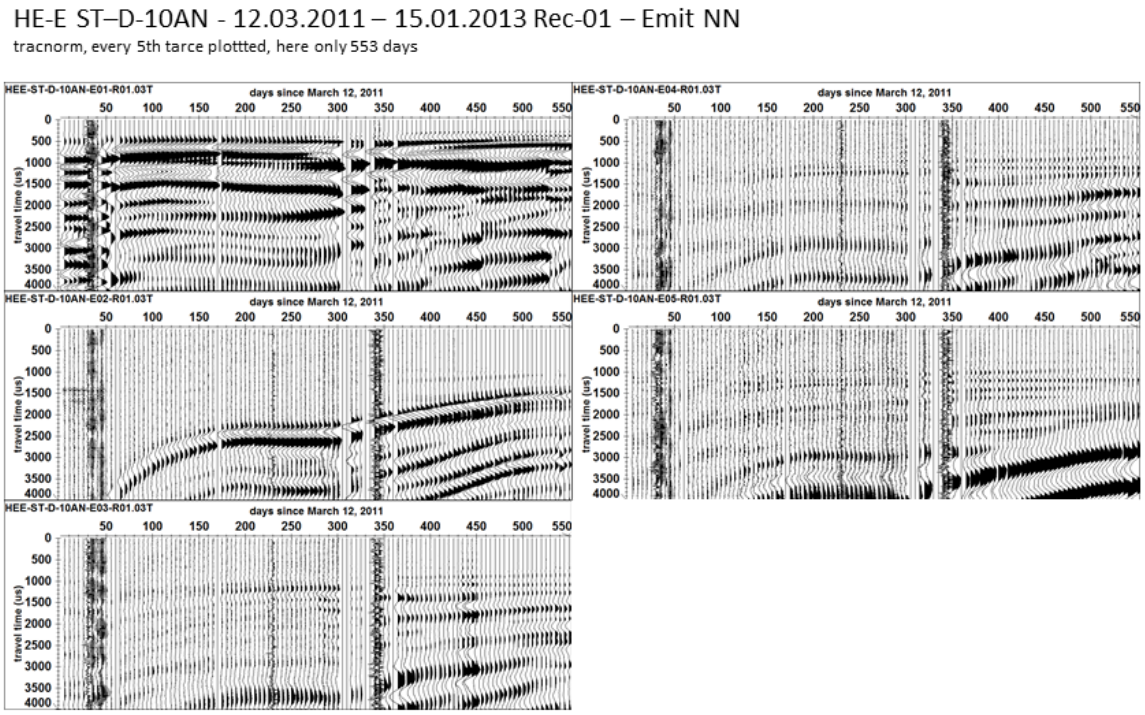

Fig. 10.2 Trace normalised seismic sections related to receiver R01 with five emitters E01 (A) – E05 (E). Only every 5th trace is plotted.

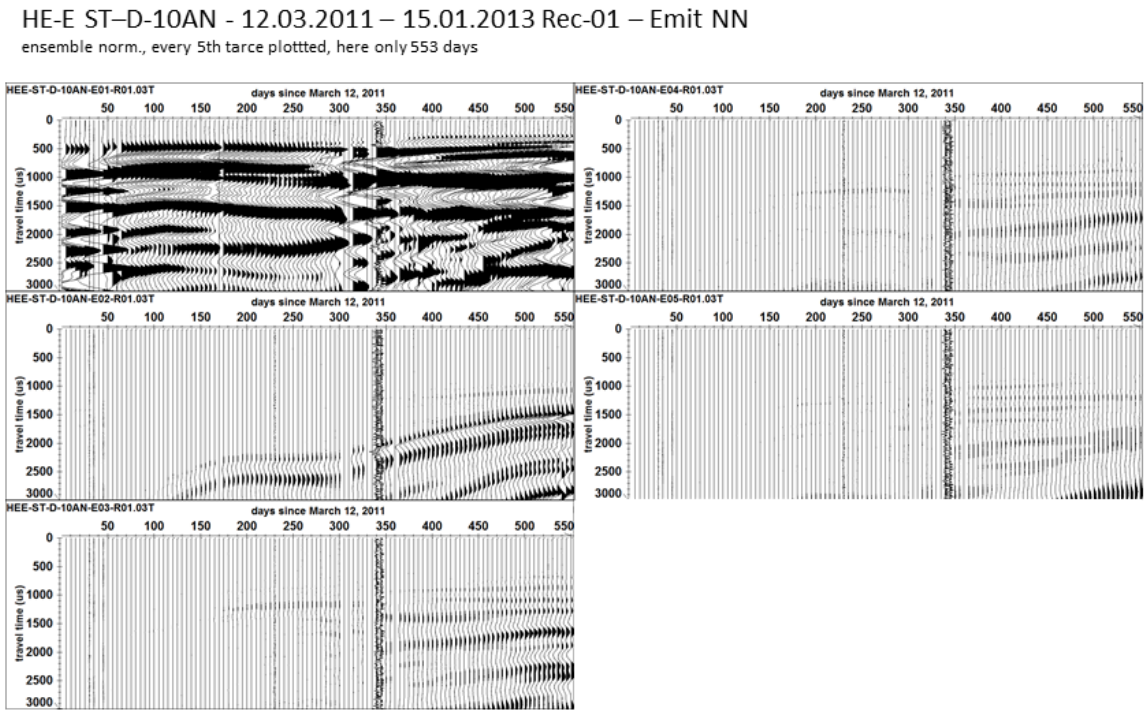

Fig. 10.3 Ensemble normalised seismic sections related to receiver R01 with five emitters E01 (A) – E05 (E). Only every 5th trace is plotted.

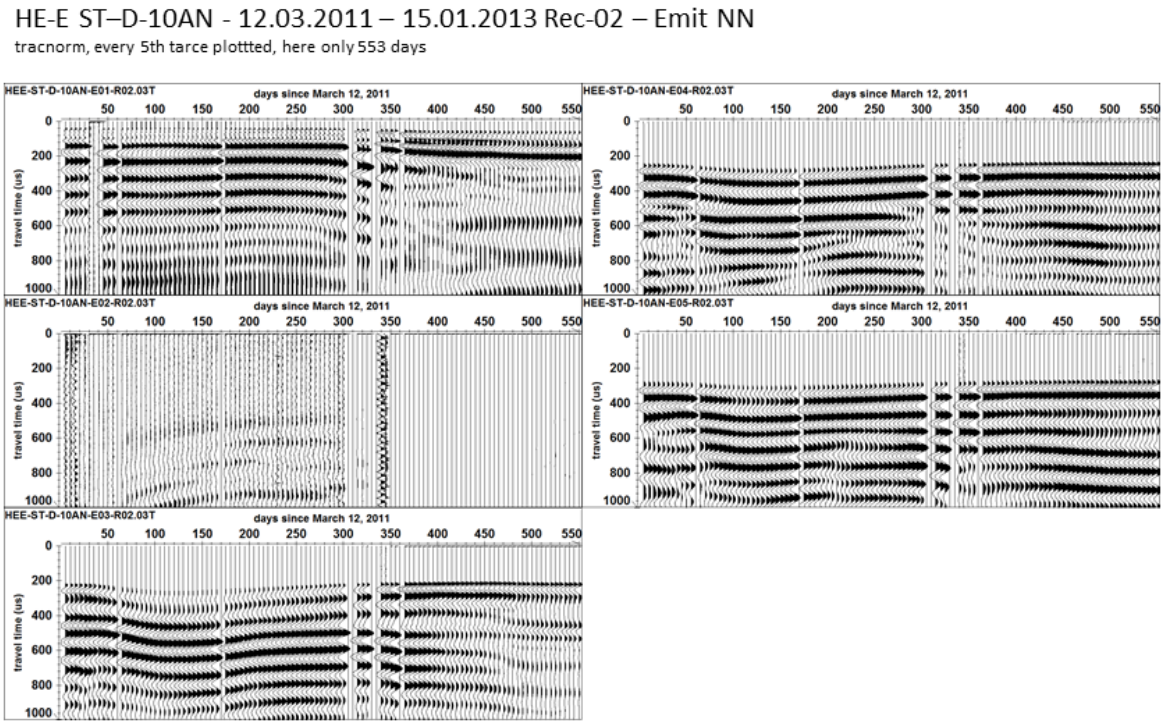

Fig. 10.4 Trace normalised seismic sections related to receiver R02 with five emitters E01 (A) – E05 (E). Only every 5th trace is plotted.

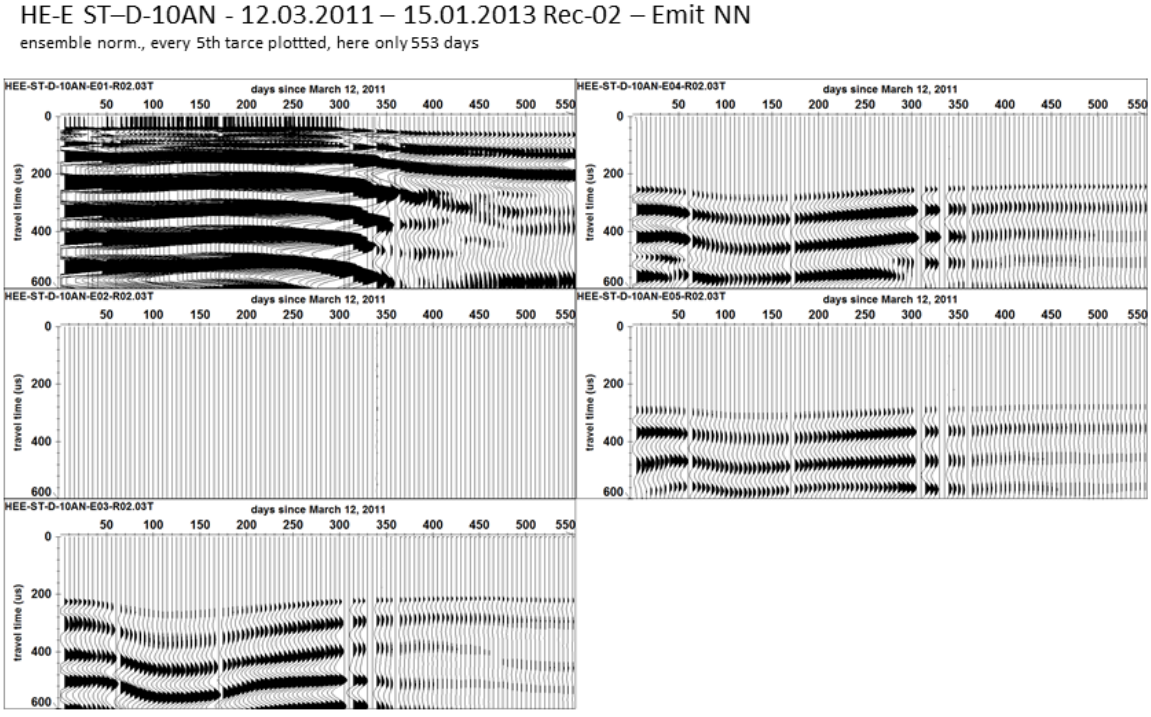

Fig. 10.5 Ensemble normalised seismic sections related to receiver R02 with five emitters E01 (A) – E05 (E). Only every 5th trace is plotted.

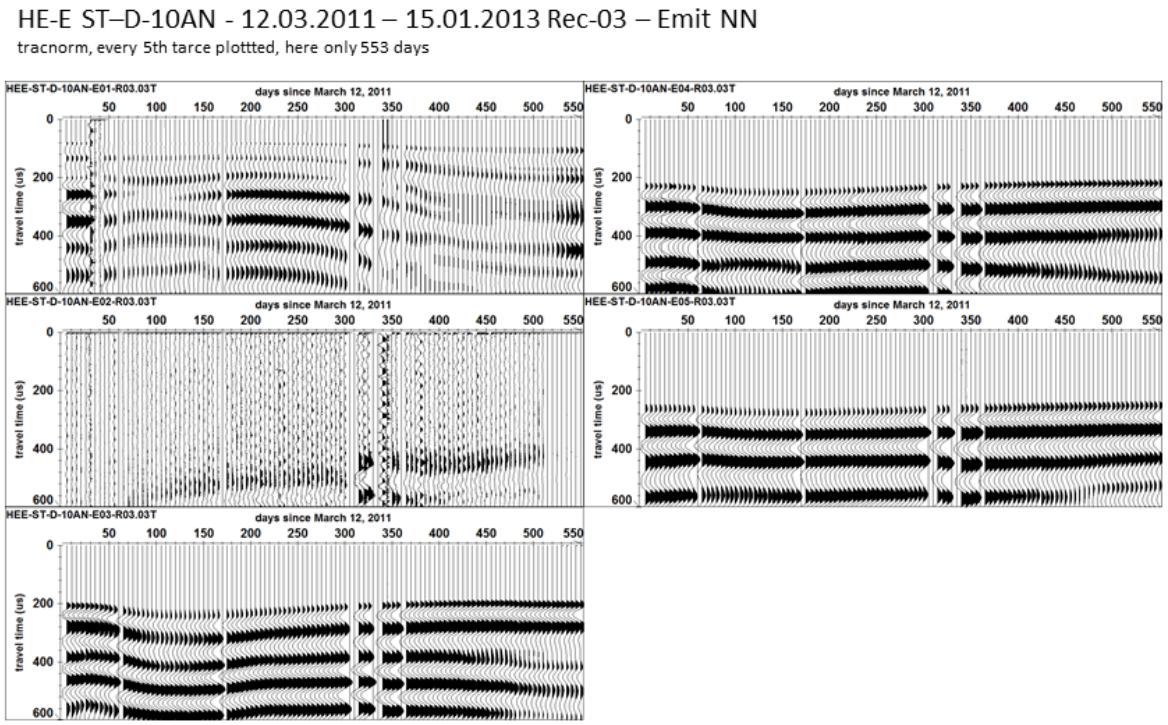

Fig. 10.6 Trace normalised seismic sections related to receiver R03 with five emitters E01 (A) – E05 (E). Only every 5th trace is plotted.

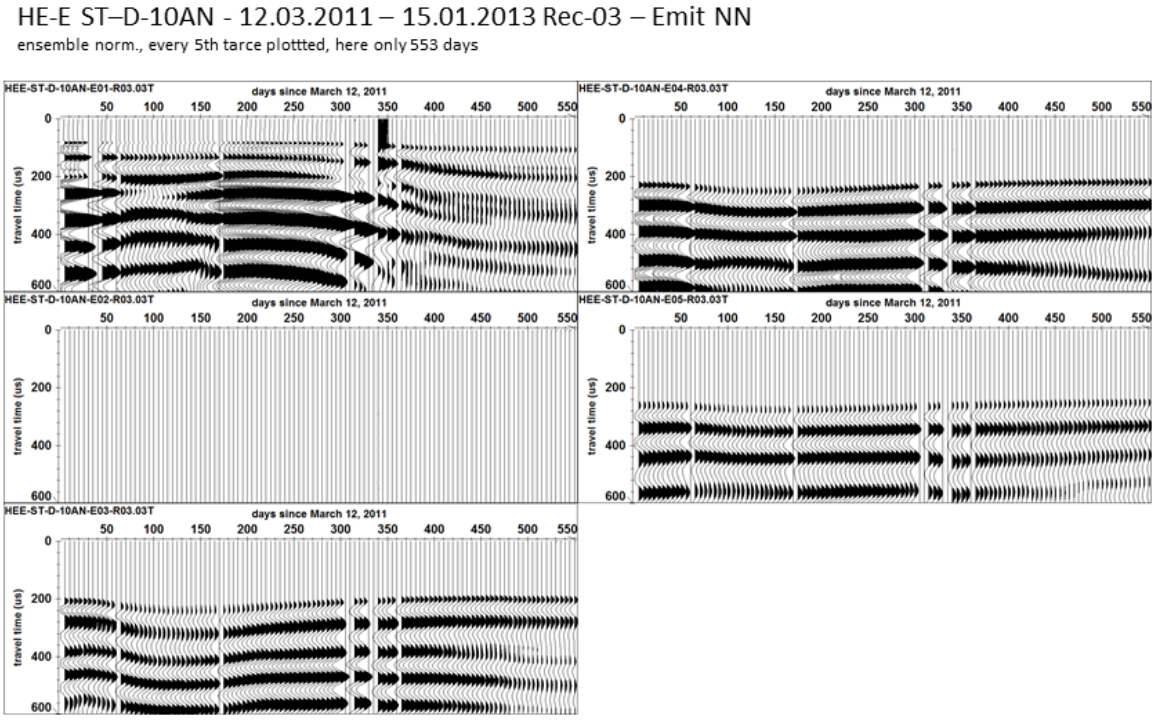

Fig. 10.7 Ensemble normalised seismic sections related to receiver R03 with five emitters E01 (A) – E05 (E). Only every 5th trace is plotted.

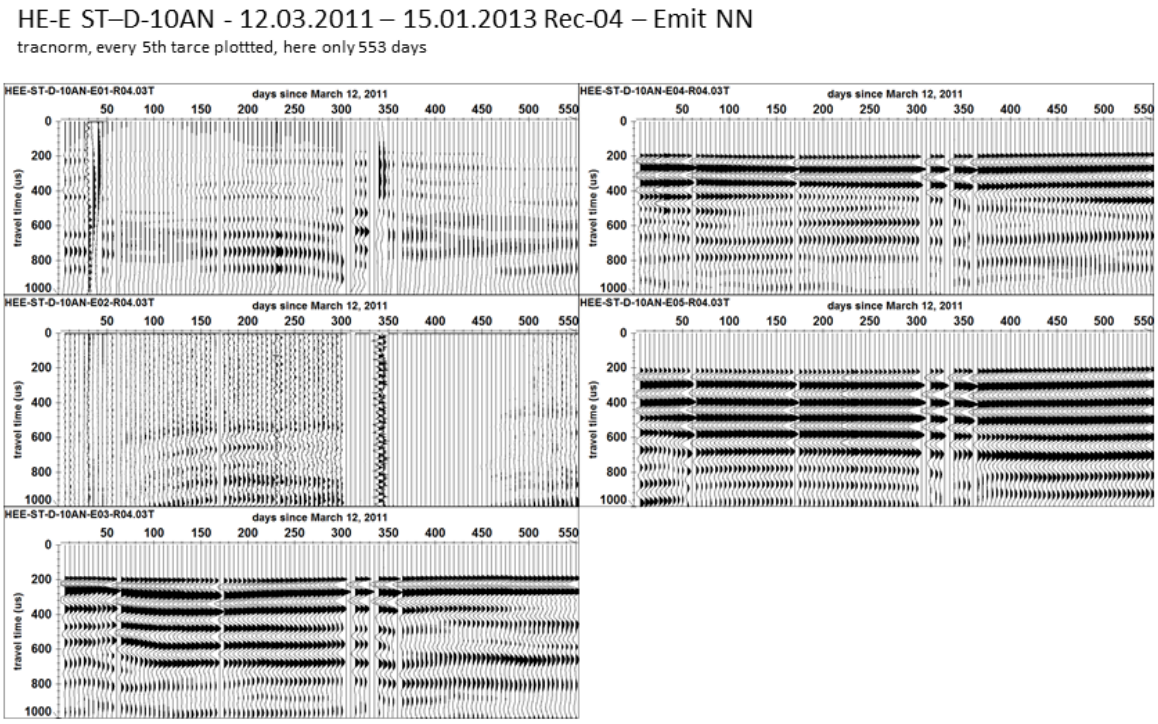

Fig. 10.8 Trace normalised seismic sections related to receiver R04 with five emitters E01 (A) – E05 (E). Only every 5th trace is plotted.

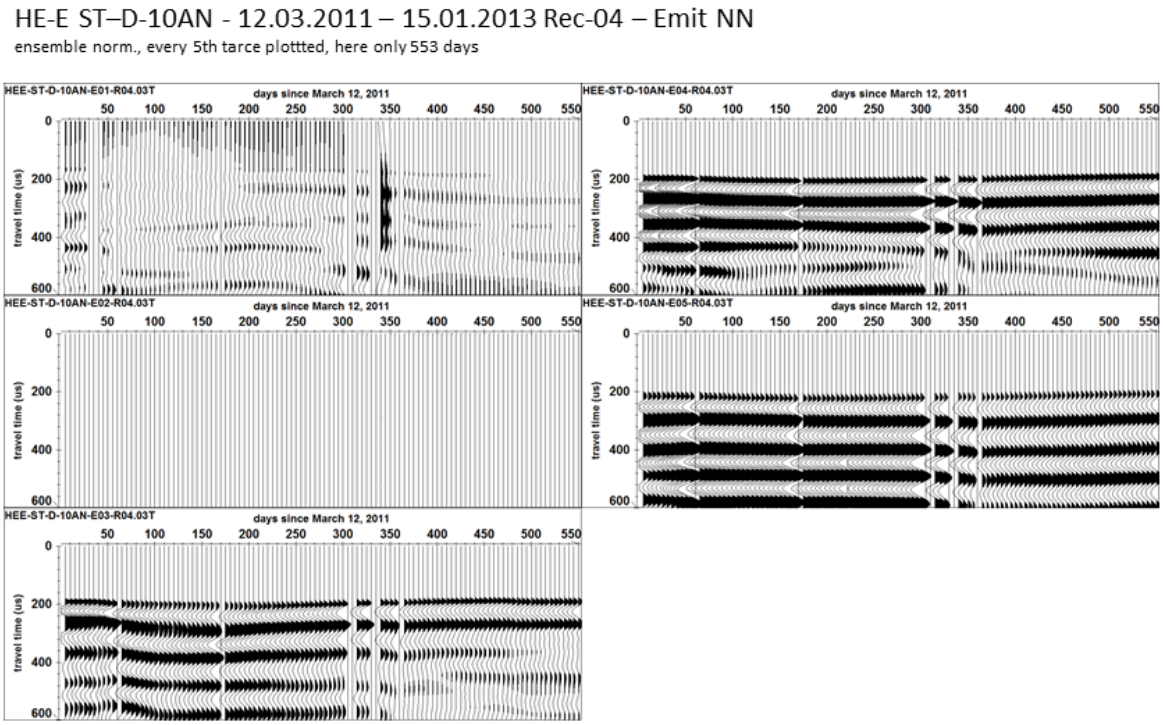

Fig. 10.9 Ensemble normalised seismic sections related to receiver R04 with five emitters E01 (A) – E05 (E). Only every 5th trace is plotted.

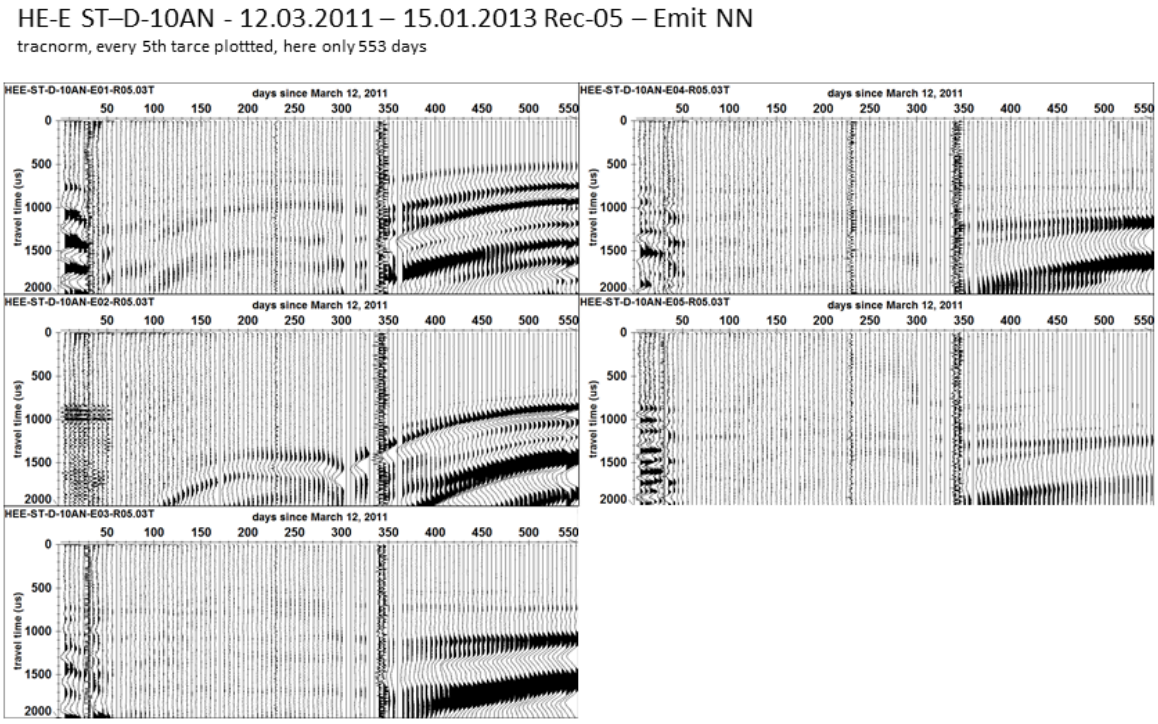

Fig. 10.10 Trace normalised seismic sections related to receiver R05 with five emitters E01 (A) – E05 (E). Only every 5th trace is plotted.

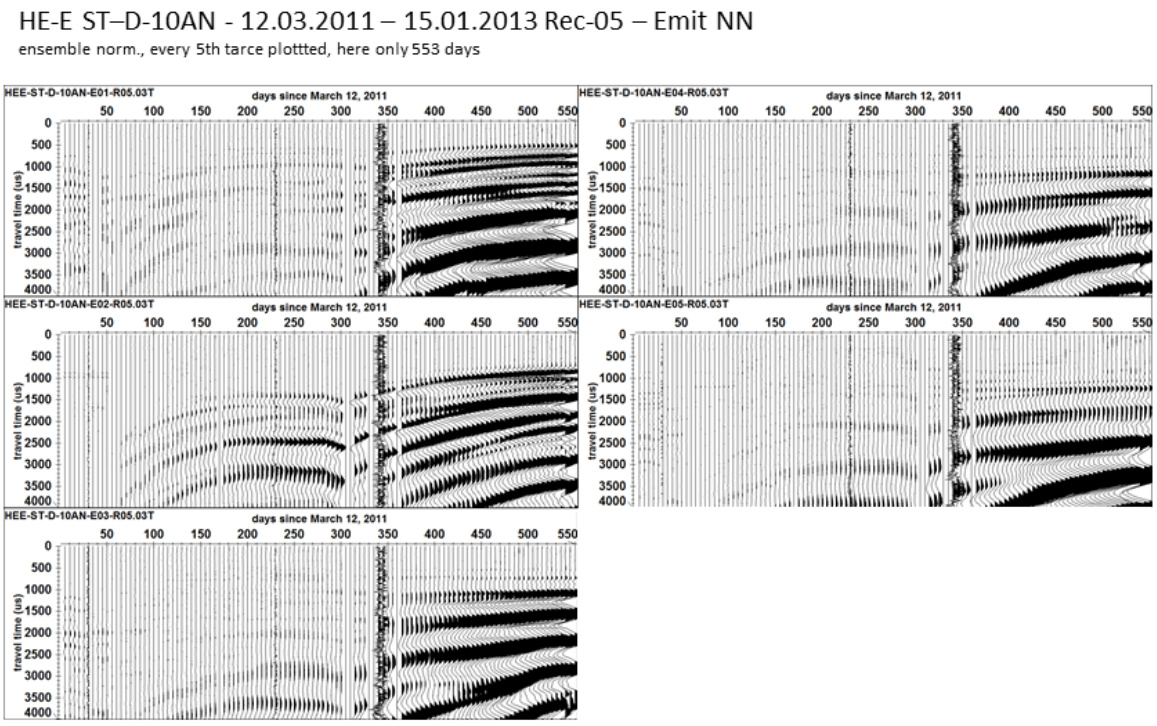

Fig. 10.11 Ensemble normalised seismic sections related to receiver R05 with five emitters E01 (A) – E05 (E). Only every 5th trace is plotted.

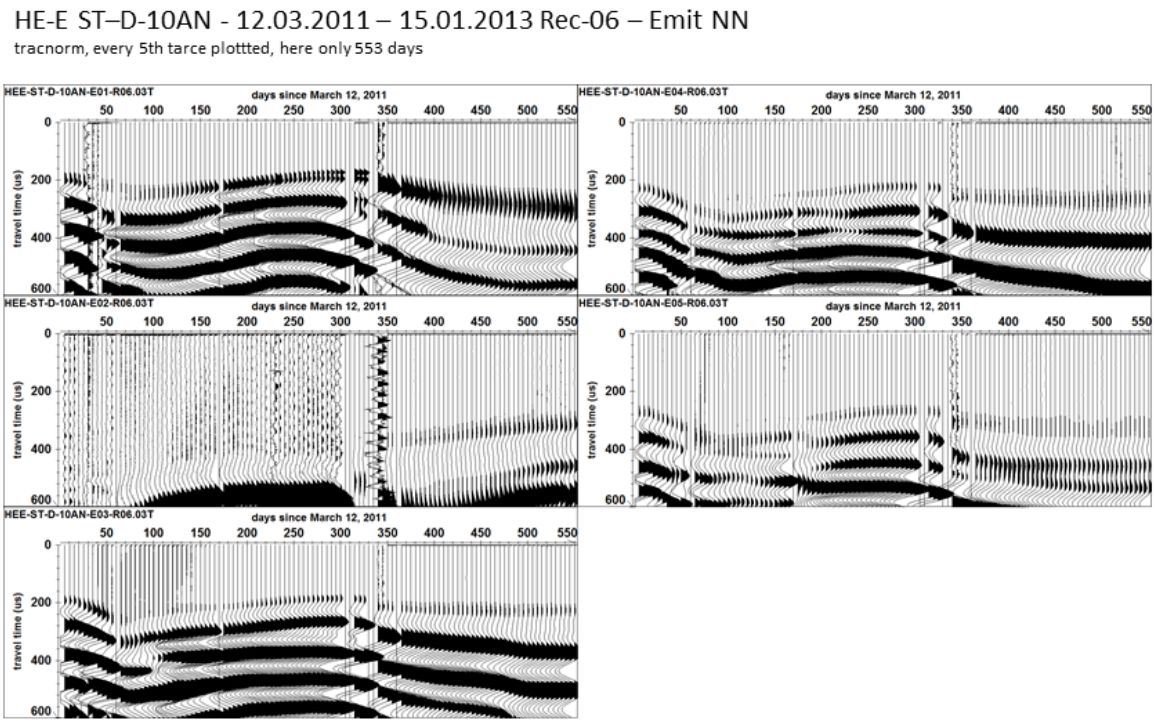

Fig. 10.12 Trace normalised seismic sections related to receiver R06 with five emitters E01 (A) – E05 (E). Only every 5th trace is plotted.

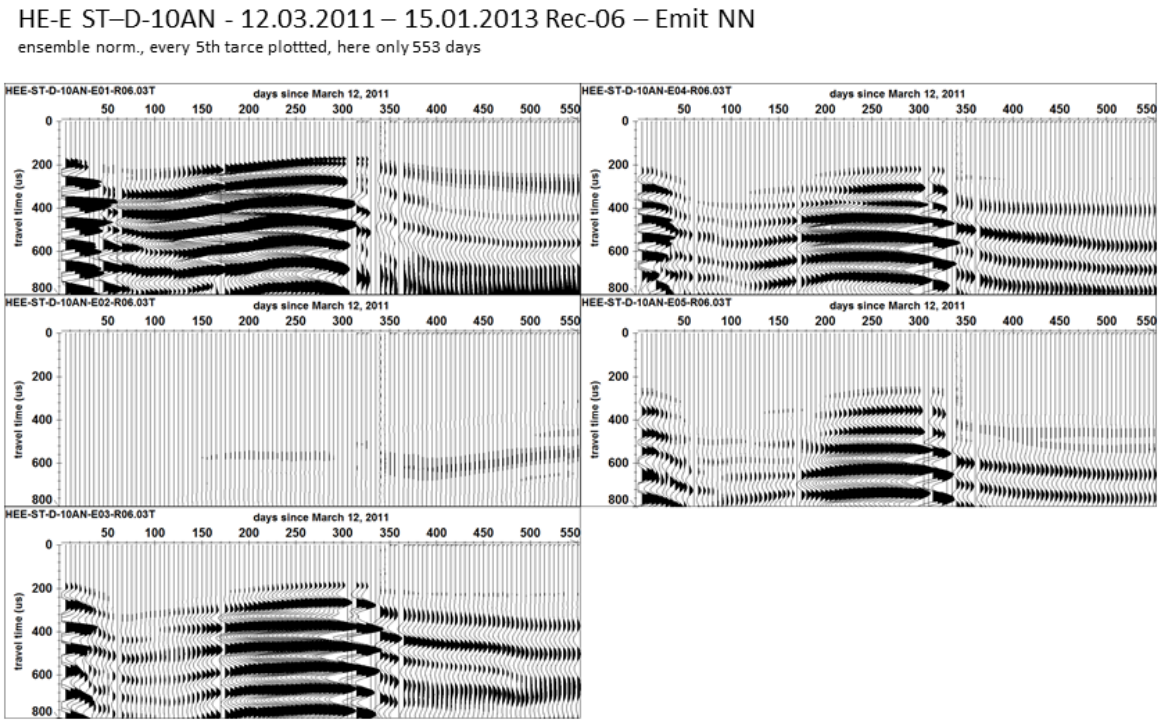

Fig. 10.13 Ensemble normalised seismic sections related to receiver R06 with five emitters E01 (A) – E05 (E). Only every 5th trace is plotted.

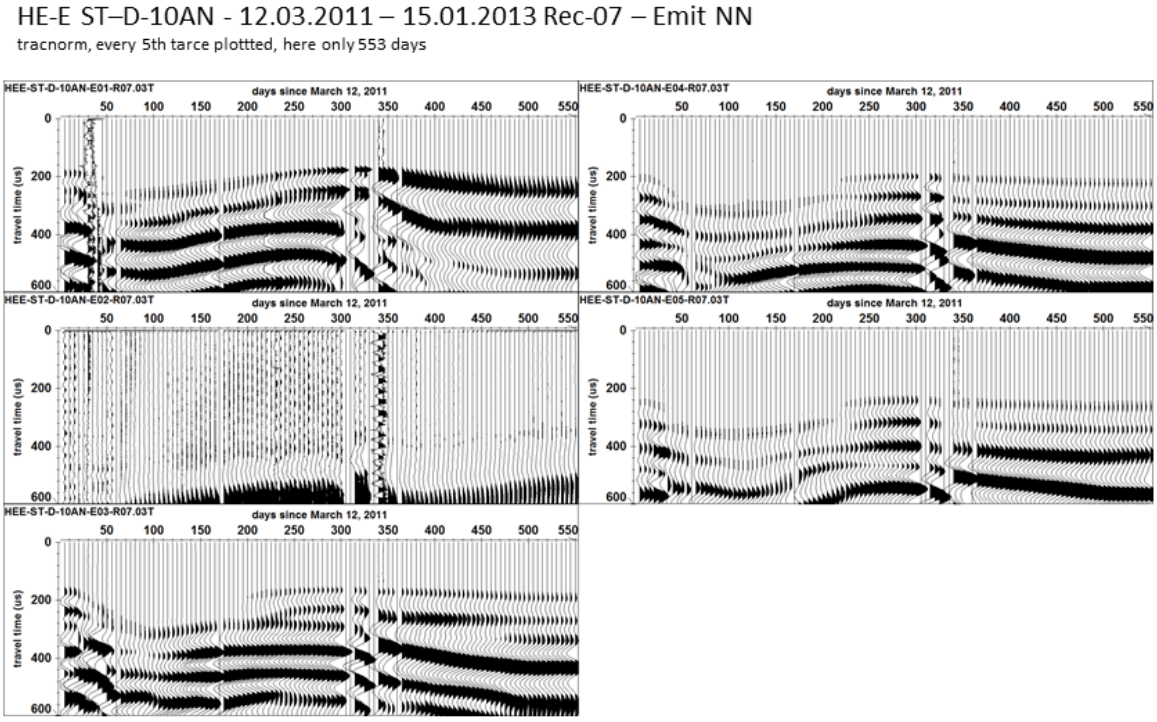

Fig. 10.14 Trace normalised seismic sections related to receiver R07 with five emitters E01 (A) – E05 (E). Only every 5th trace is plotted.

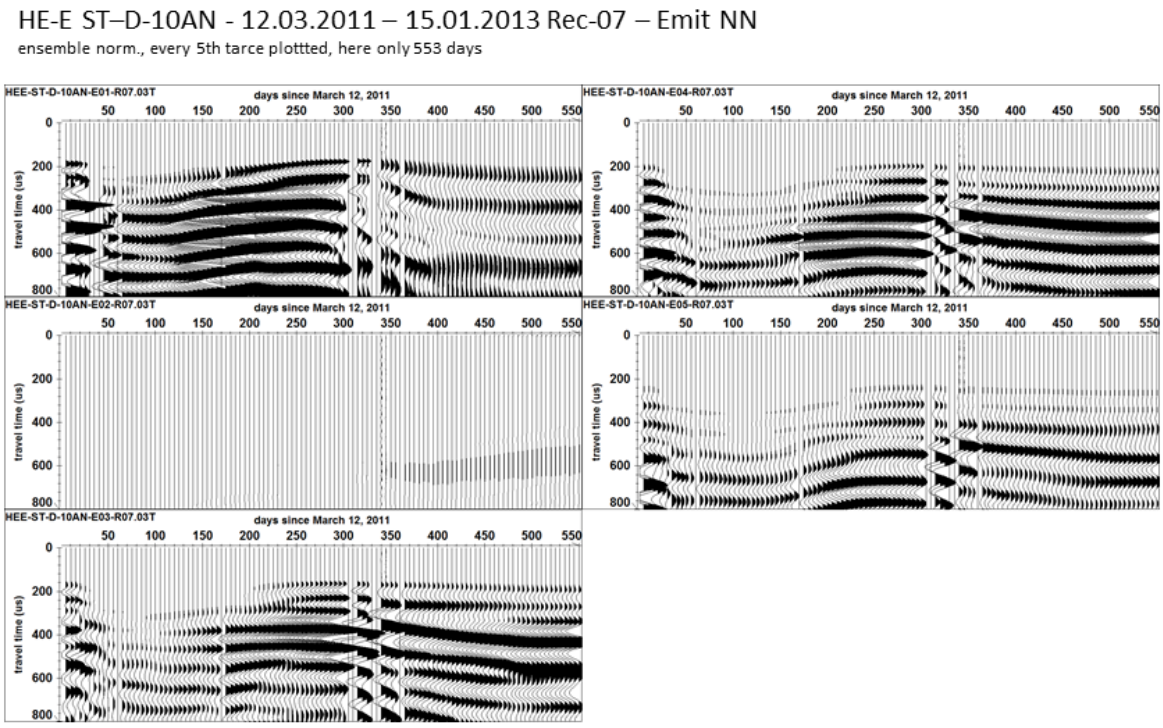

Fig. 10.15 Ensemble normalised seismic sections related to receiver R07 with five emitters E01 (A) – E05 (E). Only every 5th trace is plotted.

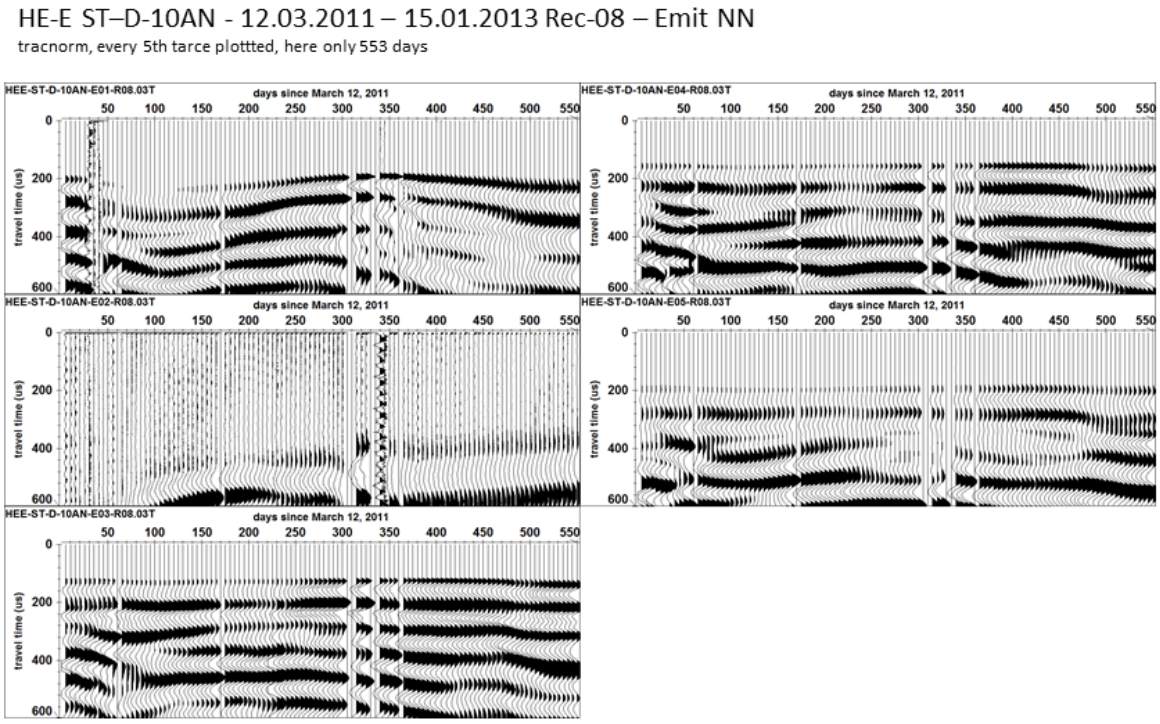

Fig. 10.16 Trace normalised seismic sections related to receiver R08 with five emitters E01 (A) – E05 (E). Only every 5th trace is plotted.

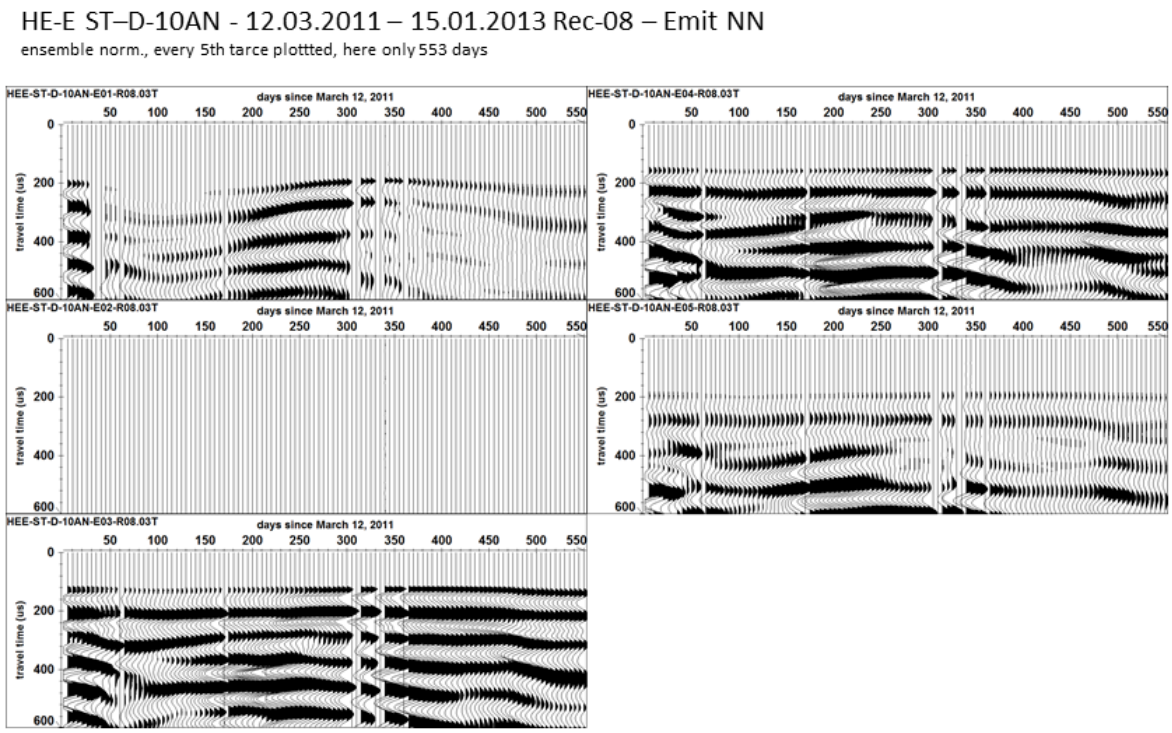

Fig. 10.17 Ensemble normalised seismic sections related to receiver R08 with five emitters E01 (A) – E05 (E). Only every 5th trace is plotted.

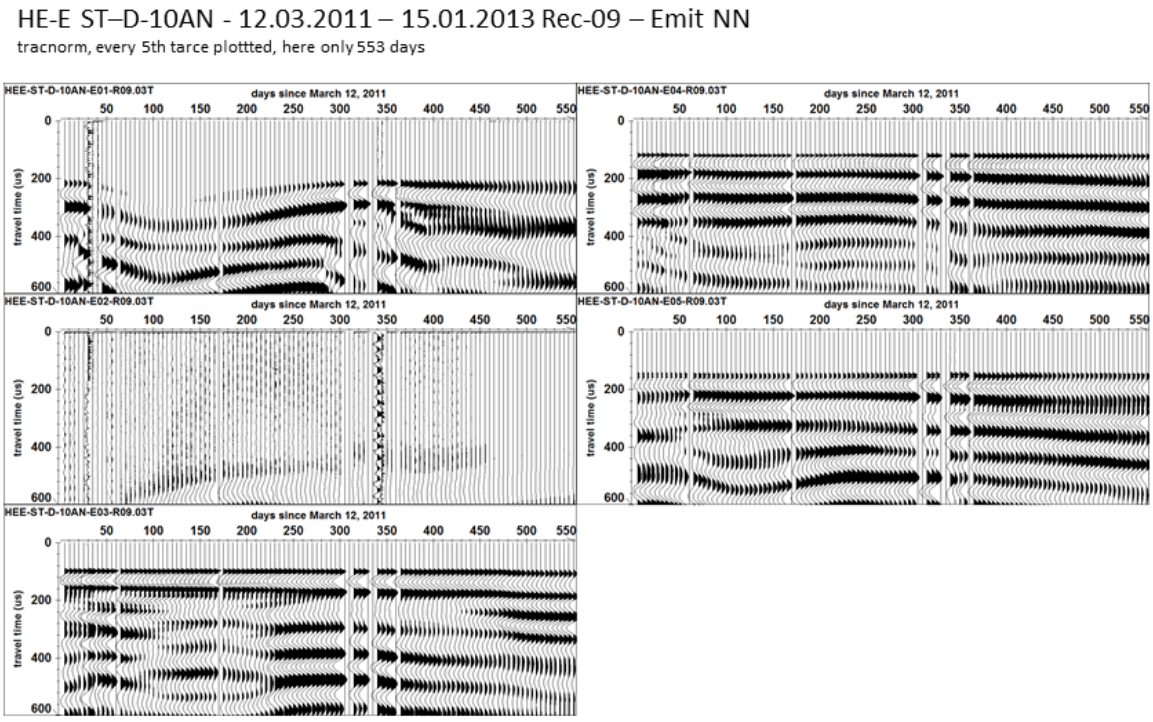

Fig. 10.18 Trace normalised seismic sections related to receiver R09 with five emitters E01 (A) – E05 (E). Only every 5th trace is plotted.

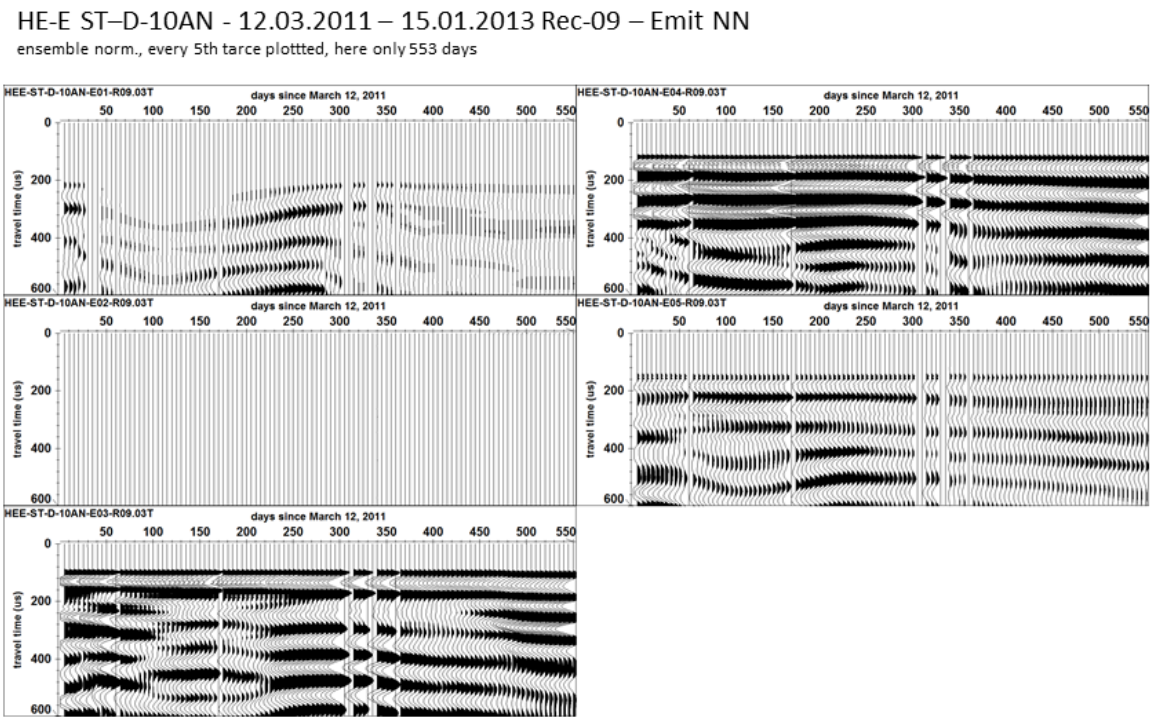

Fig. 10.19 Ensemble normalised seismic sections related to receiver R09 with five emitters E01 (A) – E05 (E). Only every 5th trace is plotted.

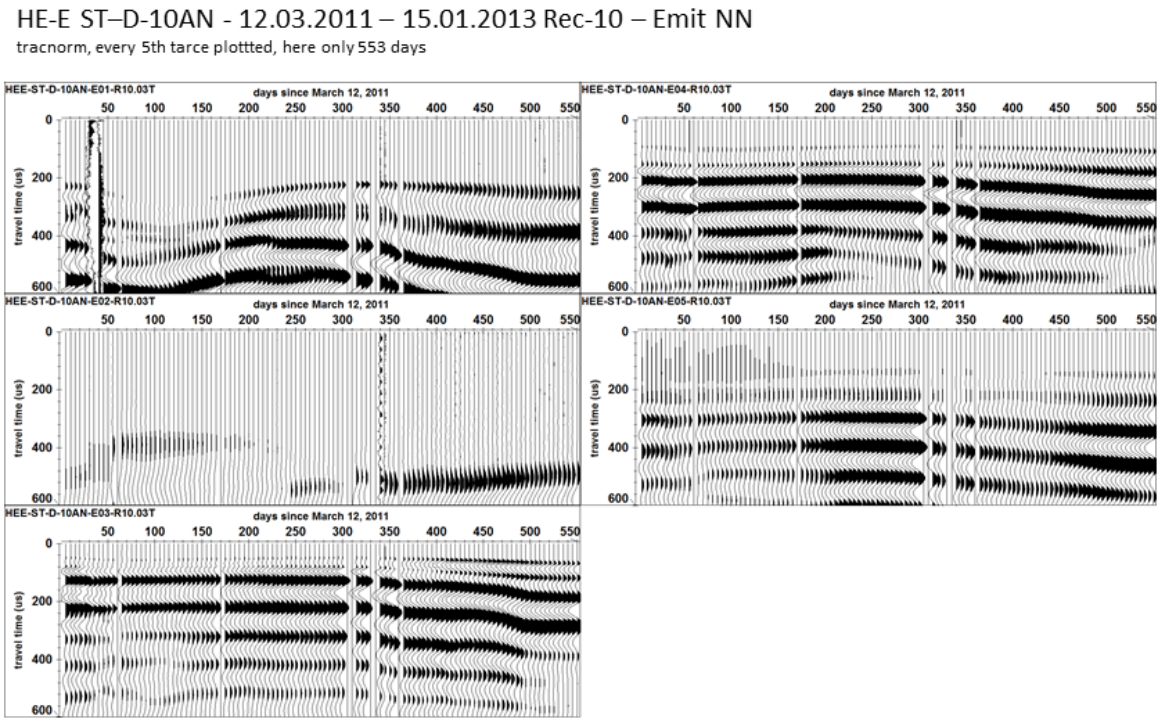

Fig. 10.20 Trace normalised seismic sections related to receiver R10 with five emitters E01 (A) – E05 (E). Only every 5th trace is plotted.

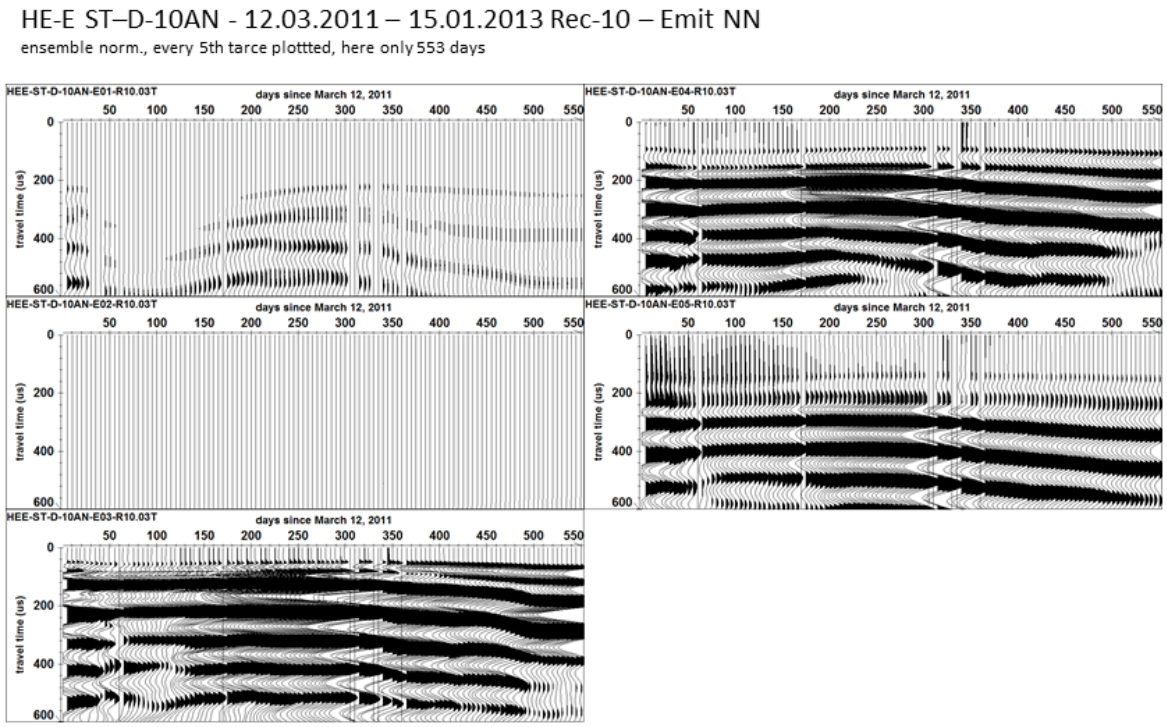

Fig. 10.21 Ensemble normalised seismic sections related to receiver R10 with five emitters E01 (A) – E05 (E). Only every 5th trace is plotted.

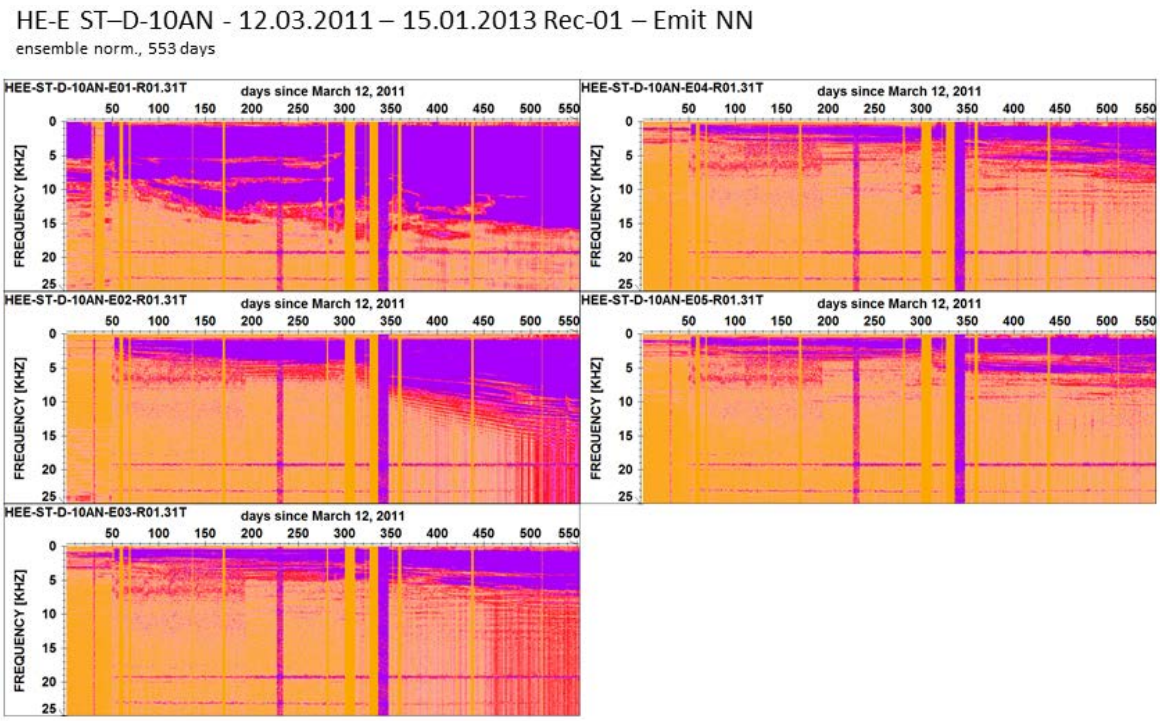

Fig. 10.22 Ensemble normalised trace spectra sections related to receiver R01 with five emitters E01 (A) – E05 (E).

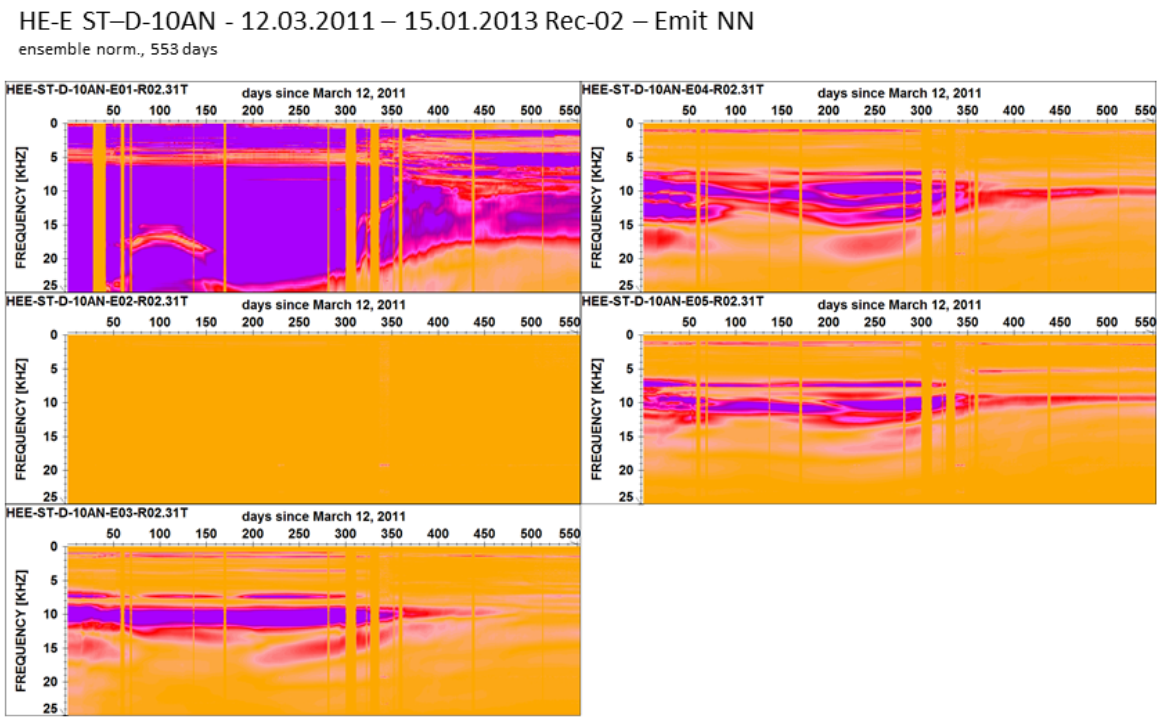

Fig. 10.23 Ensemble normalised trace spectra sections related to receiver R02 with five emitters E01 (A) – E05 (E).

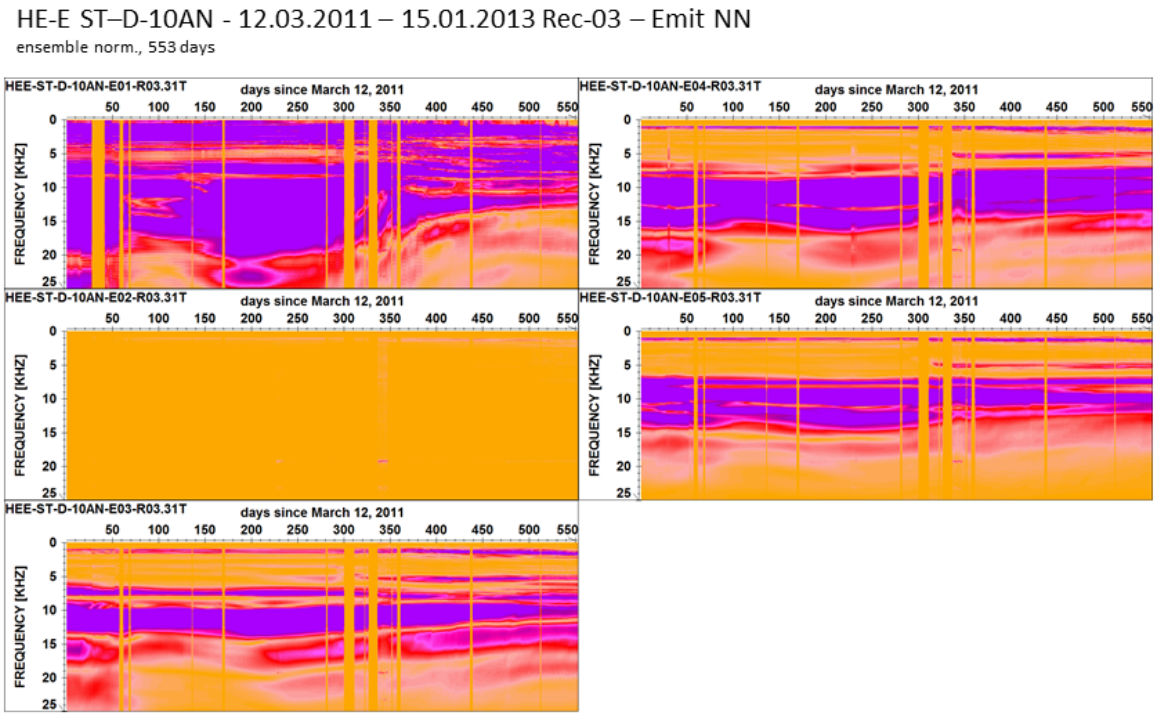

Fig. 10.24 Ensemble normalised trace spectra sections related to receiver R03 with five emitters E01 (A) – E05 (E).

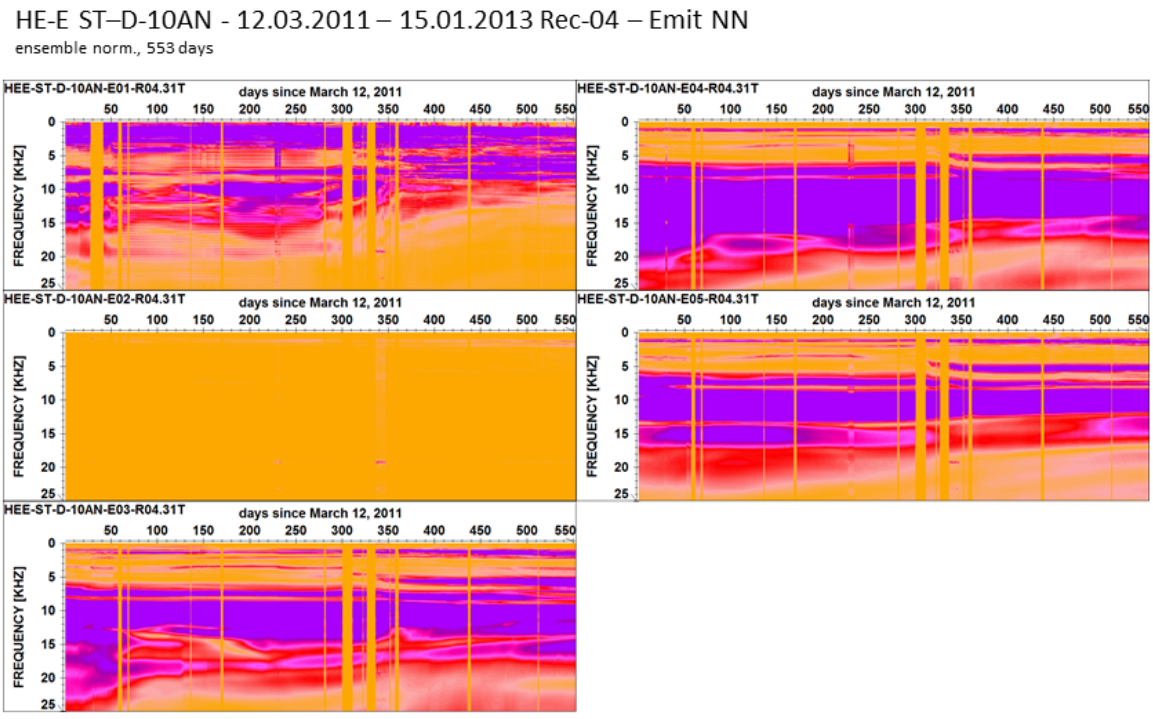

Fig. 10.25 Ensemble normalised trace spectra sections related to receiver R04 with five emitters E01 (A) – E05 (E).

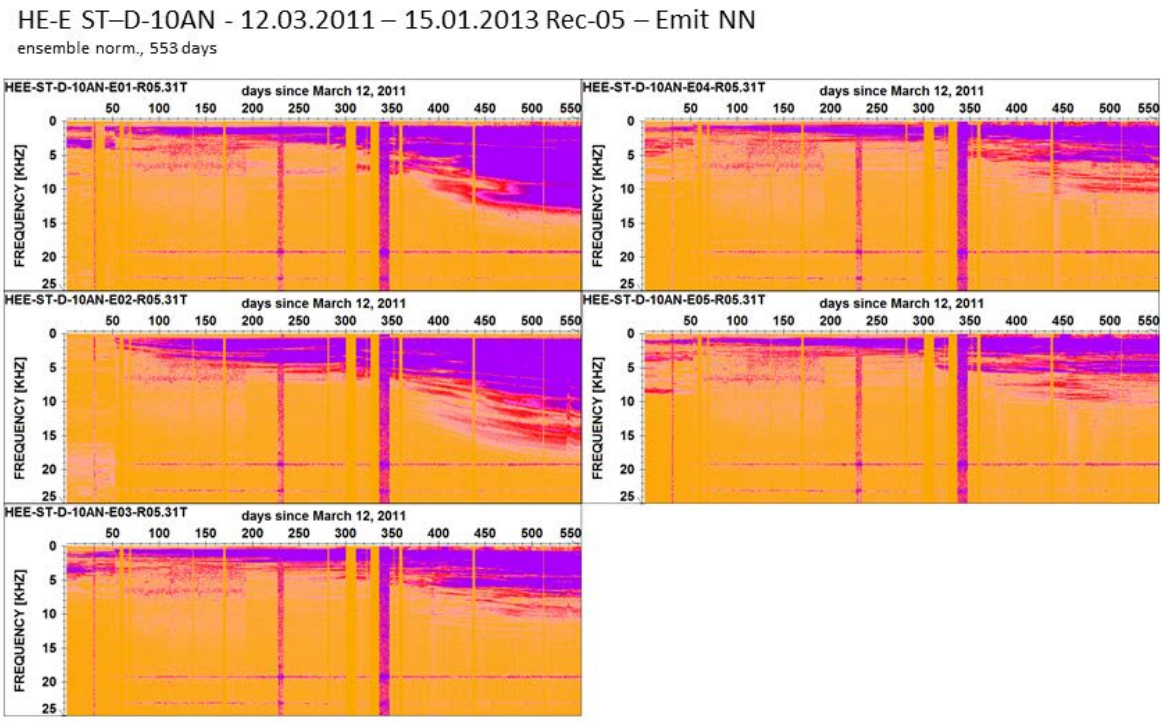

Fig. 10.26 Ensemble normalised trace spectra sections related to receiver R05 with five emitters E01 (A) – E05 (E).

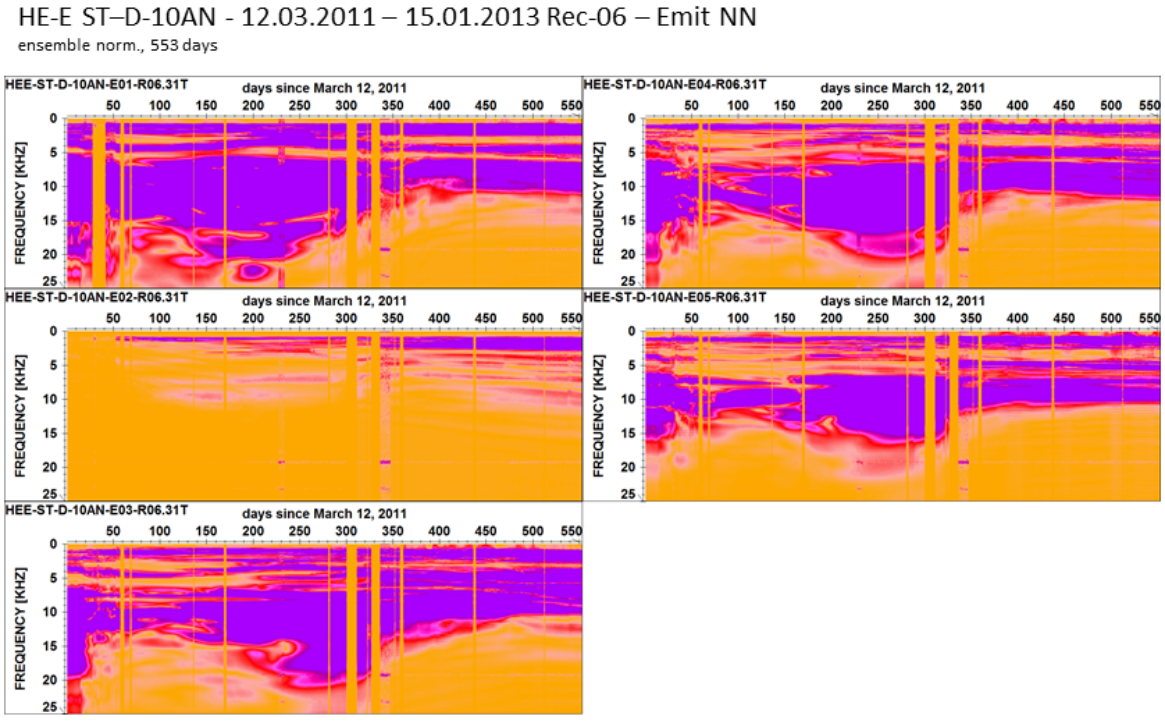

Fig. 10.27 Ensemble normalised trace spectra sections related to receiver R06 with five emitters E01 (A) – E05 (E).

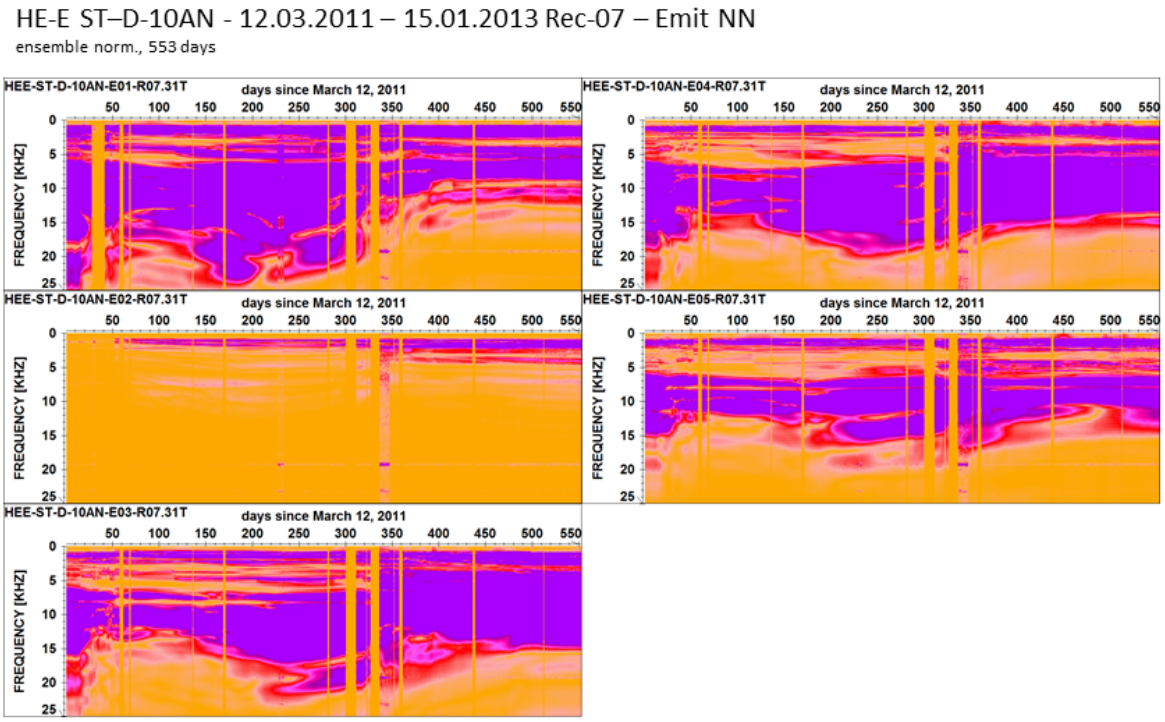

Fig. 10.28 Ensemble normalised trace spectra sections related to receiver R07 with five emitters E01 (A) – E05 (E).

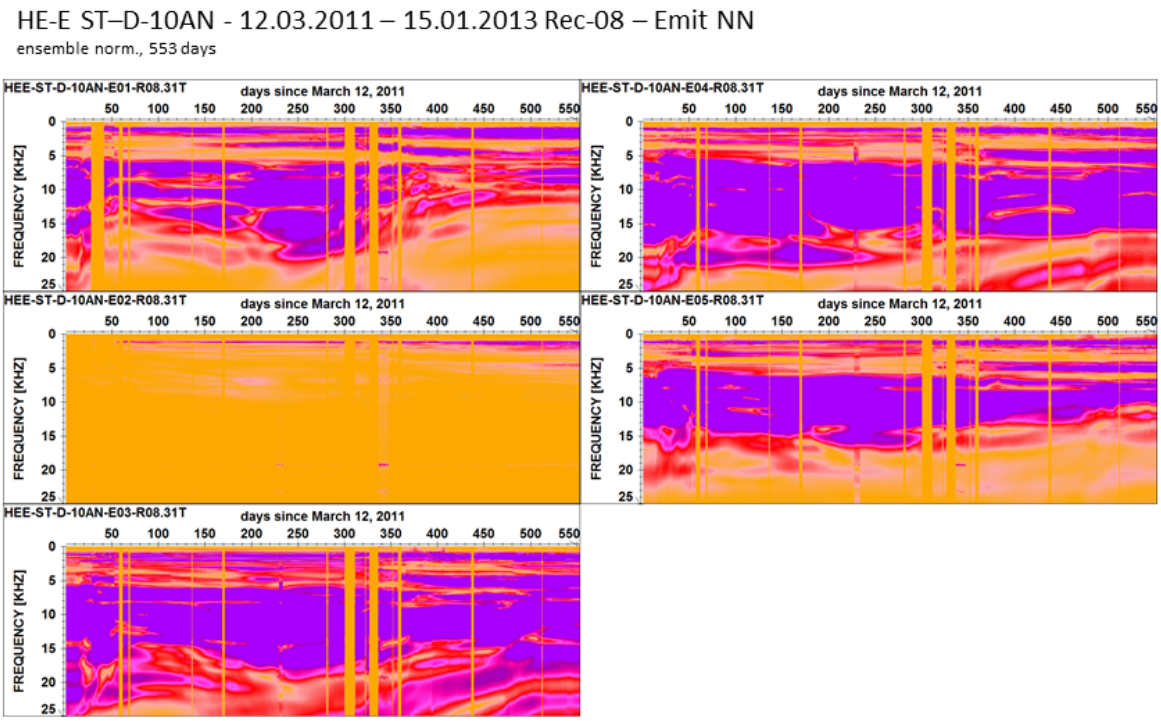

Fig. 10.29 Ensemble normalised trace spectra sections related to receiver R08 with five emitters E01 (A) – E05 (E).

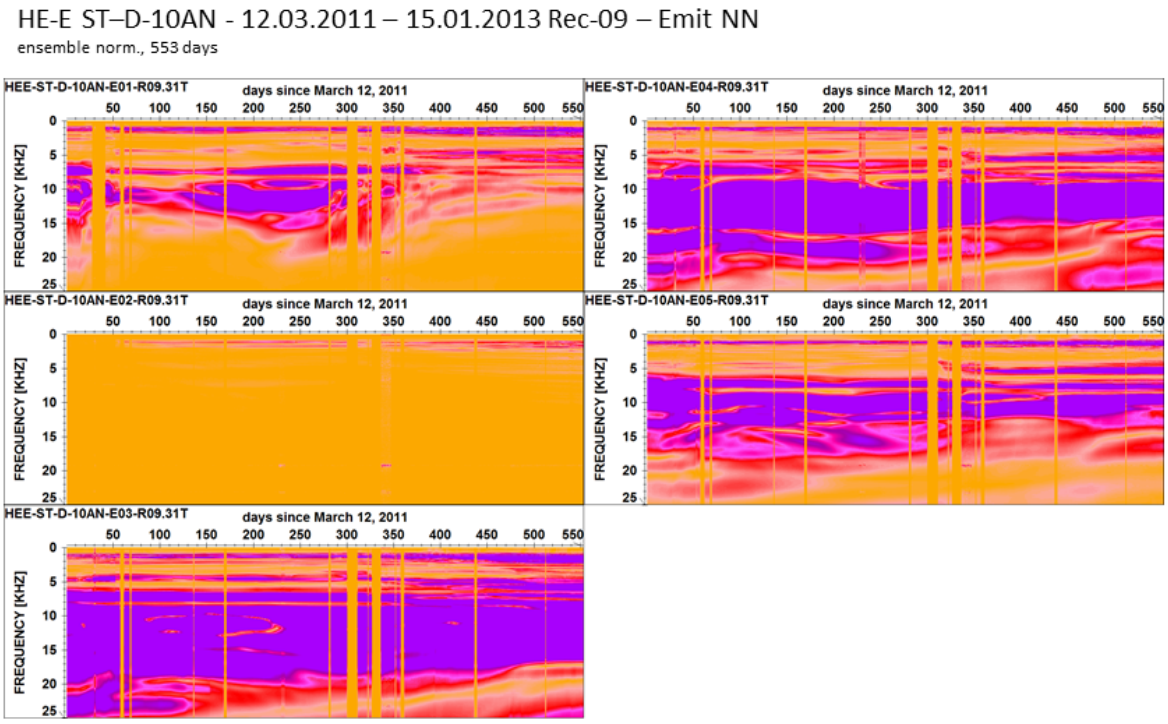

Fig. 10.30 Ensemble normalised trace spectra sections related to receiver R09 with five emitters E01 (A) – E05 (E).

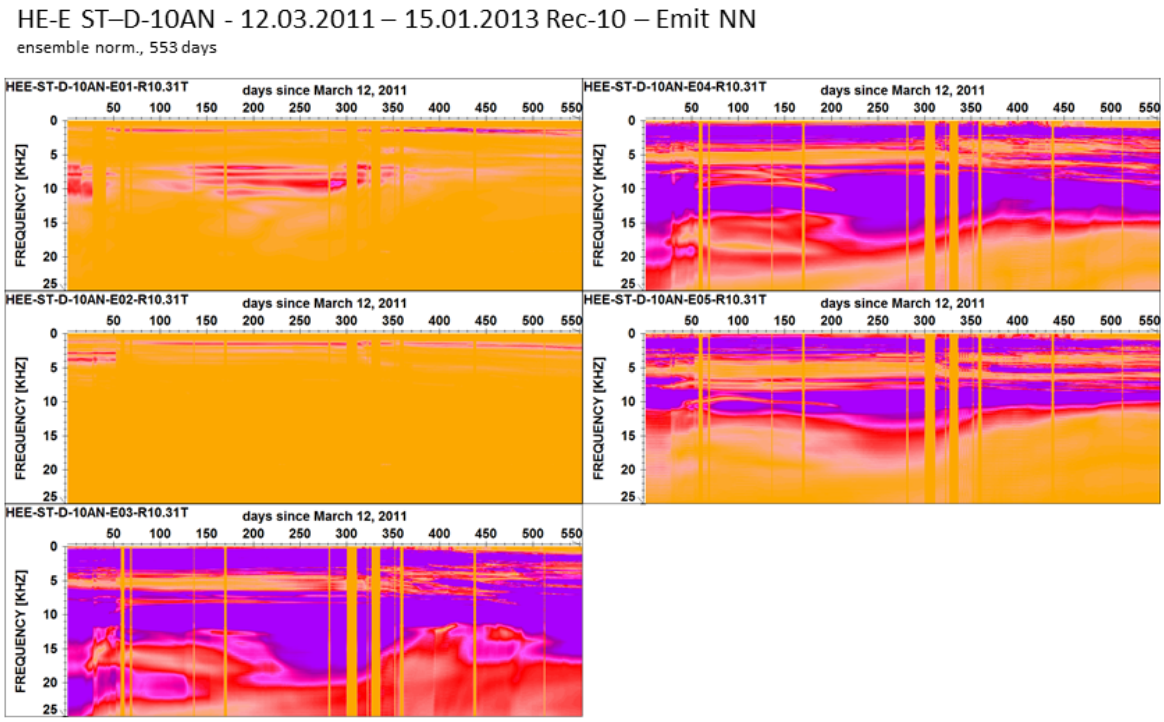

Fig. 10.31 Ensemble normalised trace spectra sections related to receiver R10 with five emitters E01 (A) – E05 (E).

11 Appendix II – Data Report in German – Stichpunktartige Protokollierung der Messungen von Thomas Fischer (GMuG)

HE-E Seismik, Mt.Terri, 2011 - 2013

Stichpunktartige Protokollierung der Messung

Author: Thomas Fischer

6. November 2013

GMuG Gesellschaft für Materialprüfung und Geophysik mbH * D-61231 Bad Nauheim

1 Beschreibung HE-E Seismic

Messanlage

Anlage für 16 Empfänger und 8 Sender
16 Kanal A-D-Wandler, 16 Bit @500kHz (dt=2us)
Elektrische Quelle: Impulsgenerator mit Relais-Umschaltung
Sonden: 15 Stück, piezoelektrisch, je 5 in einem Strang, pneumatische Ankopplung
10 Empfänger (Kanal 01 bis 10)
5 Sender (A bis E)
Verstärkungsfaktoren:
Empfänger : 40dB (30dB Vorverstärker + 10dB) + 1kHz Hochpass
Sendesignal: -40 dB , Aufzeichnung via unkompensiertem Teiler auf Kanal 11

Durchschallungsmessung

Startzeitpunkt der täglichen Messung: 01:10 Uhr
Dauer (alle Sender): ca. 50 Minuten
Je Sender: 2048 fache Wiederholung / Stapelung
Aufnahmedauer je Kanal: 32.4 ms bzw. 16384 Samples
Pretrigger: 20% (Nullpunkt-Sample = 3280)

Die Parameter wurden so gewählt, dass sowohl das gesamte Sendesignal aufgezeichnet wird als auch die hohe Empfängeramplitude bei Down-Hole Geometrie abgeklungen ist. Die Aufnahmedauer ist daher im Vergleich zu den Laufzeiten (Laufwege < 1m) sehr lang.

Impulsgenerator

Der Impulsgenerator liefert eine sägezahnförmige Ausgangsspannung mit einstellbarer Maximalamplitude für die Sende-Sonden. Der Spannungsverlauf beginnt bei 0 V und steigt linear in einigen Millisekunden auf den Maximalwert an. Dann erfolgt der Sprung zurück auf 0 V. Dies ist der zeitliche Nullpunkt der Messung. Nach dem Austausch des Impulsgenerators im Januar 2012 durch ein nicht ganz identisches Modell (der lineare Anstieg des Sendesignals ist von ca. 5 ms auf ca. 7 ms verlängert) wird der Beginn des Sendesignals nicht mehr aufgezeichnet. Die Einstellung des Pretiggers blieb konstant bei 20% und es werden manuell Kontrollmessungen mit 25% Pretrigger durchgeführt, um zumindest einige Aufnahmen mit dem gesamten Sendesignal zu haben.

Die Maximalamplitude war beim ersten Impulsgenerator auf ca. 100V eingestellt, beim zweiten nominal auf ca. 130 V. Während der erste Impulsgenerator eine relativ konstante Ausgangsspannung lieferte, zeigt der zweite einen kontinuierlichen Abfall der Ausgangsspannung - außer bei Sender B (im verfüllten Bereich). Die Ursache für den Abfall ist unbekannt (Nach dem Ohm'schen Gesetz muss die Ausgangsspannung sinken, wenn der Generator nicht genug Strom liefern kann bzw. der Innenwiderstand steigt entsprechend an). Der zeitliche Verlauf der Generator-Maximalspannung an den Sendesonden ist in **Abbildung 1** zu sehen. Weitere Einzelheiten zum Sendesignal sind in im Kapitel 'Datenbeispiele' unter 'Vorläufer Signal bei Down-Hole Messungen' zu finden.

Akustische Emission (AE)

Wenn keine Durchschallungsmessung ausgeführt wird, ist das AE Monitoring aktiv. Diese Messung ist nicht Teil der Beauftragung, wird aber dennoch durchgeführt. Die eingesetzten Messgeräte sind

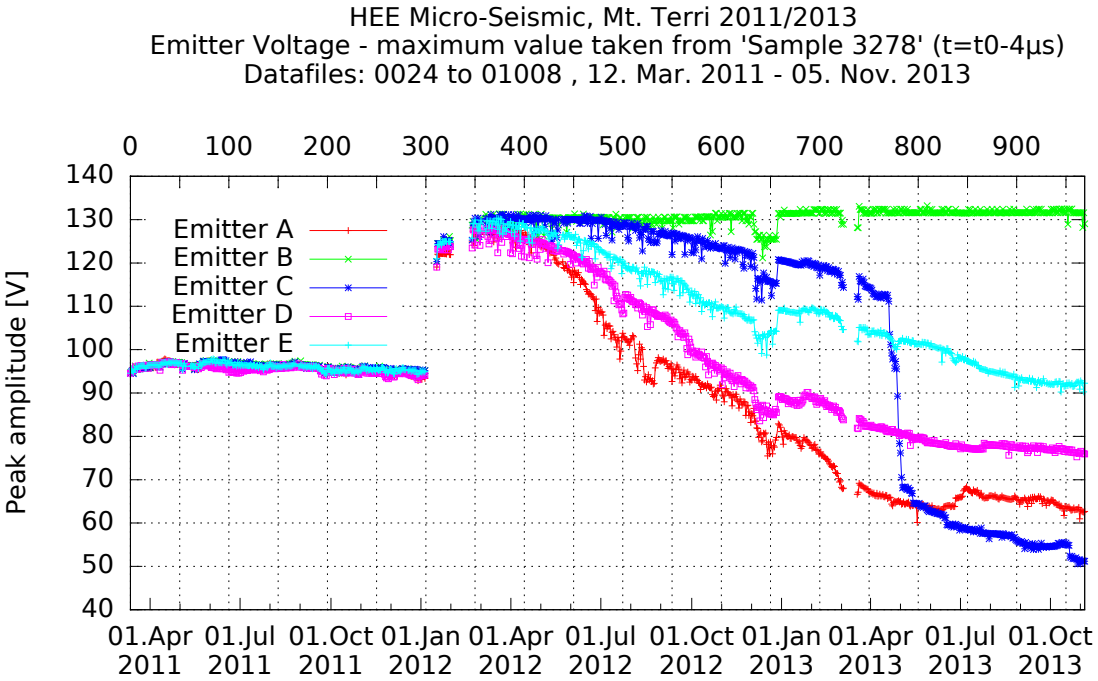

Abbildung 1: Änderung der Generatoramplitude an den Sendern.

prinzipiell auch für die AE Messung geeignet, allerdings ist das Empfänger-Layout nicht für diesen Zweck ausgelegt.

Elektrische Einstreuungen und andere Störgräusche erschweren die Messung und reduzieren die Empfindlichkeit, da der Triggerlevel entsprechend angehoben werden muss. Die Aufzeichnung erfolgt im +/- 1V Messbereich, gelegentlich sind einige Signale übersteuert. Die Trigger- bzw. Ereignisstatistik ist in **Abbildung 7** gezeigt. Die Ereignisraten sind gering, deutlich unter 10 pro Tag. Mit einer Triggerschwelle von 8-10% (Juli 2012 bis März 2012) wurden sogar nur alle paar Tage einzelne AE Ereignisse registriert. Maxima in der Trigger-Statistik - mit mehr als 50 Ereignissen pro Tag - sind meist durch plötzlich auftretende elektrische Störimpulse verursacht. Seltener, hauptsächlich im Zeitraum Mai bis Juni 2011, werden hohe Ereignisraten durch mechanische Anregung verursacht, z.B. durch Bauarbeiten oder große Maschinen.

Das an der Registrieranlage gemessene breitbandige Grundrauschen besitzt eine Amplitude von etwa +/- 3mV, kann aber an einzelnen Tagen auch auf ca. +/- 10mV steigen. Wegen elektrischer Störimpulse, die seit dem Beginn der Erhitzung auftreten, musste der Triggerlevel der AE Messung deutlich erhöht werden.

Bisher ist nicht klar, ob die wenigen registrierten akustischen Ereignisse einen natürlichen Ursprung haben. Häufig sprechen auch nur die Empfänger in einem Sondenstrang an, und an den beiden anderen Sondensträngen ist kein Signal zu beobachten.

Zeitplan AE Monitoring:
01. März 2011 - 30 Juli 2012: täglich 19:00 - 05:00 Uhr
Ab 31. Juli 2012 : permanent / ganztägig
Triggerlevel:
März 2011 - Juni 2011 : 3% (1V)
Juli 2011 - März 2012 : 8-10% (1V)
April 2012 - Juli 2012 : 3% (1V)

Ab Aug. 2012 : 4-6% (1V)

Umgebung

Im Felslabor Mt. Terri wird eine Vielzahl von Versuchen durchgeführt. Einwirkungen von notwendigen Arbeiten und Abläufen auf das Messsystem sind unvermeidlich. Ebenso mechanische und besonders elektrische Wechselwirkungen mit anderen Versuchen. Der Einfluss von Störgeräuschen auf die seismische Messung ist begrenzt, da ein Mittelwert aus 2000 Einzelmessungen gebildet wird. Eine einzelne seismische Messung kann durchaus stärkere Störungen aufweisen. Bei der AE Messung muss gegebenfalls der Triggerlevel angepasst werden, was eine häufige Kontrolle der Messanlage erfordert.
Mechanische Störgeräusche:
Vermutlich tragen laufende schwere Maschinen einen gewissen Teil zum allgemeinen akustischen Grundrauschen im Berg bei. Eher selten und temporär begrenzt treten stärkere (Arbeits-)Geräusche auf.
Elektrische Störimpulse:
Signifikante Änderungen des elektrischen Grundrauschens erfolgten bisher an zwei Tagen:
(1) ab 29. Juni 2011 (Spikes, Periode=10ms, Amplitude=10-20mV, Erhitzer eingeschaltet) und
(2) ab 26. Juli 2012 (Impulse, Breite=1ms, Periode=10ms Amplitude=20-40mV, Ursache unbekannt). Besonders letztere sind auf seismischen Einzelmessungen und bei allen AE Aufnahmen deutlich sichtar.

Sondenanordnung

Koordinatensystem

Basierend auf dem in **Abbildung 2** gezeigten Sensor-Layout wird ein Koordinatensystem gewählt. Es ist rechtshändig und wird primär zur Berechnung der Sondenabstände benötigt. Die Lage der Achsen und der Koordinaten-Ursprung wurden wie folgt festgelegt.

Lage der Achsen:

X-Achse : horizontal, senkrecht zur Achse des Mikrotunnels. Richtung: Positiv von der Tunnelwand in Richtung Bohrloch-Tiefstes BVE-11[2-4]

Y-Achse : horizontal, entlang der Achse des Microtunnels. Positiv in Richtung Tunnel Tiefstes

Z-Achse : vertikal. Positiv nach oben

Ursprung:

X0 = 0 : Tunnelwand in der Aufsicht. X-Koordinate entspricht den Tiefenangaben in Abbildung 2

Y0 = 0 : Y(BVE-114 bei X=0.5m), Schnittpunkt der Geraden entlang Bohrung BVE-114 bei X=0.5m, projeziert auf die Tunnlewand (in Abbildung 2 etwa beim 'T' von 'Tunnel Wail')

Z0 = 0 : Z(BVE-114), liegt in einer horizontalen Ebene durch BVE-114

Um die dreieckförmige Bohrloch-Anordnung in das Koordinatensystem einzuhängen, muss noch ein Winkel bestimmt werden, der nicht aus Abbildung 2 hervorgeht. Es wird angenommen, dass die Bohrungen BVE-112 und BVE-114 einen Höhenunterschied vom 50 mm aufweisen). Der resultierende Winkel zwischen einer gedachten Strecke BVE-112 nach BVE-114 und der Horizontalen beträgt dann 6°. Unter den genannten Vorraussetzungen ergeben sich die folgenden Koordinaten und gegensetigen Entfernungen für die Sensoren:

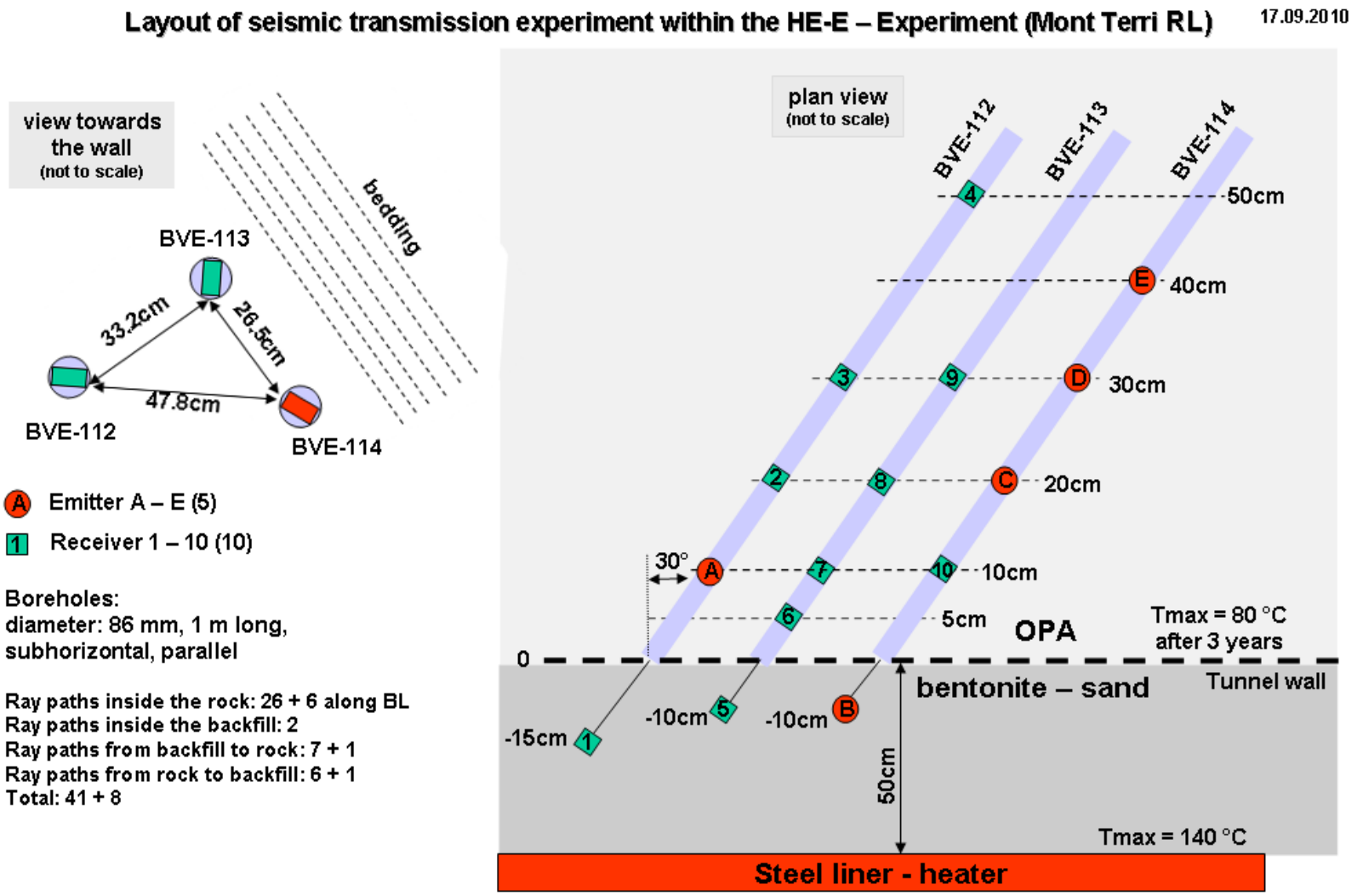

Abbildung 2: Layout HE-E Seismic, Quelle: Kristof Schuster, BGR

Sensor Koordinaten:

Receiver	x[m]	y[m]	z[m]	Bore Hole
Rec01	-0.050	0.793	0.050	BVE-112
Rec02	0.200	0.648	0.050	BVE-112
Rec03	0.300	0.591	0.050	BVE-112
Rec04	0.500	0.475	0.050	BVE-112
Rec05	-0.050	0.495	0.197	BVE-113
Rec06	0.050	0.437	0.197	BVE-113
Rec07	0.100	0.408	0.197	BVE-113
Rec08	0.200	0.350	0.197	BVE-113
Rec09	0.300	0.293	0.197	BVE-113
Rec10	0.100	0.231	0.000	BVE-114

Emitter	x[m]	y[m]	z[m]	Bore Hole
Emi01 (EA)	0.100	0.706	0.050	BVE-112
Emi02 (EB)	-0.100	0.346	0.000	BVE-114
Emi03 (EC)	0.200	0.173	0.000	BVE-114
Emi04 (ED)	0.300	0.116	0.000	BVE-114
Emi05 (EE)	0.400	0.058	0.000	BVE-114

Entfernung: Sender - Empfänger [m]

	E01 (EA)	E02 (EB)	E03 (EC)	E04 (ED)	E05 (EE)
R01	0.173	0.453	0.670	0.764	0.863
R02	0.116	0.429	0.478	0.544	0.625
R03	0.231	0.472	0.433	0.478	0.545
R04	0.462	0.616	0.429	0.414	0.432
R05	0.298	0.252	0.453	0.552	0.657
R06	0.311	0.264	0.362	0.452	0.552
R07	0.332	0.287	0.323	0.405	0.501
R08	0.398	0.359	0.265	0.322	0.405
R09	0.482	0.449	0.251	0.265	0.323
R10	0.478	0.231	0.116	0.231	0.346

Entfernung: Sender - Sender [m]

	E01 (EA)	E02 (EB)	E03 (EC)	E04 (ED)	E05 (EE)
E01 (EA)	0	0.415	0.545	0.625	0.716
E02 (EB)	0.415	0	0.346	0.461	0.577
E03 (EC)	0.545	0.346	0	0.115	0.231
E04 (ED)	0.625	0.461	0.115	0	0.116
E05 (EE)	0.716	0.577	0.231	0.116	0

Entfernung: Empfänger - Empfänger [m]

	R01	R02	R03	R04	R05	R06	R07	R08	R09	R10
R01	0	0.289	0.404	0.635	0.332	0.398	0.439	0.529	0.628	0.584
R02	0.289	0	0.115	0.346	0.328	0.298	0.299	0.332	0.397	0.432
R03	0.404	0.115	0	0.231	0.392	0.328	0.308	0.299	0.332	0.415
R04	0.635	0.346	0.231	0	0.570	0.475	0.431	0.357	0.308	0.471
R05	0.332	0.328	0.392	0.570	0	0.116	0.173	0.289	0.404	0.362
R06	0.398	0.298	0.328	0.475	0.116	0	0.058	0.173	0.289	0.289
R07	0.439	0.299	0.308	0.431	0.173	0.058	0	0.116	0.231	0.265
R08	0.529	0.332	0.299	0.357	0.289	0.173	0.116	0	0.115	0.251
R09	0.628	0.397	0.332	0.308	0.404	0.289	0.231	0.115	0	0.287
R10	0.584	0.432	0.415	0.471	0.362	0.289	0.265	0.251	0.287	0

2 Betrieb

Die Installation der Sensoren und die Inbetriebnahme der Messanlage erfolgten am 16. und 17. Februar 2011. Die im Anschluss folgende Testphase dauerte ca. einen Monat. Tägliche Durchschallungs-Messungen mit konstanten Messeinstellungen sind, mehr oder weniger kontinuierlich, seit dem 12. März 2011 vorhanden. Eine detaillierte Auflistung aller aufgenommen Durchschallungsdatenfiles ist in **Tabelle 1** zu sehen. Einen Überblick über die vorhandenen Datenfiles gibt **Abbildung 3**.

Testbetrieb

Zeitraum: 17. Februar 2011 bis 11. März 2011
Die ersten Messungen erfolgten mit folgenden Parametern: Die Aufzeichnungsdauer betrug 16.2 ms bzw. 8192 Sample und der Pretrigger 5% (Nullpunkt-Sample = 412). Mit dieser Einstellung war der Pretrigger-Bereich kürzer als das Sendesignal. Im Testbetrieb kam es gleich zu Anfang zu einem nicht mehr nachvollziehbaren Fehler bei der Durchführung der Durchschallungsmessung. Unmittelbar danach musste ein defekter Impulsgenerator ausgetasucht werden. Verwendbare Messungen aus diesem Zeitraum gibt es für vier Tage: 17. und 18. Februar, sowie 10. und 11. März.

Messbetrieb

Beginn: 12. März 2011
Die Messanlage läuft permanent und produziert täglich Datenfiles. Der normale Betrieb ist nicht weiter dokumentiert, sondern es werden häuptsächlich die aufgetretenen Störungen behandelt. Das kann den Eindruck von permanenter Fehlfunktion vermitteln, was jedoch nicht der Fall ist. Der Zeitraum vom 12. März 2011 bis 01. August 2013 umfasst 874 Tage. Es wurden an 806 Tagen gültige Datenfiles aufgenommen. Es existieren Aufnahmen von 12 weiteren Tagen, die Störungen aufweisen, aber für einige Sender-Empfänger Kombinationen verwendbar sind. Datenlücken traten wie folgt auf:

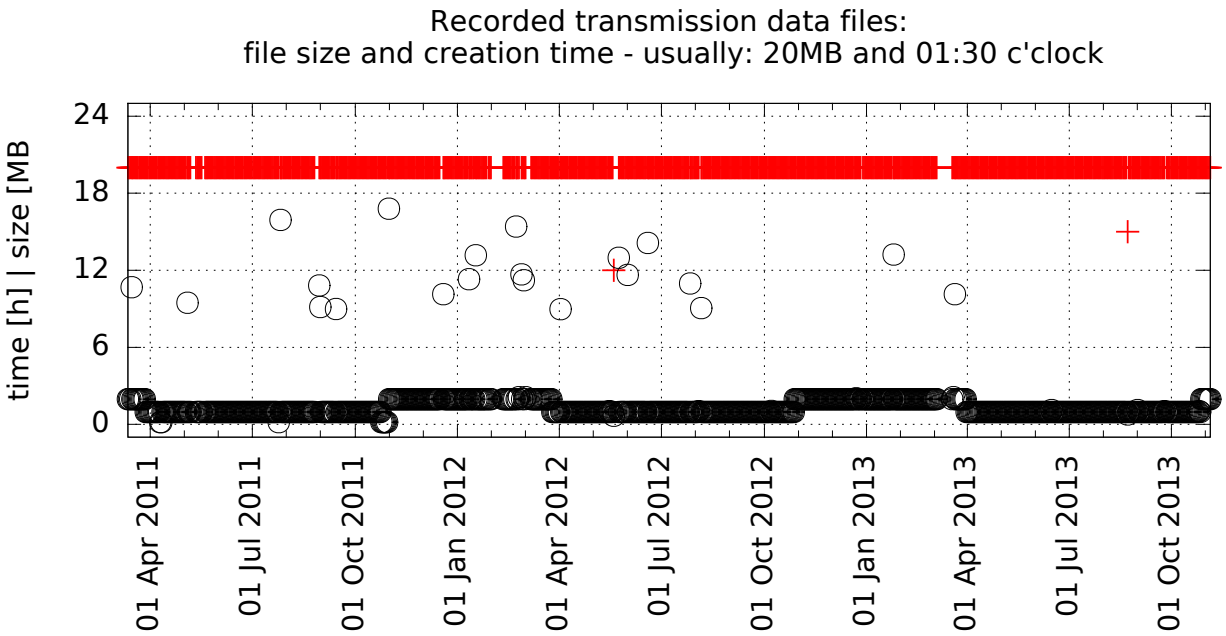

Abbildung 3: Uhrzeit (schwarz) und Größe (rot) von Datenfiles. Die Ausreisser bei der Uhrzeit zeigen manuelle Eingriffe und Fehler beim automatischen Betrieb, die Sprünge im Oktober/November und April/Mai entstehen duch die Sommerzeitumstellung.

08.-21.04.2011 (0052-0065)	Messungen mit Sender A ohne Amplitude (Bauarbeiten, BNC Stecker abgresissen)
10.-11.04.2011 (054, 055)	Error: nur 20-40 Stapelungen
08.-11.05.2011 (0084-0089)	No Data - Error: zeros only
18.-19.05.2011	No Data - System not running
06.-17.01.2012 (0333-0343)	Impulsgenerator 1 defekt, Messdaten evtl. zum Verifizieren geeignet
01.-10.02.2012 (0364-0373)	No data - Error: zeros only, Uref für Impulsgenerator defekt
11.-21.02.2012 (0373-0384)	Error : Messdaten zum Teil ok oder zum Verifizieren geeignet (Uref, Ipg=5V)
21.-23.05.2012 (0561-0562)	No Data - Messprogramm stehengeblieben
05.-06.08.2012 (0561-0562)	No Data - Relais Board Error
06.-18.03.2013	No Data Files - PC, Relais Board oder Messprogramm ?

3 Datenbeispiele

In **Abbildung 4** ist eine komplette Durchschallungsmessung mit 5 Sendern und 10 Empfängern zu sehen. Die Darstellung der Empfänger-Zeitreihen erfolgt in einer Matrixform. 5 Spalten entsprechen den Sendern A bis E, 11 Zeilen entsprechen den Empfänger 01 bis 10 sowie dem aufgezeichneten Sendesignal. Der zeitliche Nullpunkt der Messung ist bei ca. 5 ms, wenn die angelegte Sender-Spannung vom Maximum auf Null gelegt wird.

Das dreieckförmig elfte Signal ist mit einer ausgefüllten Kurve dargestellt und zeigt die Spannung am jeweiligen Sender, mit einer Peak-Amplitude von ca 100V. Bei dem Beispiel sind die Amplituden bei allen Sendern annähernd gleich, was leider nicht so geblieben ist, wie in **Abbildung 1**

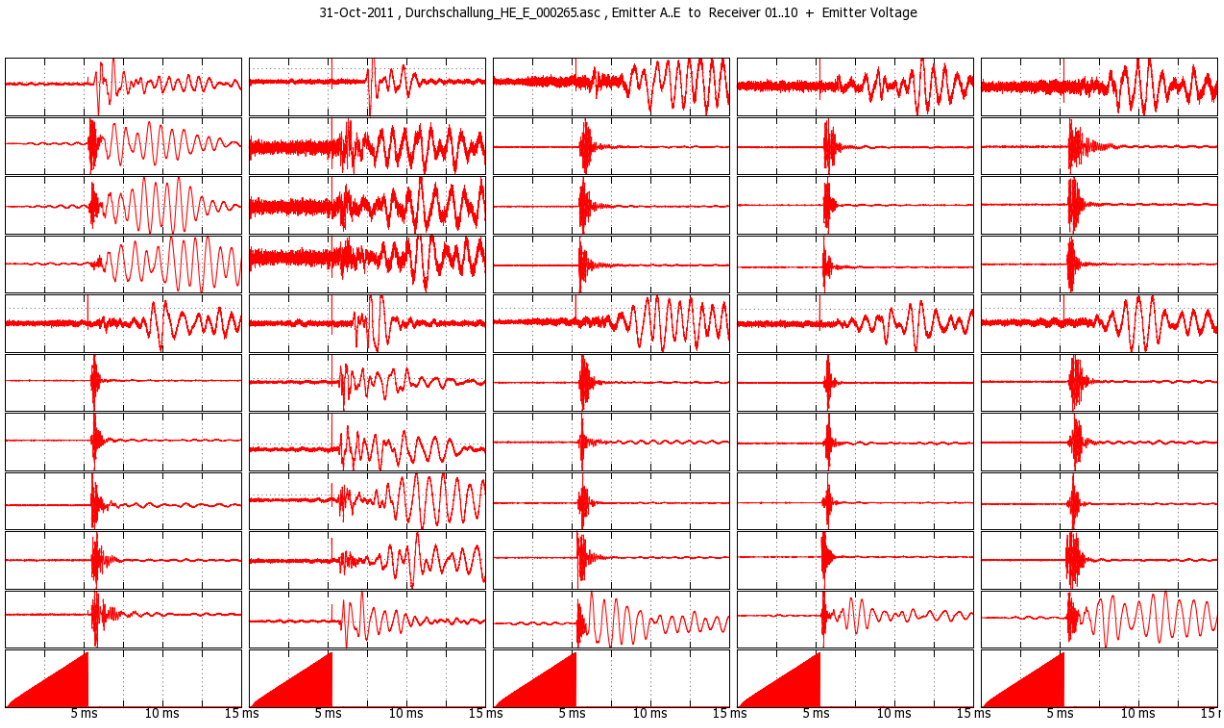

Abbildung 4: Beispiel einer Durchschallungsmessung. Der zeitliche Nullpunkt liegt ca. bei t=5ms

zu sehen. Der Zeitbereich ist mit 15 ms recht groß gewählt, so dass kaum Laufzeitdifferenzen zu sehen sind.

Vorläufer-Signal bei Down-Hole Messungen

Ausgehend von einer Durchschallungsmessung, wie z.B. in **Abbildung 4** zu sehen, scheint der P-Einsatz des Hauptimpulses von niederfrequenten Schwingungen geringer Amplitude überlagert zu sein, und zwar schon vor dem Sendezeitpunkt bei ca. 5 ms. Betroffen sind die Strecken 'Sender A auf Empfänger 2,3 und 4' sowie 'Sender C, D und E auf Empfänger 10'. Bei Down-Hole Geometrie treten sogenannte Bohrlochwellen auf (eine Art Oberflächenwelle entlang der Bohrlochwand mit geringer Phasengeschwindigkeit, langperiodisch, lange Abklingzeit, hohe Amplitude). Daher war die Vermutung, dass es sich um Bohrlochwellen eines Vorläufer-Impulses handelt.

Der Sendeimpuls ist sägezahnförmig. Der Zeitpunkt, zu dem die Spannung vom Maximalwert zurück auf 0V springt, entspricht dem zeitlichen Nullpunkt der Messung (t_0=0). Eine stark vergößerte Darstellung zeigte, dass das Vorläufersignal mit einem Spannungseinbruch am Beginn des linearen Anstiegs korreliert und auch bei Messungen mit normal hoher Sende-Amplitude zumindest nachweisbar ist **Abbildung 5**.

Die Amplitude des Vorläufer-Signals scheint unabhängig von der Sende-Amplitude des Haupt-Impulses zu sein. Wird die Sende-Amplitude des Impulsgenerators verringert, wird der Vorläufer deutlicher. Im Normalbetrieb ist das nicht der Fall (Sende-Amplitude ca. 100 V), jedoch während den partiellen Fehlfunktionen am 06.-17.01.2012 und 11.-21.02.2012, als die Sende-Amplitude kleiner als 1V bzw. 10V war. Die Wellenformen einer solchen Messung mit (ungewollt) sehr geringer Sendeamplitude ist in **Abbildung 6** zu sehen.

Die Breite des Sendeimpulses entspricht in etwa der Laufzeit maximaler Bohrlochwellenamplitude. Durch den Austausch der Impulsgenerators, durch ein Modell mit 7 ms Anstiegszeit anstatt 5

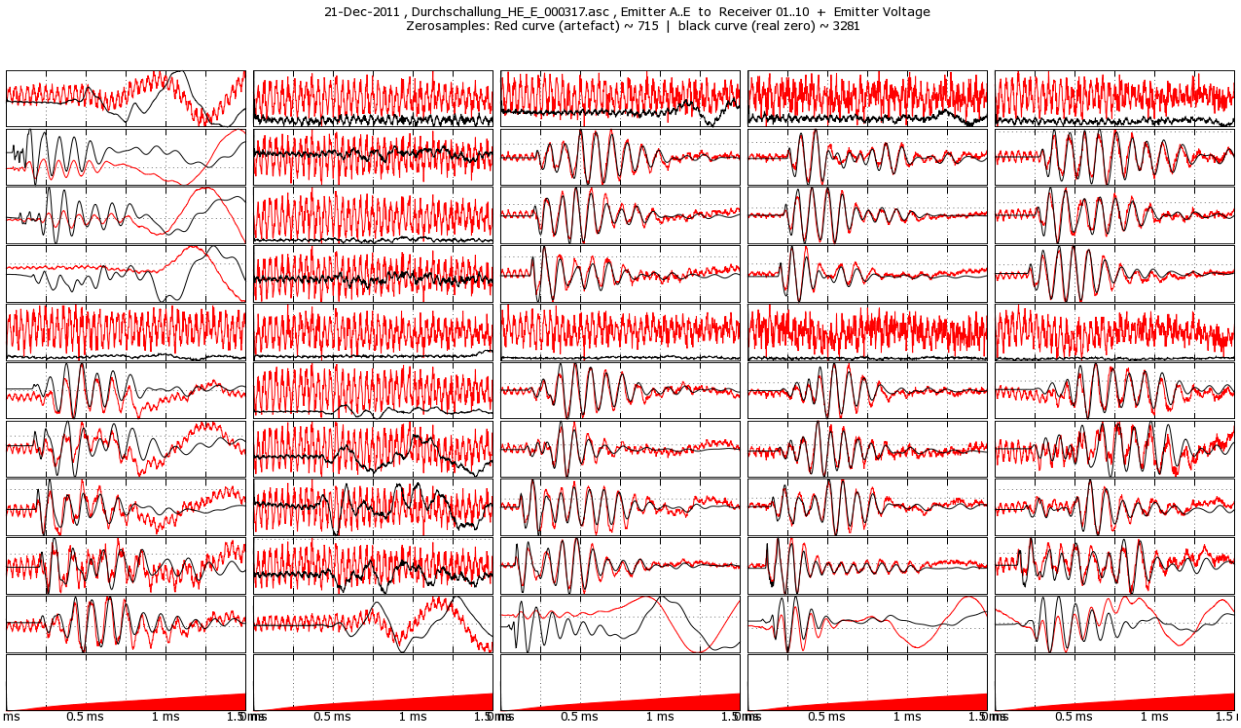

Abbildung 5: Durchschallungsmessung, 1.5ms, Vergleich: Hauptimpuls (t0=3280) mit Vorläufer (t0=714) (Spalte = Sender A - E : Zeile = Empfänger 1 - 10 + Sendesignal)

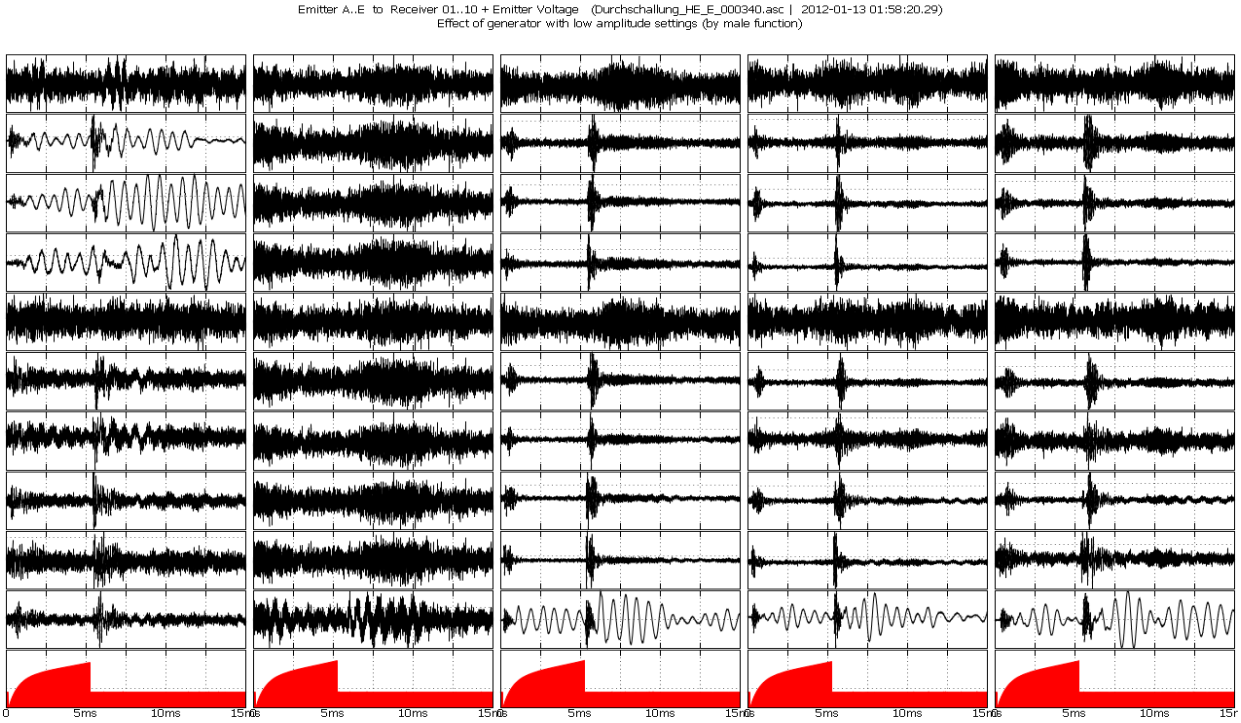

Abbildung 6: Zwei Sende-Impulse bei sehr kleiner Generatorspannung: Vorläufer bei t=0ms, Hauptimpuls bei t=5ms. In Cross-Hole Geometrie sind die Impulse deutlich getrennt, bei Down-Hole Anordnung nicht. (Spalte = Sender A - E : Zeile = Empfänger 1 - 10 + Sendesignal)

ms, ändert sich die Phasenlage von Vorläufer- zu Hauptimpuls, was in letzter Konsequenz auch zu einer leicht geänderten Signalform führt. Letztlich sollte durch die längere Anstiegszeit die Amplitude des Vorläufer-Signals reduziert werden.

Der Zweck dieser relativ genauen Untersuchung des Sendesignals besteht auch darin, möglicherweise Messdaten mit geringer Amplitude aus dem Zeitraum 06. Januar 2012 bis 21. Februar 2012 verwenden zu können.

Luftschall (12. März bis 2. Mai 2011)

Vor dem Einbau des Testkörpers und der anschließenden Verfüllung befinden sich Sender B sowie die Empfänger 01 und 05 in der Luft. Bei einer Durchschallungsmessung werden dann auch klassische akustische Signale erzeugt und aufgezeichnet. Ein händisches Picken der Einsatzzeiten ergab Geschwindigkeiten, die gut mit der Luftschallgeschwindigkeit von ca. 340 m/s übereinstimmen:
Sender B - Empfänger 01 : v = r/t = 0.453 m / 1.35 ms = 336 m/s
Sender B - Empfänger 05 : v = r/t = 0.252 m / 0.8 ms = 315 m/s

Bei den Kombinationen 'Sender B - Empfänger 10' und 'Sender A - Empfänger 01' befindet sich je ein Sensor in der Luft, während der andere am Gebirge angekoppelt ist. Bei beiden Kombinationen sind Sender und Empfänger am selben Strang montiert, der Unterschied besteht darin, dass die Position von Sender und Empfänger vertauscht ist. Es ist ein niederfrequentes Signal zu beobachten, dass von einem Wellenweg über das Gestänge oder von einer Art 'Aufschaukeln' des nicht angekoppelten Sensors stammen könnte. (Zur Zeit ist kein Datenplot vorhanden)

4 Anhang

Liste der Datenfiles

Tabelle 1: Liste der Datenfiles

File	Datum Uhrzeit	Kommentar
Installation und Testbetrieb (Aufnahmedauer=16ms, Pretrigger=5%)		
Durchschallung_HE_E_000001	2011-02-17 16:19	ok, jedoch ohne Sendesignal
Durchschallung_HE_E_000002	2011-02-18 01:35	ok, jedoch ohne Sendesignal
Durchschallung_HE_E_000003	2011-02-18 10:02	Error: Sender A ohne Amplitude
Durchschallung_HE_E_000004	2011-02-18 11:49	— incorect data (unknown error)
	...	— incorect data (unknown error)
Durchschallung_HE_E_000014	2011-02-23	— incorect data (unknown error)
	2011-02-24	System not running
	...	System not running
	2011-03-03	System not running
Durchschallung_HE_E_000015	2011-03-04	— NO DATA (zeros only)
	...	— NO DATA (zeros only)
Durchschallung_HE_E_000021	2011-03-10	— NO DATA (zeros only)
Austausch Impulsgenerator: Ipg0 –> Ipg1		
Durchschallung_HE_E_000022	2011-03-10 16:05	ok
Durchschallung_HE_E_000023	2011-03-11 01:56	ok
Messbetrieb (Aufnahmedauer=32ms, Pretrigger=20%)		
Durchschallung_HE_E_000024	2011-03-12 01:58	
Durchschallung_HE_E_000025	2011-03-13 01:58	
Durchschallung_HE_E_000026	2011-03-14 01:58	
Durchschallung_HE_E_000027	2011-03-15 01:58	— NO DATA (zeros only)
Durchschallung_HE_E_000028	2011-03-15 10:41	(+) nachgeholt
Durchschallung_HE_E_000029	2011-03-16 01:58	
Durchschallung_HE_E_000030	2011-03-17 01:58	
Durchschallung_HE_E_000031	2011-03-18 01:58	
Durchschallung_HE_E_000032	2011-03-19 01:58	
Durchschallung_HE_E_000033	2011-03-20 01:58	
Durchschallung_HE_E_000034	2011-03-21 01:58	
Durchschallung_HE_E_000035	2011-03-22 01:58	
Durchschallung_HE_E_000036	2011-03-23 01:58	
Durchschallung_HE_E_000037	2011-03-24 01:58	
Durchschallung_HE_E_000038	2011-03-25 01:58	
Durchschallung_HE_E_000039	2011-03-26 01:58	
Durchschallung_HE_E_000040	2011-03-27 01:58	
Durchschallung_HE_E_000041	2011-03-28 01:58	
Durchschallung_HE_E_000042	2011-03-29 01:58	
Durchschallung_HE_E_000043	2011-03-30 01:58	
Durchschallung_HE_E_000044	2011-03-31 01:58	
Durchschallung_HE_E_000045	2011-04-01 01:58	
Durchschallung_HE_E_000046	2011-04-02 01:58	
Durchschallung_HE_E_000047	2011-04-03 01:58	
Durchschallung_HE_E_000048	2011-04-04 01:58	
Durchschallung_HE_E_000049	2011-04-05 01:58	
Durchschallung_HE_E_000050	2011-04-06 01:58	
Durchschallung_HE_E_000051	2011-04-07 01:58	
Durchschallung_HE_E_000052	2011-04-08 01:58	- Error: Sender A ohne Amplitude
Durchschallung_HE_E_000053	2011-04-09 01:58	- Error: Sender A ohne Amplitude
Durchschallung_HE_E_000054	2011-04-10 01:10	- Error: Sender A + Stapelzahl nur 20-40
Durchschallung_HE_E_000055	2011-04-11 01:10	- Error: Sender A + Stapelzahl nur 20-40
Durchschallung_HE_E_000056	2011-04-12 01:58	- Error: Sender A ohne Amplitude

Tabelle 1: (continued)

File	Datum Uhrzeit	Kommentar
Durchschallung_HE_E_000057	2011-04-13 01:58	- Error: Sender A ohne Amplitude
Durchschallung_HE_E_000058	2011-04-14 01:58	- Error: Sender A ohne Amplitude
Durchschallung_HE_E_000059	2011-04-15 01:58	- Error: Sender A ohne Amplitude
Durchschallung_HE_E_000060	2011-04-16 01:58	- Error: Sender A ohne Amplitude
Durchschallung_HE_E_000061	2011-04-17 01:58	- Error: Sender A ohne Amplitude
Durchschallung_HE_E_000062	2011-04-18 01:58	- Error: Sender A ohne Amplitude
Durchschallung_HE_E_000063	2011-04-19 01:58	- Error: Sender A ohne Amplitude
Durchschallung_HE_E_000064	2011-04-20 01:58	- Error: Sender A ohne Amplitude
Durchschallung_HE_E_000065	2011-04-21 01:58	- Error: Sender A ohne Amplitude
Durchschallung_HE_E_000066	2011-04-22 01:58	
Durchschallung_HE_E_000067	2011-04-23 01:58	
Durchschallung_HE_E_000068	2011-04-24 01:58	
Durchschallung_HE_E_000069	2011-04-25 01:58	
Durchschallung_HE_E_000070	2011-04-26 01:58	
Durchschallung_HE_E_000071	2011-04-27 01:58	
Durchschallung_HE_E_000072	2011-04-28 01:58	
Durchschallung_HE_E_000073	2011-04-29 01:58	
Durchschallung_HE_E_000074	2011-04-30 01:58	
Durchschallung_HE_E_000075	2011-05-01 01:58	
Durchschallung_HE_E_000076	2011-05-02 01:58	
Durchschallung_HE_E_000077	2011-05-02 16:48	Kontrollmessung (zusätzlich)
Durchschallung_HE_E_000078	2011-05-03 01:58	
Durchschallung_HE_E_000079	2011-05-04 01:58	— NO DATA (zeros only)
Durchschallung_HE_E_000080	2011-05-04 10:28	(+) nachgeholt
Durchschallung_HE_E_000081	2011-05-05 01:58	
Durchschallung_HE_E_000082	2011-05-06 01:58	
Durchschallung_HE_E_000083	2011-05-07 01:58	
Durchschallung_HE_E_000084	2011-05-08 01:58	— NO DATA (zeros only)
Durchschallung_HE_E_000085	2011-05-09 01:58	— NO DATA (zeros only)
Durchschallung_HE_E_000086	2011-05-10 01:58	— NO DATA (zeros only)
Durchschallung_HE_E_000087	2011-05-11 01:58	— NO DATA (zeros only)
Durchschallung_HE_E_000088	2011-05-12 01:58	
Durchschallung_HE_E_000089	2011-05-13 01:58	
Durchschallung_HE_E_000090	2011-05-14 01:58	
Durchschallung_HE_E_000091	2011-05-15 01:58	
Durchschallung_HE_E_000092	2011-05-16 01:58	
Durchschallung_HE_E_000093	2011-05-17 01:58	
	2011-05-18	— NO DATA, System not running
	2011-05-19	— NO DATA, System not running
Durchschallung_HE_E_000094	2011-05-20 01:58	
Durchschallung_HE_E_000095	2011-05-21 01:58	
Durchschallung_HE_E_000096	2011-05-22 01:58	
Durchschallung_HE_E_000097	2011-05-23 01:58	
Durchschallung_HE_E_000098	2011-05-24 01:58	
Durchschallung_HE_E_000099	2011-05-25 01:58	
Durchschallung_HE_E_000100	2011-05-26 01:58	
Durchschallung_HE_E_000101	2011-05-27 01:58	
Durchschallung_HE_E_000102	2011-05-28 01:58	
Durchschallung_HE_E_000103	2011-05-29 01:58	
Durchschallung_HE_E_000104	2011-05-30 01:58	
Durchschallung_HE_E_000105	2011-05-31 01:58	
Durchschallung_HE_E_000106	2011-06-01 01:58	
Durchschallung_HE_E_000107	2011-06-02 01:58	
Durchschallung_HE_E_000108	2011-06-03 01:58	
Durchschallung_HE_E_000109	2011-06-04 01:58	

Tabelle 1: (continued)

File	Datum Uhrzeit	Kommentar
Durchschallung_HE_E_000110	2011-06-05 01:58	
Durchschallung_HE_E_000111	2011-06-06 01:58	
Durchschallung_HE_E_000112	2011-06-07 01:58	
Durchschallung_HE_E_000113	2011-06-08 01:58	
Durchschallung_HE_E_000114	2011-06-09 01:58	
Durchschallung_HE_E_000115	2011-06-10 01:58	
Durchschallung_HE_E_000116	2011-06-11 01:58	
Durchschallung_HE_E_000117	2011-06-12 01:58	
Durchschallung_HE_E_000118	2011-06-13 01:58	
Durchschallung_HE_E_000119	2011-06-14 01:58	
Durchschallung_HE_E_000120	2011-06-15 01:58	
Durchschallung_HE_E_000121	2011-06-16 01:58	
Durchschallung_HE_E_000122	2011-06-17 01:58	
Durchschallung_HE_E_000123	2011-06-18 01:58	
Durchschallung_HE_E_000124	2011-06-19 01:58	
Durchschallung_HE_E_000125	2011-06-20 01:58	
Durchschallung_HE_E_000126	2011-06-21 01:58	
Durchschallung_HE_E_000127	2011-06-22 01:58	
Durchschallung_HE_E_000128	2011-06-23 01:58	
Durchschallung_HE_E_000129	2011-06-24 01:58	
Durchschallung_HE_E_000130	2011-06-25 01:58	
Durchschallung_HE_E_000131	2011-06-26 01:58	
Durchschallung_HE_E_000132	2011-06-27 01:58	
Durchschallung_HE_E_000133	2011-06-28 01:58	
Durchschallung_HE_E_000134	2011-06-29 01:58	
Durchschallung_HE_E_000135	2011-06-30 01:58	
Durchschallung_HE_E_000136	2011-07-01 01:58	
Durchschallung_HE_E_000137	2011-07-02 01:58	
Durchschallung_HE_E_000138	2011-07-03 01:58	
Durchschallung_HE_E_000139	2011-07-04 01:58	
Durchschallung_HE_E_000140	2011-07-05 01:58	
Durchschallung_HE_E_000141	2011-07-06 01:58	
Durchschallung_HE_E_000142	2011-07-07 01:58	
Durchschallung_HE_E_000143	2011-07-08 01:58	
Durchschallung_HE_E_000144	2011-07-09 01:58	
Durchschallung_HE_E_000145	2011-07-10 01:58	
Durchschallung_HE_E_000146	2011-07-11 01:58	
Durchschallung_HE_E_000147	2011-07-12 01:58	
Durchschallung_HE_E_000148	2011-07-13 01:58	
Durchschallung_HE_E_000149	2011-07-14 01:58	
Durchschallung_HE_E_000150	2011-07-15 01:58	
Durchschallung_HE_E_000151	2011-07-16 01:58	
Durchschallung_HE_E_000152	2011-07-17 01:58	
Durchschallung_HE_E_000153	2011-07-18 01:58	
Durchschallung_HE_E_000154	2011-07-19 01:58	
Durchschallung_HE_E_000155	2011-07-20 01:58	
Durchschallung_HE_E_000156	2011-07-21 01:58	
Durchschallung_HE_E_000157	2011-07-22 01:58	
Durchschallung_HE_E_000158	2011-07-23 01:58	
Durchschallung_HE_E_000159	2011-07-24 01:58	
Durchschallung_HE_E_000160	2011-07-25 01:10	- Error: Stapelzahl nur 20-40
Durchschallung_HE_E_000161	2011-07-26 01:10	- Error: Stapelzahl nur 20-40
Durchschallung_HE_E_000162	2011-07-26 10:40	nachgeholt, Error: Stapelzahl nur 20-40
Durchschallung_HE_E_000163	2011-07-26 10:50	nachgeholt, Error: Stapelzahl nur 20-40
Durchschallung_HE_E_000164	2011-07-26 16:55	(+) nachgeholt

Tabelle 1: (continued)

File	Datum Uhrzeit	Kommentar
Durchschallung_HE_E_000165	2011-07-27 01:58	
Durchschallung_HE_E_000166	2011-07-28 01:58	
Durchschallung_HE_E_000167	2011-07-29 01:58	
Durchschallung_HE_E_000168	2011-07-30 01:58	
Durchschallung_HE_E_000169	2011-07-31 01:58	
Durchschallung_HE_E_000170	2011-08-01 01:58	
Durchschallung_HE_E_000171	2011-08-02 01:58	
Durchschallung_HE_E_000172	2011-08-03 01:58	
Durchschallung_HE_E_000173	2011-08-04 01:58	
Durchschallung_HE_E_000174	2011-08-05 01:58	
Durchschallung_HE_E_000175	2011-08-06 01:58	
Durchschallung_HE_E_000176	2011-08-07 01:58	
Durchschallung_HE_E_000177	2011-08-08 01:58	
Durchschallung_HE_E_000178	2011-08-09 01:58	
Durchschallung_HE_E_000179	2011-08-10 01:58	
Durchschallung_HE_E_000180	2011-08-11 01:58	
Durchschallung_HE_E_000181	2011-08-12 01:58	
Durchschallung_HE_E_000182	2011-08-13 01:58	
Durchschallung_HE_E_000183	2011-08-14 01:58	
Durchschallung_HE_E_000184	2011-08-15 01:58	
Durchschallung_HE_E_000185	2011-08-16 01:58	
Durchschallung_HE_E_000186	2011-08-17 01:58	
Durchschallung_HE_E_000187	2011-08-18 01:58	
Durchschallung_HE_E_000188	2011-08-19 01:58	
Durchschallung_HE_E_000189	2011-08-20 01:58	
Durchschallung_HE_E_000190	2011-08-21 01:58	
Durchschallung_HE_E_000191	2011-08-22 01:58	
Durchschallung_HE_E_000192	2011-08-23 01:58	
Durchschallung_HE_E_000193	2011-08-24 01:58	
Durchschallung_HE_E_000194	2011-08-25 01:58	
Durchschallung_HE_E_000195	2011-08-26 01:58	
Durchschallung_HE_E_000196	2011-08-27 01:30	— NO DATA (zeros only)
Durchschallung_HE_E_000197	2011-08-28 01:30	— NO DATA (zeros only)
Durchschallung_HE_E_000198	2011-08-29 01:30	— NO DATA (zeros only)
Durchschallung_HE_E_000199	2011-08-30 01:30	— NO DATA (zeros only)
Durchschallung_HE_E_000200	2011-08-30 11:49	— NO DATA (zeros only)
Durchschallung_HE_E_000201	2011-08-31 01:30	— NO DATA (zeros only)
Durchschallung_HE_E_000202	2011-08-31 10:08	(+) nachgeholt
Durchschallung_HE_E_000203	2011-09-01 01:58	
Durchschallung_HE_E_000204	2011-09-02 01:58	
Durchschallung_HE_E_000205	2011-09-03 01:58	
Durchschallung_HE_E_000206	2011-09-04 01:58	
Durchschallung_HE_E_000207	2011-09-05 01:58	
Durchschallung_HE_E_000208	2011-09-06 01:58	
Durchschallung_HE_E_000209	2011-09-07 01:58	
Durchschallung_HE_E_000210	2011-09-08 01:58	
Durchschallung_HE_E_000211	2011-09-09 01:58	
Durchschallung_HE_E_000212	2011-09-10 01:58	
Durchschallung_HE_E_000213	2011-09-11 01:58	
Durchschallung_HE_E_000214	2011-09-12 01:58	
Durchschallung_HE_E_000215	2011-09-13 01:58	
Durchschallung_HE_E_000216	2011-09-14 01:30	— NO DATA (zeros only)
Durchschallung_HE_E_000217	2011-09-14 09:59	(+) nachgeholt
Durchschallung_HE_E_000218	2011-09-15 01:58	
Durchschallung_HE_E_000219	2011-09-16 01:58	

Tabelle 1: (continued)

File	Datum Uhrzeit	Kommentar
Durchschallung_HE_E_000220	2011-09-17 01:58	
Durchschallung_HE_E_000221	2011-09-18 01:58	
Durchschallung_HE_E_000222	2011-09-19 01:58	
Durchschallung_HE_E_000223	2011-09-20 01:58	
Durchschallung_HE_E_000224	2011-09-21 01:58	
Durchschallung_HE_E_000225	2011-09-22 01:58	
Durchschallung_HE_E_000226	2011-09-23 01:58	
Durchschallung_HE_E_000227	2011-09-24 01:58	
Durchschallung_HE_E_000228	2011-09-25 01:58	
Durchschallung_HE_E_000229	2011-09-26 01:58	
Durchschallung_HE_E_000230	2011-09-27 01:58	
Durchschallung_HE_E_000231	2011-09-28 01:58	
Durchschallung_HE_E_000232	2011-09-29 01:58	
Durchschallung_HE_E_000233	2011-09-30 01:58	
Durchschallung_HE_E_000234	2011-10-01 01:58	
Durchschallung_HE_E_000235	2011-10-02 01:58	
Durchschallung_HE_E_000236	2011-10-03 01:58	
Durchschallung_HE_E_000237	2011-10-04 01:58	
Durchschallung_HE_E_000238	2011-10-05 01:58	
Durchschallung_HE_E_000239	2011-10-06 01:58	
Durchschallung_HE_E_000240	2011-10-07 01:58	
Durchschallung_HE_E_000241	2011-10-08 01:58	
Durchschallung_HE_E_000242	2011-10-09 01:58	
Durchschallung_HE_E_000243	2011-10-10 01:58	
Durchschallung_HE_E_000244	2011-10-11 01:58	
Durchschallung_HE_E_000245	2011-10-12 01:58	
Durchschallung_HE_E_000246	2011-10-13 01:58	
Durchschallung_HE_E_000247	2011-10-14 01:58	
Durchschallung_HE_E_000248	2011-10-15 01:58	
Durchschallung_HE_E_000249	2011-10-16 01:58	
Durchschallung_HE_E_000250	2011-10-17 01:58	
Durchschallung_HE_E_000251	2011-10-18 01:58	
Durchschallung_HE_E_000252	2011-10-19 01:58	
Durchschallung_HE_E_000253	2011-10-20 01:58	
Durchschallung_HE_E_000254	2011-10-21 01:58	
Durchschallung_HE_E_000255	2011-10-22 01:58	
Durchschallung_HE_E_000256	2011-10-23 01:58	
Durchschallung_HE_E_000257	2011-10-24 01:58	
Durchschallung_HE_E_000258	2011-10-25 01:10	- Error: Stapelzahl nur 20-40
Durchschallung_HE_E_000259	2011-10-26 01:10	- Error: Stapelzahl nur 20-40
Durchschallung_HE_E_000260	2011-10-27 01:10	- Error: Stapelzahl nur 20-40
Durchschallung_HE_E_000261	2011-10-28 01:10	- Error: Stapelzahl nur 20-40
Durchschallung_HE_E_000262	2011-10-29 01:10	- Error: Stapelzahl nur 20-40
Durchschallung_HE_E_000263	2011-10-30 01:10	- Error: Stapelzahl nur 20-40
Durchschallung_HE_E_000264	2011-10-31 01:10	- Error: Stapelzahl nur 20-40
Durchschallung_HE_E_000265	2011-10-31 16:48	(+) nachgeholt
Durchschallung_HE_E_000266	2011-11-01 01:58	
Durchschallung_HE_E_000267	2011-11-02 01:58	
Durchschallung_HE_E_000268	2011-11-03 01:58	
Durchschallung_HE_E_000269	2011-11-04 01:58	
Durchschallung_HE_E_000270	2011-11-05 01:58	
Durchschallung_HE_E_000271	2011-11-06 01:58	
Durchschallung_HE_E_000272	2011-11-07 01:58	
Durchschallung_HE_E_000273	2011-11-08 01:58	
Durchschallung_HE_E_000274	2011-11-09 01:58	

Tabelle 1: (continued)

File	Datum Uhrzeit	Kommentar
Durchschallung_HE_E_000275	2011-11-10 01:58	
Durchschallung_HE_E_000276	2011-11-11 01:58	
Durchschallung_HE_E_000277	2011-11-12 01:58	
Durchschallung_HE_E_000278	2011-11-13 01:58	
Durchschallung_HE_E_000279	2011-11-14 01:58	
Durchschallung_HE_E_000280	2011-11-15 01:58	
Durchschallung_HE_E_000281	2011-11-16 01:58	
Durchschallung_HE_E_000282	2011-11-17 01:58	— NO DATA (zeros only)
Durchschallung_HE_E_000283	2011-11-18 01:58	— NO DATA (zeros only)
Durchschallung_HE_E_000284	2011-11-19 01:58	— NO DATA (zeros only)
Durchschallung_HE_E_000285	2011-11-20 01:58	
Durchschallung_HE_E_000286	2011-11-21 01:58	
Durchschallung_HE_E_000287	2011-11-22 01:58	
Durchschallung_HE_E_000288	2011-11-23 01:58	
Durchschallung_HE_E_000289	2011-11-24 01:58	
Durchschallung_HE_E_000290	2011-11-25 01:58	
Durchschallung_HE_E_000291	2011-11-26 01:58	
Durchschallung_HE_E_000292	2011-11-27 01:58	
Durchschallung_HE_E_000293	2011-11-28 01:58	
Durchschallung_HE_E_000294	2011-11-29 01:58	
Durchschallung_HE_E_000295	2011-11-30 01:58	
Durchschallung_HE_E_000296	2011-12-01 01:58	
Durchschallung_HE_E_000297	2011-12-02 01:58	
Durchschallung_HE_E_000298	2011-12-03 01:58	
Durchschallung_HE_E_000299	2011-12-04 01:58	
Durchschallung_HE_E_000300	2011-12-05 01:58	
Durchschallung_HE_E_000301	2011-12-06 01:58	
Durchschallung_HE_E_000302	2011-12-07 01:58	
Durchschallung_HE_E_000303	2011-12-08 01:58	
Durchschallung_HE_E_000304	2011-12-09 01:58	
Durchschallung_HE_E_000305	2011-12-10 01:58	
Durchschallung_HE_E_000306	2011-12-11 01:58	
Durchschallung_HE_E_000307	2011-12-12 01:58	
Durchschallung_HE_E_000308	2011-12-13 01:58	
Durchschallung_HE_E_000309	2011-12-14 01:58	
Durchschallung_HE_E_000310	2011-12-15 01:58	
Durchschallung_HE_E_000311	2011-12-16 01:58	
Durchschallung_HE_E_000312	2011-12-17 01:30	
Durchschallung_HE_E_000313	2011-12-18 01:30	
Durchschallung_HE_E_000314	2011-12-19 01:30	
Durchschallung_HE_E_000315	2011-12-19 10:08	
Durchschallung_HE_E_000316	2011-12-20 01:58	
Durchschallung_HE_E_000317	2011-12-21 01:58	
Durchschallung_HE_E_000318	2011-12-22 01:58	
Durchschallung_HE_E_000319	2011-12-23 01:58	
Durchschallung_HE_E_000320	2011-12-24 01:58	
Durchschallung_HE_E_000321	2011-12-25 01:58	
Durchschallung_HE_E_000322	2011-12-26 01:58	
Durchschallung_HE_E_000323	2011-12-27 01:58	
Durchschallung_HE_E_000324	2011-12-28 01:58	
Durchschallung_HE_E_000325	2011-12-29 01:58	
Durchschallung_HE_E_000326	2011-12-30 01:58	
Durchschallung_HE_E_000327	2011-12-31 01:58	
Durchschallung_HE_E_000328	2012-01-01 01:58	
Durchschallung_HE_E_000329	2012-01-02 01:58	

Tabelle 1: (continued)

File	Datum Uhrzeit	Kommentar
Durchschallung_HE_E_000330	2012-01-03 01:58	
Durchschallung_HE_E_000331	2012-01-04 01:58	
Durchschallung_HE_E_000332	2012-01-05 01:58	
Durchschallung_HE_E_000333	2012-01-06 01:58	– Error: Ipg Sendespannung nur 1V
Durchschallung_HE_E_000334	2012-01-07 01:58	– Error: Ipg Sendespannung nur 1V
Durchschallung_HE_E_000335	2012-01-08 01:58	– Error: Ipg Sendespannung nur 1V
Durchschallung_HE_E_000336	2012-01-09 01:58	– Error: Ipg Sendespannung nur 1V
Durchschallung_HE_E_000337	2012-01-10 01:58	– Error: Ipg Sendespannung nur 1V
Durchschallung_HE_E_000338	2012-01-11 11:18	– Error: Ipg Sendespannung nur 1V
Durchschallung_HE_E_000339	2012-01-12 01:58	– Error: Ipg Sendespannung nur 1V
Durchschallung_HE_E_000340	2012-01-13 01:58	– Error: Ipg Sendespannung nur 1V
Durchschallung_HE_E_000341	2012-01-14 01:58	– Error: Ipg Sendespannung nur 1V
Durchschallung_HE_E_000342	2012-01-15 01:58	– Error: Ipg Sendespannung nur 1V
Durchschallung_HE_E_000343	2012-01-16 01:58	– Error: Ipg Sendespannung nur 1V
Durchschallung_HE_E_000344	2012-01-17 01:58	– Error: Ipg Sendespannung nur 1V
Austausch Impulsgenerator: Ipg 1(5ms) –> Ipg 2(7ms)		
Durchschallung_HE_E_000345	2012-01-17 10:45	Testmessung nach Ipg 2 Installation
Durchschallung_HE_E_000346	2012-01-17 13:10	(+) nachgeholt Ipg 2
Durchschallung_HE_E_000347	2012-01-17 14:37	25% Pretrigger (zusätzlich)
Durchschallung_HE_E_000348	2012-01-18 01:58	
Durchschallung_HE_E_000349	2012-01-19 01:58	
Durchschallung_HE_E_000350	2012-01-20 01:58	
Durchschallung_HE_E_000351	2012-01-21 01:58	
Durchschallung_HE_E_000352	2012-01-22 01:58	
Durchschallung_HE_E_000353	2012-01-23 01:58	
Durchschallung_HE_E_000354	2012-01-24 01:58	
Durchschallung_HE_E_000355	2012-01-25 01:58	
Durchschallung_HE_E_000356	2012-01-25 10:50	Kontrollmessung (zusätzlich)
Durchschallung_HE_E_000357	2012-01-26 01:58	
Durchschallung_HE_E_000358	2012-01-26 16:18	Pretrigger 25% (zusätzlich)
Durchschallung_HE_E_000359	2012-01-27 01:58	
Durchschallung_HE_E_000361	2012-01-29 01:58	
Durchschallung_HE_E_000362	2012-01-30 01:58	
Durchschallung_HE_E_000363	2012-01-31 01:58	
Durchschallung_HE_E_000364	2012-02-01 01:17	— NO DATA (zeros only), Uref=0V
Durchschallung_HE_E_000365	2012-02-02 01:17	— NO DATA (zeros only), Uref=0V
Durchschallung_HE_E_000366	2012-02-03 01:17	— NO DATA (zeros only), Uref=0V
Durchschallung_HE_E_000367	2012-02-04 01:17	— NO DATA (zeros only), Uref=0V
Durchschallung_HE_E_000368	2012-02-05 01:17	— NO DATA (zeros only), Uref=0V
Durchschallung_HE_E_000369	2012-02-06 01:17	— NO DATA (zeros only), Uref=0V
Durchschallung_HE_E_000370	2012-02-07 01:17	— NO DATA (zeros only), Uref=0V
Durchschallung_HE_E_000371	2012-02-08 01:17	— NO DATA (zeros only), Uref=0V
Durchschallung_HE_E_000372	2012-02-09 01:17	— NO DATA (zeros only), Uref=0V
Durchschallung_HE_E_000373	2012-02-10 01:17	— NO DATA (zeros only), Uref=0V
Durchschallung_HE_E_000374	2012-02-11 01:58	- Error: 5V Sendespannung (Uref=noise)
Durchschallung_HE_E_000375	2012-02-12 01:58	- Error: 5V Sendespannung (Uref=noise)
Durchschallung_HE_E_000376	2012-02-13 01:58	- Error: 5V Sendespannung (Uref=noise)
Durchschallung_HE_E_000377	2012-02-14 01:58	- Error: 5V Sendespannung (Uref=noise)
Durchschallung_HE_E_000378	2012-02-15 01:58	- Error: 5V Sendespannung (Uref=noise)
Durchschallung_HE_E_000379	2012-02-16 01:58	- Error: 5V Sendespannung (Uref=noise)
Durchschallung_HE_E_000380	2012-02-17 01:58	- Error: 5V Sendespannung (Uref=noise)
Durchschallung_HE_E_000381	2012-02-18 01:58	- Error: 5V Sendespannung (Uref=noise)
Durchschallung_HE_E_000382	2012-02-19 01:58	- Error: 5V Sendespannung (Uref=noise)
Durchschallung_HE_E_000383	2012-02-20 01:58	- Error: 5V Sendespannung (Uref=noise)
Durchschallung_HE_E_000384	2012-02-21 01:58	- Error: 5V Sendespannung (Uref=noise)

Tabelle 1: (continued)

File	Datum Uhrzeit	Kommentar
Durchschallung_HE_E_000385	2012-02-22 01:58	- Error: 5V Sendespannung (Uref=noise)
Durchschallung_HE_E_000386	2012-02-22 15:24	(+) nachgeholt (neue Uref für Ipg2 installiert)
Durchschallung_HE_E_000387	2012-02-22 17:22	25% Pretrigger (zusätzlich)
Durchschallung_HE_E_000388	2012-02-23 01:58	
Durchschallung_HE_E_000389	2012-02-24 01:58	
Durchschallung_HE_E_000390	2012-02-25 02:07	ok (Error Transmitter 7 + 8 only)
Durchschallung_HE_E_000391	2012-02-26 02:34	— NO DATA (Relais-Board)
Durchschallung_HE_E_000392	2012-02-27 02:34	— NO DATA (Relais-Board)
Durchschallung_HE_E_000393	2012-02-27 11:41	(+) nachgeholt
Durchschallung_HE_E_000394	2012-02-28 01:58	
Durchschallung_HE_E_000395	2012-02-29 01:30	
Durchschallung_HE_E_000396	2012-02-29 11:13	
Durchschallung_HE_E_000397	2012-03-01 01:58	
Durchschallung_HE_E_000398	2012-03-02 02:07	ok (Error Transmitter 7 + 8 only)
Durchschallung_HE_E_000399	2012-03-03 02:34	— NO DATA (Relais-Board)
Durchschallung_HE_E_000400	2012-03-04 02:34	— NO DATA (Relais-Board)
Durchschallung_HE_E_000401	2012-03-05 02:34	— NO DATA (Relais-Board)
Durchschallung_HE_E_000402	2012-03-06 02:34	— NO DATA (Relais-Board)
Durchschallung_HE_E_000403	2012-03-07 01:58	
Durchschallung_HE_E_000404	2012-03-07 09:59	Kontrollmessung (zusätzlich)
Durchschallung_HE_E_000405	2012-03-08 01:58	
Durchschallung_HE_E_000406	2012-03-09 01:58	
Durchschallung_HE_E_000407	2012-03-10 01:58	
Durchschallung_HE_E_000408	2012-03-11 01:58	
Durchschallung_HE_E_000409	2012-03-12 01:58	
Durchschallung_HE_E_000410	2012-03-13 01:58	
Durchschallung_HE_E_000411	2012-03-14 01:58	
Durchschallung_HE_E_000412	2012-03-15 01:58	
Durchschallung_HE_E_000413	2012-03-16 01:58	
Durchschallung_HE_E_000413	2012-03-16 01:58	
Durchschallung_HE_E_000414	2012-03-17 01:58	
Durchschallung_HE_E_000415	2012-03-18 01:58	
Durchschallung_HE_E_000416	2012-03-19 01:58	
Durchschallung_HE_E_000417	2012-03-20 01:58	
Durchschallung_HE_E_000418	2012-03-21 01:58	
Durchschallung_HE_E_000419	2012-03-22 01:58	
Durchschallung_HE_E_000420	2012-03-23 01:58	
Durchschallung_HE_E_000421	2012-03-24 01:58	
Durchschallung_HE_E_000422	2012-03-25 01:58	
Durchschallung_HE_E_000423	2012-03-26 01:58	
Durchschallung_HE_E_000424	2012-03-27 01:58	
Durchschallung_HE_E_000425	2012-03-27 13:08	25% Pretrigger (zusätzlich)
Durchschallung_HE_E_000426	2012-03-28 01:58	
Durchschallung_HE_E_000427	2012-03-29 01:58	
Durchschallung_HE_E_000428	2012-03-30 01:58	
Durchschallung_HE_E_000429	2012-03-31 01:58	
Durchschallung_HE_E_000430	2012-04-01 01:58	
Durchschallung_HE_E_000431	2012-04-02 01:58	- Error: Stapelzahl nur 20-40
Durchschallung_HE_E_000432	2012-04-02 09:58	(+) nachgeholt
Durchschallung_HE_E_000433	2012-04-03 01:58	
Durchschallung_HE_E_000434	2012-04-04 01:58	
Durchschallung_HE_E_000435	2012-04-05 01:58	
Durchschallung_HE_E_000436	2012-04-06 01:58	
Durchschallung_HE_E_000437	2012-04-07 01:58	
Durchschallung_HE_E_000438	2012-04-08 01:58	

Tabelle 1: (continued)

File	Datum Uhrzeit	Kommentar
Durchschallung_HE_E_000439	2012-04-09 01:58	
Durchschallung_HE_E_000440	2012-04-10 01:58	
Durchschallung_HE_E_000441	2012-04-11 01:58	
Durchschallung_HE_E_000442	2012-04-12 01:58	
Durchschallung_HE_E_000443	2012-04-13 01:58	
Durchschallung_HE_E_000444	2012-04-14 01:58	
Durchschallung_HE_E_000445	2012-04-15 01:58	
Durchschallung_HE_E_000446	2012-04-16 01:58	
Durchschallung_HE_E_000447	2012-04-17 01:58	
Durchschallung_HE_E_000448	2012-04-18 01:58	
Durchschallung_HE_E_000449	2012-04-19 01:58	
Durchschallung_HE_E_000450	2012-04-19 13:08	25% Pretrigger (zusätzlich)
Durchschallung_HE_E_000451	2012-04-20 01:58	
Durchschallung_HE_E_000452	2012-04-21 01:58	
Durchschallung_HE_E_000453	2012-04-22 01:58	
Durchschallung_HE_E_000454	2012-04-23 01:58	
Durchschallung_HE_E_000455	2012-04-24 01:58	
Durchschallung_HE_E_000456	2012-04-25 01:58	
Durchschallung_HE_E_000457	2012-04-26 01:58	
Durchschallung_HE_E_000458	2012-04-27 01:58	
Durchschallung_HE_E_000459	2012-04-28 01:58	
Durchschallung_HE_E_000460	2012-04-29 01:58	
Durchschallung_HE_E_000461	2012-04-30 01:58	
Durchschallung_HE_E_000462	2012-05-01 01:58	
Durchschallung_HE_E_000463	2012-05-02 01:58	
Durchschallung_HE_E_000464	2012-05-03 01:58	
Durchschallung_HE_E_000465	2012-05-04 01:58	
Durchschallung_HE_E_000466	2012-05-05 01:58	
Durchschallung_HE_E_000467	2012-05-06 01:58	
Durchschallung_HE_E_000468	2012-05-07 01:58	
Durchschallung_HE_E_000469	2012-05-08 01:58	
Durchschallung_HE_E_000470	2012-05-09 01:58	
Durchschallung_HE_E_000471	2012-05-10 01:58	
Durchschallung_HE_E_000472	2012-05-11 01:58	
Durchschallung_HE_E_000473	2012-05-12 01:58	
Durchschallung_HE_E_000474	2012-05-13 01:58	
Durchschallung_HE_E_000475	2012-05-14 01:58	
Durchschallung_HE_E_000476	2012-05-15 01:58	
Durchschallung_HE_E_000477	2012-05-16 02:02	ok (Error: Relais-Board, Transmitter 8 only)
Durchschallung_HE_E_000478	2012-05-17 01:58	
Durchschallung_HE_E_000479	2012-05-18 01:58	
Durchschallung_HE_E_000480	2012-05-19 01:58	
Durchschallung_HE_E_000481	2012-05-20 01:40	Transmitter 1-5 ok, Messprogramm stehen geblieben
	2012-05-21	Messprogramm stehen geblieben
	2012-05-22	Messprogramm stehen geblieben
	2012-05-23	Messprogramm stehen geblieben
Durchschallung_HE_E_000482	2012-05-24 13:58	(+) nachgeholt
Durchschallung_HE_E_000483	2012-05-24 14:58	25% Pretrigger (zusätzlich)
Durchschallung_HE_E_000484	2012-05-25 01:58	
Durchschallung_HE_E_000485	2012-05-26 01:58	
Durchschallung_HE_E_000486	2012-05-27 01:58	
Durchschallung_HE_E_000487	2012-05-28 01:58	
Durchschallung_HE_E_000488	2012-05-29 01:58	
Durchschallung_HE_E_000489	2012-05-30 01:58	
Durchschallung_HE_E_000490	2012-05-31 01:58	

Tabelle 1: (continued)

File	Datum Uhrzeit	Kommentar
Durchschallung_HE_E_000491	2012-06-01 01:30	— NO DATA (zeros only)
Durchschallung_HE_E_000492	2012-06-01 12:38	(+) nachgeholt
Durchschallung_HE_E_000493	2012-06-02 01:58	
Durchschallung_HE_E_000494	2012-06-03 01:58	
Durchschallung_HE_E_000495	2012-06-04 01:58	
Durchschallung_HE_E_000496	2012-06-05 01:58	
Durchschallung_HE_E_000497	2012-06-06 01:58	
Durchschallung_HE_E_000498	2012-06-07 01:58	
Durchschallung_HE_E_000499	2012-06-08 01:58	
Durchschallung_HE_E_000500	2012-06-09 01:58	
Durchschallung_HE_E_000501	2012-06-10 01:58	
Durchschallung_HE_E_000502	2012-06-11 01:58	
Durchschallung_HE_E_000503	2012-06-12 01:58	
Durchschallung_HE_E_000504	2012-06-13 01:58	
Durchschallung_HE_E_000505	2012-06-14 01:58	
Durchschallung_HE_E_000506	2012-06-15 01:58	
Durchschallung_HE_E_000507	2012-06-16 01:58	
Durchschallung_HE_E_000508	2012-06-17 01:58	
Durchschallung_HE_E_000509	2012-06-18 01:58	
Durchschallung_HE_E_000510	2012-06-19 01:30	— NO DATA (zeros only)
Durchschallung_HE_E_000511	2012-06-19 11:28	25% Pretrigger (zusätzlich)
Durchschallung_HE_E_000512	2012-06-19 15:08	(+) nachgeholt
Durchschallung_HE_E_000513	2012-06-20 01:58	
Durchschallung_HE_E_000514	2012-06-21 01:58	
Durchschallung_HE_E_000515	2012-06-22 01:58	
Durchschallung_HE_E_000516	2012-06-23 01:58	
Durchschallung_HE_E_000517	2012-06-24 01:58	
Durchschallung_HE_E_000518	2012-06-25 01:58	
Durchschallung_HE_E_000519	2012-06-26 01:58	
Durchschallung_HE_E_000520	2012-06-27 01:58	
Durchschallung_HE_E_000521	2012-06-28 01:58	
Durchschallung_HE_E_000522	2012-06-29 01:58	
Durchschallung_HE_E_000523	2012-06-30 01:58	
Durchschallung_HE_E_000524	2012-07-01 01:58	
Durchschallung_HE_E_000525	2012-07-02 01:58	
Durchschallung_HE_E_000526	2012-07-03 01:58	
Durchschallung_HE_E_000527	2012-07-04 01:58	
Durchschallung_HE_E_000528	2012-07-05 01:58	
Durchschallung_HE_E_000529	2012-07-06 01:58	
Durchschallung_HE_E_000530	2012-07-07 01:58	
Durchschallung_HE_E_000531	2012-07-08 01:58	
Durchschallung_HE_E_000532	2012-07-09 01:58	
Durchschallung_HE_E_000533	2012-07-10 01:58	
Durchschallung_HE_E_000534	2012-07-11 01:58	
Durchschallung_HE_E_000535	2012-07-12 01:58	
Durchschallung_HE_E_000536	2012-07-13 01:58	
Durchschallung_HE_E_000537	2012-07-14 01:58	
Durchschallung_HE_E_000538	2012-07-15 01:58	
Durchschallung_HE_E_000539	2012-07-16 01:58	
Durchschallung_HE_E_000540	2012-07-17 01:58	
Durchschallung_HE_E_000541	2012-07-18 01:58	
Durchschallung_HE_E_000542	2012-07-19 01:58	
Durchschallung_HE_E_000543	2012-07-20 01:58	
Durchschallung_HE_E_000544	2012-07-21 01:58	
Durchschallung_HE_E_000545	2012-07-22 01:58	

Tabelle 1: (continued)

File	Datum Uhrzeit	Kommentar
Durchschallung_HE_E_000546	2012-07-23 01:58	
Durchschallung_HE_E_000547	2012-07-24 01:58	
Durchschallung_HE_E_000548	2012-07-25 01:58	
Durchschallung_HE_E_000549	2012-07-26 01:58	
Durchschallung_HE_E_000550	2012-07-27 01:11	– Error: Verrauscht (Ohne Stapelung?)
Durchschallung_HE_E_000551	2012-07-27 11:58	(+) nachgeholt
Durchschallung_HE_E_000552	2012-07-27 12:58	25% Pretrigger (zusätzlich)
Durchschallung_HE_E_000553	2012-07-28 01:58	
Durchschallung_HE_E_000554	2012-07-29 01:58	
Durchschallung_HE_E_000555	2012-07-30 01:58	
Durchschallung_HE_E_000556	2012-07-31 01:58	
Durchschallung_HE_E_000557	2012-08-01 01:58	
Durchschallung_HE_E_000558	2012-08-02 01:58	
Durchschallung_HE_E_000559	2012-08-03 01:58	
Durchschallung_HE_E_000560	2012-08-04 02:02	ok (Error: Relais-Board, Transmitter 8 only)
Durchschallung_HE_E_000561	2012-08-05 02:34	— NO DATA (Relais-Board)
Durchschallung_HE_E_000562	2012-08-06 02:34	— NO DATA (Relais-Board)
Durchschallung_HE_E_000563	2012-08-06 10:03	(+) nachgeholt
Durchschallung_HE_E_000564	2012-08-07 01:58	
Durchschallung_HE_E_000565	2012-08-08 01:58	
Durchschallung_HE_E_000566	2012-08-09 01:58	
Durchschallung_HE_E_000567	2012-08-10 01:58	
Durchschallung_HE_E_000568	2012-08-11 01:58	
Durchschallung_HE_E_000569	2012-08-12 01:58	
Durchschallung_HE_E_000570	2012-08-13 01:58	
Durchschallung_HE_E_000571	2012-08-14 01:58	
Durchschallung_HE_E_000572	2012-08-15 01:58	
Durchschallung_HE_E_000573	2012-08-16 01:58	
Durchschallung_HE_E_000574	2012-08-17 01:58	
Durchschallung_HE_E_000575	2012-08-18 01:58	
Durchschallung_HE_E_000576	2012-08-19 01:58	
Durchschallung_HE_E_000577	2012-08-20 01:58	
Durchschallung_HE_E_000578	2012-08-21 01:58	
Durchschallung_HE_E_000579	2012-08-22 01:58	
Durchschallung_HE_E_000580	2012-08-23 01:58	
Durchschallung_HE_E_000581	2012-08-24 01:58	
Durchschallung_HE_E_000582	2012-08-25 01:58	
Durchschallung_HE_E_000583	2012-08-26 01:58	
Durchschallung_HE_E_000584	2012-08-27 01:58	
Durchschallung_HE_E_000585	2012-08-28 01:58	
Durchschallung_HE_E_000586	2012-08-29 01:58	
Durchschallung_HE_E_000587	2012-08-30 01:58	
Durchschallung_HE_E_000588	2012-08-31 01:58	
Durchschallung_HE_E_000589	2012-09-01 01:58	
Durchschallung_HE_E_000590	2012-09-02 01:58	
Durchschallung_HE_E_000591	2012-09-03 01:58	
Durchschallung_HE_E_000592	2012-09-04 01:58	
Durchschallung_HE_E_000593	2012-09-05 01:58	
Durchschallung_HE_E_000594	2012-09-06 01:58	
Durchschallung_HE_E_000595	2012-09-07 01:58	
Durchschallung_HE_E_000596	2012-09-08 01:58	
Durchschallung_HE_E_000597	2012-09-09 01:58	
Durchschallung_HE_E_000598	2012-09-10 01:58	
Durchschallung_HE_E_000599	2012-09-11 01:58	
Durchschallung_HE_E_000600	2012-09-12 01:58	

Tabelle 1: (continued)

File	Datum Uhrzeit	Kommentar
Durchschallung_HE_E_000601	2012-09-13 01:58	
Durchschallung_HE_E_000602	2012-09-14 01:58	
Durchschallung_HE_E_000603	2012-09-15 01:58	
Durchschallung_HE_E_000604	2012-09-16 01:58	
Durchschallung_HE_E_000605	2012-09-17 01:58	
Durchschallung_HE_E_000606	2012-09-18 01:58	
Durchschallung_HE_E_000607	2012-09-19 01:58	
Durchschallung_HE_E_000608	2012-09-20 01:58	
Durchschallung_HE_E_000609	2012-09-21 01:58	
Durchschallung_HE_E_000610	2012-09-22 01:58	
Durchschallung_HE_E_000611	2012-09-23 01:58	
Durchschallung_HE_E_000612	2012-09-24 01:58	
Durchschallung_HE_E_000613	2012-09-25 01:58	
Durchschallung_HE_E_000614	2012-09-26 01:58	
Durchschallung_HE_E_000615	2012-09-27 01:58	
Durchschallung_HE_E_000616	2012-09-28 01:58	
Durchschallung_HE_E_000617	2012-09-29 01:58	
Durchschallung_HE_E_000618	2012-09-30 01:58	
Durchschallung_HE_E_000619	2012-10-01 01:58	
Durchschallung_HE_E_000620	2012-10-02 01:58	
Durchschallung_HE_E_000621	2012-10-03 01:58	
Durchschallung_HE_E_000622	2012-10-04 01:58	
Durchschallung_HE_E_000623	2012-10-05 01:58	
Durchschallung_HE_E_000624	2012-10-06 01:58	
Durchschallung_HE_E_000625	2012-10-07 01:58	
Durchschallung_HE_E_000626	2012-10-08 02:03	
Durchschallung_HE_E_000627	2012-10-09 01:58	
Durchschallung_HE_E_000628	2012-10-10 01:58	
Durchschallung_HE_E_000629	2012-10-11 01:58	
Durchschallung_HE_E_000630	2012-10-12 01:58	
Durchschallung_HE_E_000631	2012-10-13 01:58	
Durchschallung_HE_E_000632	2012-10-14 01:58	
Durchschallung_HE_E_000633	2012-10-15 01:58	
Durchschallung_HE_E_000634	2012-10-16 01:58	
Durchschallung_HE_E_000635	2012-10-17 01:58	
Durchschallung_HE_E_000636	2012-10-18 01:58	
Durchschallung_HE_E_000637	2012-10-19 01:58	
Durchschallung_HE_E_000638	2012-10-20 01:58	
Durchschallung_HE_E_000639	2012-10-21 01:58	
Durchschallung_HE_E_000640	2012-10-22 01:58	
Durchschallung_HE_E_000641	2012-10-23 01:58	
Durchschallung_HE_E_000642	2012-10-24 01:58	
Durchschallung_HE_E_000643	2012-10-25 01:58	
Durchschallung_HE_E_000644	2012-10-26 01:58	
Durchschallung_HE_E_000645	2012-10-27 01:58	
Durchschallung_HE_E_000646	2012-10-28 01:58	
Durchschallung_HE_E_000647	2012-10-29 01:58	
Durchschallung_HE_E_000648	2012-10-30 01:58	
Durchschallung_HE_E_000649	2012-10-31 01:58	
Durchschallung_HE_E_000650	2012-11-01 01:58	
Durchschallung_HE_E_000651	2012-11-02 01:58	
Durchschallung_HE_E_000652	2012-11-03 01:58	
Durchschallung_HE_E_000653	2012-11-04 01:58	
Durchschallung_HE_E_000654	2012-11-05 01:58	
Durchschallung_HE_E_000655	2012-11-06 01:58	

Tabelle 1: (continued)

File	Datum Uhrzeit	Kommentar
Durchschallung_HE_E_000656	2012-11-07 01:58	
Durchschallung_HE_E_000657	2012-11-08 01:58	
Durchschallung_HE_E_000658	2012-11-09 01:58	
Durchschallung_HE_E_000659	2012-11-10 01:58	
Durchschallung_HE_E_000660	2012-11-11 01:58	
Durchschallung_HE_E_000661	2012-11-12 01:58	
Durchschallung_HE_E_000662	2012-11-13 01:58	
Durchschallung_HE_E_000663	2012-11-14 01:58	
Durchschallung_HE_E_000664	2012-11-15 01:58	
Durchschallung_HE_E_000665	2012-11-16 01:58	
Durchschallung_HE_E_000666	2012-11-17 01:58	
Durchschallung_HE_E_000667	2012-11-18 01:58	
Durchschallung_HE_E_000668	2012-11-19 01:58	
Durchschallung_HE_E_000669	2012-11-20 01:58	
Durchschallung_HE_E_000670	2012-11-21 01:58	
Durchschallung_HE_E_000671	2012-11-22 01:58	
Durchschallung_HE_E_000672	2012-11-23 01:58	
Durchschallung_HE_E_000673	2012-11-24 01:58	
Durchschallung_HE_E_000674	2012-11-25 01:58	
Durchschallung_HE_E_000675	2012-11-26 01:58	
Durchschallung_HE_E_000676	2012-11-27 01:58	
Durchschallung_HE_E_000677	2012-11-28 01:58	
Durchschallung_HE_E_000678	2012-11-29 01:58	
Durchschallung_HE_E_000679	2012-11-30 01:58	
Durchschallung_HE_E_000680	2012-12-01 01:58	
Durchschallung_HE_E_000681	2012-12-02 01:58	
Durchschallung_HE_E_000682	2012-12-03 01:58	
Durchschallung_HE_E_000683	2012-12-04 01:58	
Durchschallung_HE_E_000684	2012-12-05 01:58	
Durchschallung_HE_E_000685	2012-12-06 01:58	
Durchschallung_HE_E_000686	2012-12-07 01:58	
Durchschallung_HE_E_000687	2012-12-08 01:58	
Durchschallung_HE_E_000688	2012-12-09 01:58	
Durchschallung_HE_E_000689	2012-12-10 01:58	
Durchschallung_HE_E_000690	2012-12-11 01:58	
Durchschallung_HE_E_000691	2012-12-12 01:58	
Durchschallung_HE_E_000692	2012-12-13 01:58	
Durchschallung_HE_E_000693	2012-12-14 01:58	
Durchschallung_HE_E_000694	2012-12-15 01:58	
Durchschallung_HE_E_000695	2012-12-16 01:58	
Durchschallung_HE_E_000696	2012-12-17 01:58	
Durchschallung_HE_E_000697	2012-12-18 01:58	
Durchschallung_HE_E_000698	2012-12-19 01:58	
Durchschallung_HE_E_000699	2012-12-20 01:58	
Durchschallung_HE_E_000700	2012-12-21 01:58	
Durchschallung_HE_E_000701	2012-12-22 01:58	
Durchschallung_HE_E_000702	2012-12-23 02:02	
Durchschallung_HE_E_000703	2012-12-24 01:58	
Durchschallung_HE_E_000704	2012-12-25 01:58	
Durchschallung_HE_E_000705	2012-12-26 01:58	
Durchschallung_HE_E_000706	2012-12-27 01:58	
	2012-12-28	no file for this day (Relais-Board Error) afaik
Durchschallung_HE_E_000707	2012-12-29 01:58	
Durchschallung_HE_E_000708	2012-12-30 01:58	
Durchschallung_HE_E_000709	2012-12-31 01:58	

Tabelle 1: (continued)

File	Datum Uhrzeit	Kommentar
Durchschallung_HE_E_000710	2013-01-01 01:58	
Durchschallung_HE_E_000711	2013-01-02 01:58	
Durchschallung_HE_E_000712	2013-01-03 01:58	
Durchschallung_HE_E_000713	2013-01-04 01:58	
Durchschallung_HE_E_000714	2013-01-05 01:58	
Durchschallung_HE_E_000715	2013-01-06 01:58	
Durchschallung_HE_E_000716	2013-01-07 01:58	
Durchschallung_HE_E_000717	2013-01-08 01:58	
Durchschallung_HE_E_000718	2013-01-09 01:58	
Durchschallung_HE_E_000719	2013-01-10 01:58	
Durchschallung_HE_E_000720	2013-01-11 01:58	
Durchschallung_HE_E_000721	2013-01-12 01:58	
Durchschallung_HE_E_000722	2013-01-13 01:58	
Durchschallung_HE_E_000723	2013-01-14 01:58	
Durchschallung_HE_E_000724	2013-01-15 01:58	
Durchschallung_HE_E_000725	2013-01-15 11:58	25% Pretrigger (zusätzlich)
Durchschallung_HE_E_000726	2013-01-16 01:58	
Durchschallung_HE_E_000727	2013-01-17 01:58	
Durchschallung_HE_E_000728	2013-01-18 01:58	
Durchschallung_HE_E_000729	2013-01-19 01:58	
Durchschallung_HE_E_000730	2013-01-20 01:58	
Durchschallung_HE_E_000731	2013-01-21 01:58	
Durchschallung_HE_E_000732	2013-01-22 01:58	
Durchschallung_HE_E_000733	2013-01-23 01:58	
Durchschallung_HE_E_000734	2013-01-24 01:58	
Durchschallung_HE_E_000736	2013-01-25 13:13	
Durchschallung_HE_E_000737	2013-01-26 01:58	
Durchschallung_HE_E_000738	2013-01-27 01:58	
Durchschallung_HE_E_000739	2013-01-28 01:58	
Durchschallung_HE_E_000740	2013-01-29 01:58	
Durchschallung_HE_E_000741	2013-01-30 01:58	
Durchschallung_HE_E_000742	2013-01-31 01:58	
Durchschallung_HE_E_000743	2013-02-01 01:58	
Durchschallung_HE_E_000744	2013-02-02 01:58	
Durchschallung_HE_E_000745	2013-02-03 01:58	
Durchschallung_HE_E_000746	2013-02-04 01:58	
Durchschallung_HE_E_000747	2013-02-05 01:58	
Durchschallung_HE_E_000748	2013-02-06 01:58	
Durchschallung_HE_E_000749	2013-02-07 01:58	
Durchschallung_HE_E_000750	2013-02-08 01:58	
Durchschallung_HE_E_000751	2013-02-09 01:58	
Durchschallung_HE_E_000752	2013-02-10 01:58	
Durchschallung_HE_E_000753	2013-02-11 01:58	
Durchschallung_HE_E_000754	2013-02-12 01:58	
Durchschallung_HE_E_000755	2013-02-13 01:58	
Durchschallung_HE_E_000756	2013-02-14 01:58	
Durchschallung_HE_E_000757	2013-02-15 01:58	
Durchschallung_HE_E_000758	2013-02-16 01:58	
Durchschallung_HE_E_000759	2013-02-17 01:58	
Durchschallung_HE_E_000760	2013-02-18 01:58	
Durchschallung_HE_E_000761	2013-02-19 01:58	
Durchschallung_HE_E_000762	2013-02-20 01:58	
Durchschallung_HE_E_000763	2013-02-21 01:58	
Durchschallung_HE_E_000764	2013-02-22 01:58	
Durchschallung_HE_E_000765	2013-02-23 01:58	

Tabelle 1: (continued)

File	Datum Uhrzeit	Kommentar
Durchschallung_HE_E_000766	2013-02-24 01:58	
Durchschallung_HE_E_000767	2013-02-25 01:58	
Durchschallung_HE_E_000768	2013-02-26 01:58	
Durchschallung_HE_E_000769	2013-02-27 01:58	
Durchschallung_HE_E_000770	2013-02-28 01:58	
Durchschallung_HE_E_000771	2013-03-01 01:58	
Durchschallung_HE_E_000772	2013-03-02 01:58	
Durchschallung_HE_E_000773	2013-03-03 01:58	
Durchschallung_HE_E_000774	2013-03-04 01:58	
Durchschallung_HE_E_000775	2013-03-05 01:58	
	2013-03-06	— NO DATA (unknown reason)
	...	— NO DATA (unknown reason)
	2013-03-18	— NO DATA (unknown reason)
Durchschallung_HE_E_000776	2013-03-19 01:58	
Durchschallung_HE_E_000777	2013-03-20 02:07	
Durchschallung_HE_E_000779	2013-03-21 10:08	
Durchschallung_HE_E_000780	2013-03-22 01:58	
Durchschallung_HE_E_000781	2013-03-23 01:58	
Durchschallung_HE_E_000782	2013-03-24 01:58	
Durchschallung_HE_E_000783	2013-03-25 01:58	
Durchschallung_HE_E_000784	2013-03-26 01:58	
Durchschallung_HE_E_000785	2013-03-27 01:58	
Durchschallung_HE_E_000786	2013-03-28 01:58	
Durchschallung_HE_E_000787	2013-03-29 01:58	
Durchschallung_HE_E_000788	2013-03-30 01:58	
Durchschallung_HE_E_000789	2013-03-31 01:58	
Durchschallung_HE_E_000790	2013-04-01 01:58	
Durchschallung_HE_E_000791	2013-04-02 01:58	
Durchschallung_HE_E_000792	2013-04-03 01:58	
Durchschallung_HE_E_000793	2013-04-04 01:58	
Durchschallung_HE_E_000794	2013-04-05 01:58	
Durchschallung_HE_E_000795	2013-04-06 01:58	
Durchschallung_HE_E_000796	2013-04-07 01:58	
Durchschallung_HE_E_000797	2013-04-08 01:58	
Durchschallung_HE_E_000798	2013-04-09 01:58	
Durchschallung_HE_E_000799	2013-04-10 01:58	
Durchschallung_HE_E_000800	2013-04-11 01:58	
Durchschallung_HE_E_000801	2013-04-12 01:58	
Durchschallung_HE_E_000802	2013-04-13 01:58	
Durchschallung_HE_E_000803	2013-04-14 01:58	
Durchschallung_HE_E_000804	2013-04-15 01:58	
Durchschallung_HE_E_000805	2013-04-16 01:58	
Durchschallung_HE_E_000806	2013-04-17 01:58	
Durchschallung_HE_E_000807	2013-04-18 01:58	
Durchschallung_HE_E_000808	2013-04-19 01:58	
Durchschallung_HE_E_000809	2013-04-20 01:58	
Durchschallung_HE_E_000810	2013-04-21 01:58	
Durchschallung_HE_E_000811	2013-04-22 01:58	
Durchschallung_HE_E_000812	2013-04-23 01:58	
Durchschallung_HE_E_000813	2013-04-24 01:58	
Durchschallung_HE_E_000814	2013-04-25 01:58	
Durchschallung_HE_E_000815	2013-04-26 01:58	
Durchschallung_HE_E_000816	2013-04-27 01:58	
Durchschallung_HE_E_000817	2013-04-28 01:58	
Durchschallung_HE_E_000818	2013-04-29 01:58	

Tabelle 1: (continued)

File	Datum Uhrzeit	Kommentar
Durchschallung_HE_E_000819	2013-04-30 01:58	
Durchschallung_HE_E_000820	2013-05-01 01:58	
Durchschallung_HE_E_000821	2013-05-02 01:58	
Durchschallung_HE_E_000822	2013-05-03 01:58	
Durchschallung_HE_E_000823	2013-05-04 01:58	
Durchschallung_HE_E_000824	2013-05-05 01:58	
Durchschallung_HE_E_000825	2013-05-06 01:58	
Durchschallung_HE_E_000826	2013-05-07 01:58	
Durchschallung_HE_E_000827	2013-05-08 01:58	
Durchschallung_HE_E_000828	2013-05-09 01:58	
Durchschallung_HE_E_000829	2013-05-10 01:58	
Durchschallung_HE_E_000830	2013-05-11 01:58	
Durchschallung_HE_E_000831	2013-05-12 01:58	
Durchschallung_HE_E_000832	2013-05-13 01:58	
Durchschallung_HE_E_000833	2013-05-14 01:58	
Durchschallung_HE_E_000834	2013-05-15 01:58	
Durchschallung_HE_E_000835	2013-05-16 01:58	
Durchschallung_HE_E_000836	2013-05-17 01:58	
Durchschallung_HE_E_000837	2013-05-18 01:58	
Durchschallung_HE_E_000838	2013-05-19 01:58	
Durchschallung_HE_E_000839	2013-05-20 01:58	
Durchschallung_HE_E_000840	2013-05-21 01:58	
Durchschallung_HE_E_000841	2013-05-22 01:58	
Durchschallung_HE_E_000842	2013-05-23 01:58	
Durchschallung_HE_E_000843	2013-05-24 01:58	
Durchschallung_HE_E_000844	2013-05-25 01:58	
Durchschallung_HE_E_000845	2013-05-26 01:58	
Durchschallung_HE_E_000846	2013-05-27 01:58	
Durchschallung_HE_E_000847	2013-05-28 01:58	
Durchschallung_HE_E_000848	2013-05-29 01:58	
Durchschallung_HE_E_000849	2013-05-30 01:58	
Durchschallung_HE_E_000850	2013-05-31 01:58	
Durchschallung_HE_E_000851	2013-06-01 01:58	
Durchschallung_HE_E_000852	2013-06-02 01:58	
Durchschallung_HE_E_000853	2013-06-03 01:58	
Durchschallung_HE_E_000854	2013-06-04 01:58	
Durchschallung_HE_E_000855	2013-06-05 01:58	
Durchschallung_HE_E_000856	2013-06-06 01:58	
Durchschallung_HE_E_000857	2013-06-07 01:58	
Durchschallung_HE_E_000858	2013-06-08 01:58	
Durchschallung_HE_E_000859	2013-06-09 01:58	
Durchschallung_HE_E_000860	2013-06-10 01:58	
Durchschallung_HE_E_000861	2013-06-11 01:58	
Durchschallung_HE_E_000862	2013-06-12 01:58	
Durchschallung_HE_E_000863	2013-06-13 01:58	
Durchschallung_HE_E_000864	2013-06-14 01:58	
Durchschallung_HE_E_000865	2013-06-15 01:58	
Durchschallung_HE_E_000866	2013-06-16 02:07	ok (Error: Relais-Board, Transmitter 8 only)
Durchschallung_HE_E_000867	2013-06-17 01:58	
Durchschallung_HE_E_000868	2013-06-18 01:58	
Durchschallung_HE_E_000869	2013-06-19 01:58	
Durchschallung_HE_E_000870	2013-06-20 01:58	
Durchschallung_HE_E_000871	2013-06-21 01:58	
Durchschallung_HE_E_000872	2013-06-22 01:58	
Durchschallung_HE_E_000873	2013-06-23 01:58	

Tabelle 1: (continued)

File	Datum Uhrzeit	Kommentar
Durchschallung_HE_E_000874	2013-06-24 01:58	
Durchschallung_HE_E_000875	2013-06-25 01:58	
Durchschallung_HE_E_000876	2013-06-26 01:58	
Durchschallung_HE_E_000877	2013-06-27 01:58	
Durchschallung_HE_E_000878	2013-06-28 01:58	
Durchschallung_HE_E_000879	2013-06-29 01:58	
Durchschallung_HE_E_000880	2013-06-30 01:58	
Durchschallung_HE_E_000881	2013-07-01 01:58	
Durchschallung_HE_E_000882	2013-07-02 01:58	
Durchschallung_HE_E_000883	2013-07-03 01:58	
Durchschallung_HE_E_000884	2013-07-04 01:58	
Durchschallung_HE_E_000885	2013-07-05 01:58	
Durchschallung_HE_E_000886	2013-07-06 01:58	
Durchschallung_HE_E_000887	2013-07-07 01:58	
Durchschallung_HE_E_000888	2013-07-08 01:58	
Durchschallung_HE_E_000889	2013-07-09 01:58	
Durchschallung_HE_E_000890	2013-07-10 01:58	
Durchschallung_HE_E_000891	2013-07-11 01:58	
Durchschallung_HE_E_000892	2013-07-12 01:58	
Durchschallung_HE_E_000893	2013-07-13 01:58	
Durchschallung_HE_E_000894	2013-07-14 01:58	
Durchschallung_HE_E_000895	2013-07-15 01:58	
Durchschallung_HE_E_000896	2013-07-16 01:58	
Durchschallung_HE_E_000897	2013-07-17 01:58	
Durchschallung_HE_E_000898	2013-07-18 01:58	
Durchschallung_HE_E_000899	2013-07-19 01:58	
Durchschallung_HE_E_000900	2013-07-20 01:58	
Durchschallung_HE_E_000901	2013-07-21 01:58	
Durchschallung_HE_E_000902	2013-07-22 01:58	
Durchschallung_HE_E_000903	2013-07-23 01:58	
Durchschallung_HE_E_000904	2013-07-24 01:58	
Durchschallung_HE_E_000905	2013-07-25 01:58	
Durchschallung_HE_E_000906	2013-07-26 01:58	
Durchschallung_HE_E_000907	2013-07-27 01:58	
Durchschallung_HE_E_000908	2013-07-28 01:58	
Durchschallung_HE_E_000909	2013-07-29 01:58	
Durchschallung_HE_E_000910	2013-07-30 01:58	
Durchschallung_HE_E_000911	2013-07-31 01:58	
Durchschallung_HE_E_000912	2013-08-01 01:58	
Durchschallung_HE_E_000913	2013-08-02 01:58	
Durchschallung_HE_E_000914	2013-08-03 01:58	
Durchschallung_HE_E_000915	2013-08-04 01:58	
Durchschallung_HE_E_000916	2013-08-05 01:58	
Durchschallung_HE_E_000917	2013-08-06 01:58	
Durchschallung_HE_E_000918	2013-08-07 01:58	
Durchschallung_HE_E_000919	2013-08-08 01:58	
Durchschallung_HE_E_000920	2013-08-09 01:58	
Durchschallung_HE_E_000921	2013-08-10 01:58	
Durchschallung_HE_E_000922	2013-08-11 01:58	
Durchschallung_HE_E_000923	2013-08-12 01:58	
Durchschallung_HE_E_000924	2013-08-13 01:58	
Durchschallung_HE_E_000925	2013-08-14 01:58	
Durchschallung_HE_E_000926	2013-08-15 01:58	
Durchschallung_HE_E_000927	2013-08-16 01:58	
Durchschallung_HE_E_000928	2013-08-17 01:58	

Tabelle 1: (continued)

File	Datum Uhrzeit	Kommentar
Durchschallung_HE_E_000929	2013-08-18 01:58	
Durchschallung_HE_E_000930	2013-08-19 01:58	
Durchschallung_HE_E_000931	2013-08-20 01:58	
Durchschallung_HE_E_000932	2013-08-21 01:58	
Durchschallung_HE_E_000933	2013-08-22 01:58	
Durchschallung_HE_E_000934	2013-08-23 01:46	ok (Error: Relais-Board, Transmitter 7 + 8 only)
Durchschallung_HE_E_000935	2013-08-24 01:58	
Durchschallung_HE_E_000936	2013-08-25 01:58	
Durchschallung_HE_E_000937	2013-08-26 01:58	
Durchschallung_HE_E_000938	2013-08-27 01:58	
Durchschallung_HE_E_000939	2013-08-28 01:58	
Durchschallung_HE_E_000940	2013-08-29 01:58	
Durchschallung_HE_E_000941	2013-08-30 01:58	
Durchschallung_HE_E_000942	2013-08-31 01:58	
Durchschallung_HE_E_000943	2013-09-01 02:07	Uhrzeit nicht 01:58 ?
Durchschallung_HE_E_000944	2013-09-02 01:58	
Durchschallung_HE_E_000945	2013-09-03 01:58	
Durchschallung_HE_E_000946	2013-09-04 01:58	
Durchschallung_HE_E_000947	2013-09-05 01:58	
Durchschallung_HE_E_000948	2013-09-06 01:58	
Durchschallung_HE_E_000949	2013-09-07 01:58	
Durchschallung_HE_E_000950	2013-09-08 01:58	
Durchschallung_HE_E_000951	2013-09-09 01:58	
Durchschallung_HE_E_000952	2013-09-10 01:58	
Durchschallung_HE_E_000953	2013-09-11 01:58	
Durchschallung_HE_E_000954	2013-09-12 01:58	
Durchschallung_HE_E_000955	2013-09-13 01:58	
Durchschallung_HE_E_000956	2013-09-14 01:58	
Durchschallung_HE_E_000957	2013-09-15 01:58	
Durchschallung_HE_E_000958	2013-09-16 01:58	
Durchschallung_HE_E_000959	2013-09-17 01:58	
Durchschallung_HE_E_000960	2013-09-18 01:58	
Durchschallung_HE_E_000961	2013-09-19 01:58	
Durchschallung_HE_E_000962	2013-09-20 01:58	
Durchschallung_HE_E_000963	2013-09-21 01:58	
Durchschallung_HE_E_000964	2013-09-22 01:58	
Durchschallung_HE_E_000965	2013-09-23 01:58	
Durchschallung_HE_E_000966	2013-09-24 01:58	
Durchschallung_HE_E_000967	2013-09-25 02:02	
	2013-09-26	— NO DATA (Relais-Board Error)
Durchschallung_HE_E_000969	2013-09-27 01:58	
Durchschallung_HE_E_000970	2013-09-28 01:58	
Durchschallung_HE_E_000971	2013-09-29 01:58	
Durchschallung_HE_E_000972	2013-09-30 01:58	
Durchschallung_HE_E_000973	2013-10-01 01:58	
Durchschallung_HE_E_000974	2013-10-02 01:58	
Durchschallung_HE_E_000975	2013-10-03 01:58	
Durchschallung_HE_E_000976	2013-10-04 01:58	
Durchschallung_HE_E_000977	2013-10-05 01:58	
Durchschallung_HE_E_000978	2013-10-06 01:58	
Durchschallung_HE_E_000979	2013-10-07 01:58	
Durchschallung_HE_E_000980	2013-10-08 01:58	
Durchschallung_HE_E_000981	2013-10-09 01:58	
Durchschallung_HE_E_000982	2013-10-10 01:58	
Durchschallung_HE_E_000983	2013-10-11 01:58	

Tabelle 1: (continued)

File	Datum Uhrzeit	Kommentar
Durchschallung_HE_E_000984	2013-10-12 01:58	
Durchschallung_HE_E_000985	2013-10-13 01:58	
Durchschallung_HE_E_000986	2013-10-14 01:58	
Durchschallung_HE_E_000987	2013-10-15 01:58	
Durchschallung_HE_E_000988	2013-10-16 01:58	
Durchschallung_HE_E_000989	2013-10-17 01:58	
Durchschallung_HE_E_000990	2013-10-18 01:58	
Durchschallung_HE_E_000991	2013-10-19 01:58	
Durchschallung_HE_E_000992	2013-10-20 01:58	
Durchschallung_HE_E_000993	2013-10-21 01:58	
Durchschallung_HE_E_000994	2013-10-22 01:58	
Durchschallung_HE_E_000995	2013-10-23 01:58	
Durchschallung_HE_E_000996	2013-10-24 01:58	
Durchschallung_HE_E_000997	2013-10-25 01:58	
Durchschallung_HE_E_000998	2013-10-26 02:02	
Durchschallung_HE_E_000999	2013-10-27 01:58	
Durchschallung_HE_E_001000	2013-10-28 01:58	
Durchschallung_HE_E_001001	2013-10-29 01:58	
Durchschallung_HE_E_001002	2013-10-30 01:58	
Durchschallung_HE_E_001003	2013-10-31 01:58	
Durchschallung_HE_E_001004	2013-11-01 01:58	
Durchschallung_HE_E_001005	2013-11-02 01:58	
Durchschallung_HE_E_001006	2013-11-03 01:58	
Durchschallung_HE_E_001007	2013-11-04 01:58	
Durchschallung_HE_E_001008	2013-11-05 01:58	

Erläuterung und Zusammenfassung der Kommentar-Spalte in Tabelle 1

'Leeres Feld'	die Messung ist normal und ohne Fehler abgelaufen.
- Error	Weniger kritischer Fehler, Daten sind teilweise gestört.
– Error	Daten mit starken Störungen, teilweise noch zum validieren geeignet.
— NO DATA	Fehlende automatische Messung (fatal)
(+) nachgeholt	Manuell nachgeholte Messung, falls Error bei automatischer Messung.
Kontrollmessung	zusätzliche Messung
25% Pretrigger	Seit Impulsgenerator 2: Manuelle zusätzliche Messung, die den Beginn des Sendesignals enthält (Ansteigszeit 5ms ->7ms)

Mehrfach aufgetretene Fehler:

'Stapelzahl nur 20-40'	Verrauschte Daten, Durchschallungs-Messung wird nach 10 x Timout abgebrochen, unbekannte Ursache
'Relasi Board'	Keine Daten, Timout beim Relaisboard, PC muss neu gestartet werden
'Zeros only'	Keine Daten, unbekannte Ursache, letztmalig aufgetreten am 19. Juni 2012

Einmalig aufgetretene Fehler:

'incorect data (unknown error)'	im Testbetrieb, 18.-23. Februar 2011
'Kabel von Sender A beschädigt'	08.-21. April 2011
'Impulsgenerator defekt'	06.-17. Januar 2012
'Steuerspannung für Impulsgenerator defekt'	01.-22. Februar 2012
'System stromlos'	17./18. bis 19. Mai 2011, 16:00
'Messprogramm stehen geblieben'	20. Mai 2012, Neustart am 24. Mai 2012

Nachgeholte Messungen: (Uhrzeit nicht 01:58):
15.03.2011 (0028)
04.05.2011 (0080)
26.07.2011 (0164)
31.08.2011 (0202)
14.09.2011 (0217)
31.10.2011 (0265)

17.01.2012 (0346)
22.02.2012 (0386)
27.02.2012 (0393)
02.04.2012 (0432)
24.05.2012 (0482)
01.06.2012 (0492)
19.06.2012 (0512)
27.07.2012 (0551)
06.08.2012 (0563)

Messdaten ok, Fehler irrelevant:
25.02.2012 (0390) : Error Transmitter 7 - 8
02.03.2012 (0398) : Error Transmitter 7 - 8
20.05.2012 (0481) : Error Transmitter 6 - 8
04.08.2012 (0560) : Error Transmitter 8
16.06.2013 (0866) : Error Transmitter 8

Messungen mit 25% Pretrigger mit Impulsgenerator 2:
17.01.2012 (0347)
26.01.2012 (0358)
22.02.2012 (0387)
27.03.2012 (0425)
19.04.2012 (0450)
24.05.2012 (0483)
19.06.2012 (0511)
27.07.2012 (0552)
15.01.2013 (0724)

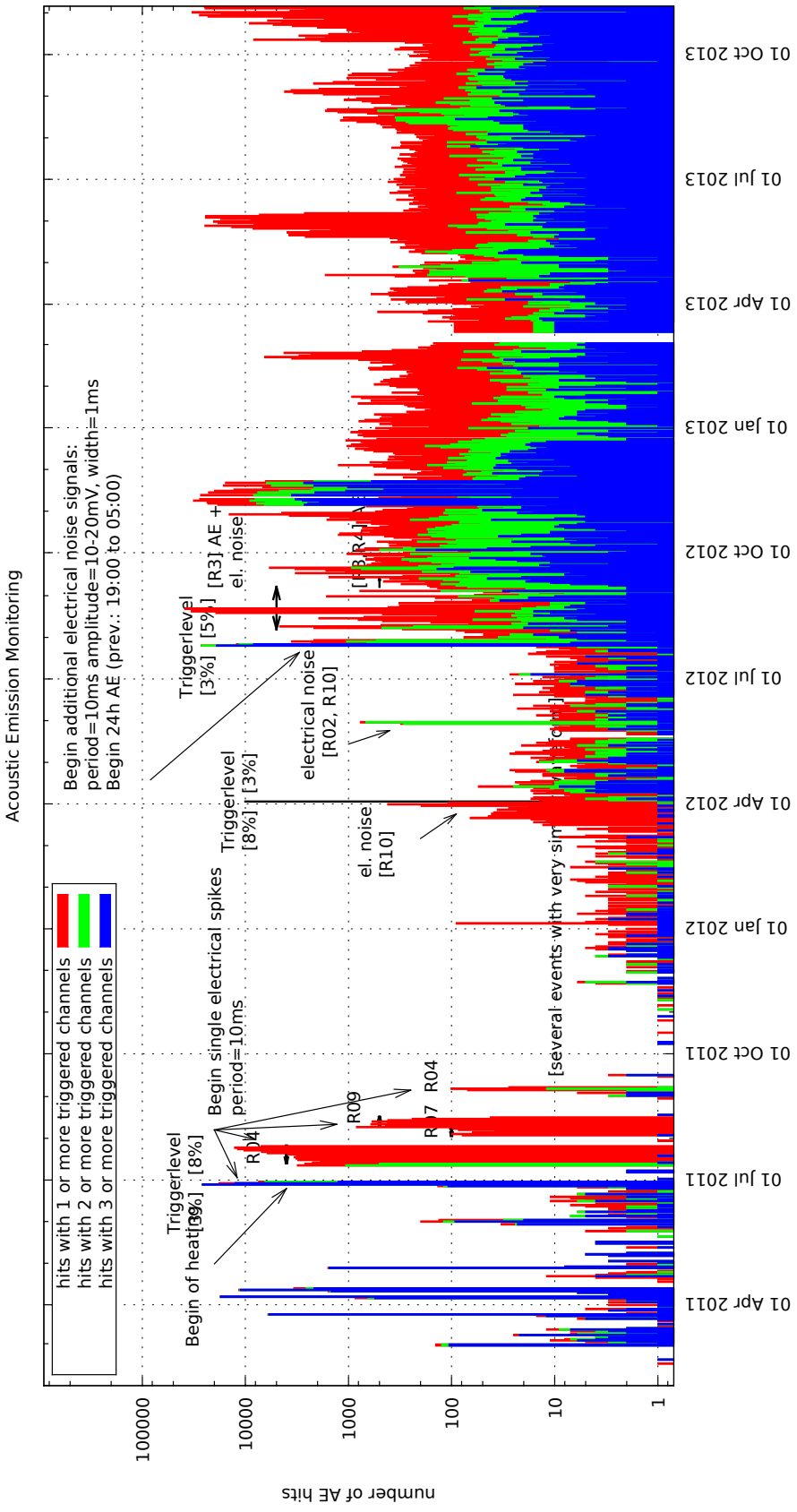

Abbildung 7: AE Trigger Statistik in halblogarithmischer Darstellung. Ereignisse mit nur einem getriggerten Kanal sind (in der Regel) keine AE Ereignisse sondern Störungen.

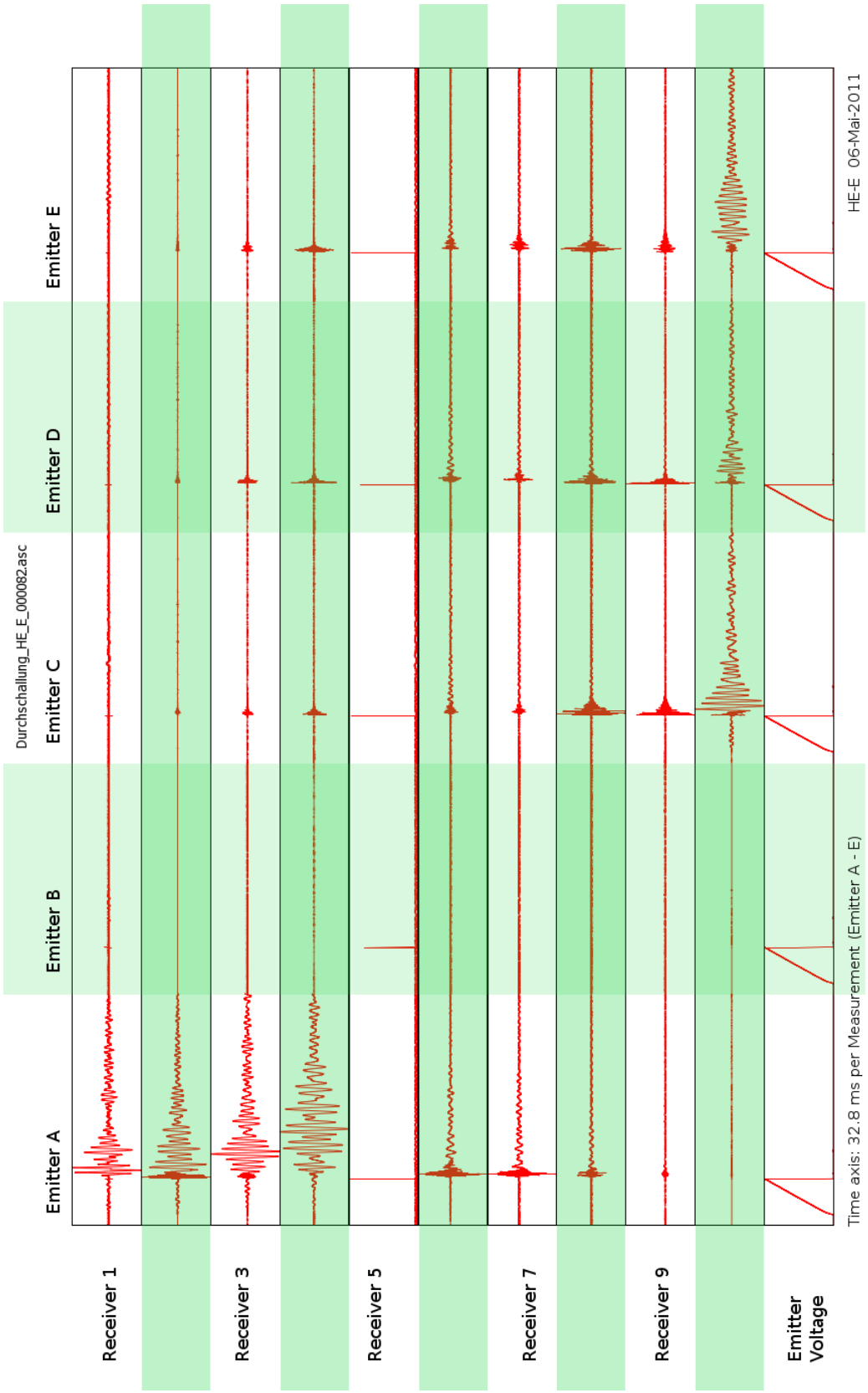

Abbildung 8: Darstellung aller Durchschallungsstrecken incl. Sendesignal. Deutlich zu unterscheiden sind Down Hole (’Sender A auf Empfänger 1..4’ und ’Sender C..E auf Empfänger 10’) von Cross Hole (’Sender D..E auf Empfänger 02..09’) Strecken. Sender B ist nicht angekoppelt